

ScholarWorks@GSU

Spectroscopic and mechanistic investigation of two flavin-dependent enzymes: nitronate monooxygenase and choline oxidase

Authors	Su, Dan
Citation	Su, Dan. (2019). "Spectroscopic and mechanistic investigation of two flavin-dependent enzymes: nitronate monooxygenase and choline oxidase". Georgia State University. https://doi.org/15009583
DOI	https://doi.org/10.57709/15009583
Download date	2026-06-06 19:33:27
Link to Item	https://hdl.handle.net/20.500.14694/2682

SPECTROSCOPIC AND MECHANISTIC INVESTIGATION OF TWO FLAVIN-
DEPENDENT ENZYMES: NITRONATE MONOOXYGENASE AND CHOLINE OXIDASE

by

DAN SU

Under the Direction of Giovanni Gadda, PhD

ABSTRACT

Propionate 3-nitronate (P3N) is a natural toxin that irreversibly inhibits mitochondrial succinate dehydrogenase. P3N poisoning leads to a variety of neurological disorders and even death. Nitronate monooxygenase (NMO) from *Cyberlindnera saturnus* (*Cs*NMO) and *Pseudomonas aeruginosa* PAO1 (*Pa*NMO) serve as paradigms for Class I NMO, which catalyze the oxidation of P3N involving single electron transfer. In this dissertation, the crystallographic structure of *Cs*NMO was solved and demonstrated a highly conserved three-dimensional structure and active site with respect to NMO from *Pa*NMO. The role of conserved residues in the active site of Class I NMO, e.g. Y109, Y254, Y299, Y303, and K307 in *Pa*NMO in substrate binding and catalysis were investigated using site-directed mutagenesis, steady-state kinetics and pH

effects on the UV-visible absorption spectrum. The study revealed that a protonated tyrosine is required for binding of the negatively charged P3N substrate. We also report that *Pa*NMO can stabilize both the neutral and anionic semiquinones anaerobically for hours, providing a constant protein environment to study their photochemical and photophysical properties.

Choline oxidase catalyzes two-step oxidation of choline to glycine betaine with betaine aldehyde as an intermediate. The FAD cofactor is covalently attached to the choline oxidase via H99 through an 8α -N³-histidyl linkage. In the active site of choline oxidase, S101 and H466 are located on two extent loops, ~ 4 Å from the flavin C4a atom. In this dissertation, a charge-induced, reversible C4a-S-cysteinyl- 8α -N³-histidyl FAD was engineered by replacing S101 with a cysteine. The mechanistic rationale for the stabilization of *de novo* C4a-S-cysteinyl-flavins was illustrated with rapid kinetics, pH, kinetic isotope effects and proton inventory. A photoinduced transient C4a-N-histidyl- 8α -N³-histidyl FAD in choline oxidase wild-type was also observed with the aid of fluorescence excitation spectroscopy. Site-directed mutagenesis, solvent equilibrium isotope effects and pH effects on the stoke shifts of flavin in choline oxidase wild-type demonstrated H466 as the adduct on the C4a atom of flavin upon excitation, and provided a mechanistic rationale involving photoinduced electron transfer (PET) for the formation of the novel photoinduced transient flavin C4a adduct.

INDEX WORDS: Nitronate monooxygenase, Flavin semiquinones, Tyrosine ionization, TD-DFT, Choline oxidase, Flavin C4a adduct, Photoinduced electron transfer, Fluorescence

SPECTROSCOPIC AND MECHANISTIC INVESTIGATION OF TWO FLAVIN-
DEPENDENT ENZYMES: NITRONATE MONOOXYGENASE AND CHOLOINE OXIDASE

by

DAN SU

A Dissertation Submitted in Partial Fulfillment of the Requirements for the Degree of

Doctor of Philosophy

in the College of Arts and Sciences

Georgia State University

2019

Copyright by
Dan Su
2019

SPECTROSCOPIC AND MECHANISTIC INVESTIGATION OF TWO FLAVIN-
DEPENDENT ENZYMES: NITRONATE MONOOXYGENASE AND CHOLINE OXIDASE

by

DAN SU

Committee Chair: Giovanni Gadda

Committee: Markus W. Germann

Jun Yin

Samer Gozem

Electronic Version Approved:

Office of Graduate Studies

College of Arts and Sciences

Georgia State University

August 2019

DEDICATION

This dissertation is dedicated to my parents, Shikui Su and Haiyan Wan, for their unconditional love and support.

ACKNOWLEDGEMENTS

I am deeply grateful to my advisor, Dr. Giovanni Gadda, for his support throughout my graduate career. Without the rigorous training received from him, I would not be able to present any of the work in this dissertation. The quality of being critical and meticulous he instilled prepares me for the ongoing scientific venture.

I would like to express my appreciation to my committee members, Dr. Markus Germann, Dr. Samer Gozem and Dr. Jun Yin, for their insightful suggestions and encouragement.

I am thankful to my senior colleagues, Dr. Elvira Romero, Dr. Swathi Gannavaram, Dr. Francesca Salvi, Dr. Crystal Smitherman, Dr. Renata Reis, and Dr. Hongling Yuan for being constant inspirations. I would like to extend my sincere thanks to Daniel Ouedraogo, Quan Bui, and Jacob Ball for their friendship since we were novice in science. Also, I cannot leave Georgia State without mentioning Shan, Maria Vodovoz, Archana Iyer and Shingo Esaki for their unwavering support and help.

The last but not the least, special thanks to my daughter, Wanyi Su, for bringing so much joy and motivation to my life.

TABLE OF CONTENTS

DEDICATION.....	IV
ACKNOWLEDGEMENTS	V
LIST OF TABLES	X
LIST OF FIGURES	XI
1 CHAPTER 1: INTRODUCTION.....	1
1.1 Chemical Properties of 3-NPA	1
1.2 Natural Occurrence of 3-NPA.....	2
1.3 Toxicity of 3-NPA	4
<i>1.3.1 Impairment of Energy Metabolism by 3-NPA.....</i>	<i>6</i>
<i>1.3.2 Oxidative Stress Induced by 3-NPA.....</i>	<i>7</i>
<i>1.3.3 Excitotoxicity of 3-NPA.....</i>	<i>8</i>
1.4 Biosynthesis of 3-NPA.....	9
<i>1.4.1 Biosynthesis of 3-NPA in Fungi.....</i>	<i>9</i>
<i>1.4.2 Biosynthesis of 3-NPA in Plants.....</i>	<i>11</i>
<i>1.4.3 Biosynthesis of 3-NPA in Insects.....</i>	<i>12</i>
1.5 Detoxification of 3-NPA	13
1.6 Specific Goals.....	15
1.7 References	17

2	CHAPTER 2: CRYSTAL STRUCTURE OF YEAST NITRONATE MONOOXYGENASE FROM <i>CYBERLINDNERA SATURNUS</i>	23
2.1	Abstract	23
2.2	Introduction	23
2.3	Materials and Methods	25
2.4	Results and Discussion	28
2.5	Conclusion.....	38
2.6	Acknowledgement	39
2.7	References	39
3	CHAPTER 3: CHARACTERIZATION OF CONSERVED ACTIVE SITE RESIDUES IN CLASS I NITRONATE MONOOXYGENASE	42
3.1	Abstract	42
3.2	Introduction	43
3.3	Materials and Methods	46
3.4	Results	49
3.5	Discussion.....	55
3.5	Conclusion.....	57
3.6	References	58
4	CHAPTER 4: FLUORESCENCE PROPERTIES OF FLAVIN SEMIQUINONE RADICALS IN NITRONATE MONOOXYGENASE.....	61

4.1	Abstract	61
4.2	Introduction	61
4.3	Materials and Methods	65
4.4	Results and Discussion	67
4.4	Conclusion.....	78
4.5	Acknowledgement	79
4.6	References	79
5	CHAPTER 5: A REVERSIBLE, CHARGE-INDUCED INTRAMOLECULAR C4A-S-CYSTEINYL-FLAVIN IN CHOLINE OXIDASE VARIANT S101C	86
5.1	Abstract	86
5.2	Introduction	87
5.3	Material and Methods.....	90
5.4	Results	93
5.4	Discussion.....	109
5.5	Conclusion.....	120
5.7	Acknowledgement	120
5.8	References	121
6	CHAPTER 6: A TRANSIENT, PHOTOINDUCED INTRAMOLECULAR C4A-N- HISTIDYL-FLAVIN IN CHOLINE OXIDASE.....	125
6.1	Abstract	125

6.2	Introduction	125
6.3	Material and Methods.....	128
6.4	Results	130
6.5	Discussion.....	136
6.6	Conclusion.....	140
6.7	Acknowledgement	141
6.8	References	141
7	CHAPTER 7: GENERAL DISCUSSION AND CONCLUSIONS	144
7.1	References	148

LIST OF TABLES

Table 2.1 X-ray Diffraction Data Collection and Refinement Statistics.....	29
Table 2.2 Comparison of Steady-State Kinetic Parameters of CsNMO and PaNMO	36
Table 3.1 UV-Visible Absorption Maxima and FMN/Protein Stoichiometry of Wild-Type and Mutated <i>Pa</i> NMO	51
Table 3.2 Effects of pH on Steady-State Kinetic Parameters of Wild-Type PaNMO	52
Table 3.3 Steady-State Kinetic Parameters of Wild-Type and Mutated PaNMO at pH 8.0.....	55
Table 4.1 Fluorescence properties of FMN in bulk solution and bound to NMO at 15°C ^a	70
Table 4.2 Computed vertical and adiabatic energies for LFH [•] and LF ^{• -} at the B3LYP/cc-pVTZ/PCM level of theory	75
Table 4.3 Solvent effect on the computed energies of D ₁ ππ* and n _O π* for LFH [•] and D ₁ ππ* and n _N π* for LF ^{• -}	76
Table 5.1 Kinetic rate constants for the reversible formation of the C4a-S-cysteinyl-flavin in the S101C enzyme with Tris ^a	108
Table 5.2 Solvent kinetic isotope effects on the reversible formation of the C4a-S-cysteinyl-flavin in the S101C enzyme with Tris ^a	108

LIST OF FIGURES

Figure 1.1 Ionization of 3-NPA (left) to P3N (right).....	2
Figure 1.2 Chemical structures of select compounds containing 3-NPA moieties (in red).....	2
Figure 1.3 Proposed biosynthetic pathway for 3-NPA from aspartate in the fungus <i>P.atrovenetum</i>	11
Figure 1.4 Alternative proposed biosynthetic pathway for 3-NPA from aspartate in the fungus <i>P. atrovenetum</i>	11
Figure 2.1 Structure of yeast CsNMO (PDB ID 6BKA). (A) Cartoon representation of the overall structure.	30
Figure 2.2 Close-up view of the FMN binding-site showing the residues around FMN. Protein side chains are displayed in sticks with carbon atoms colored in gray.....	31
Figure 2.3 CsNMO crystal packing around PEG molecule.	34
Figure 2.4 Comparison of the three-dimensional structure of CsNMO (light-blue, PDB ID 6BKA) with PaNMO (gray, PDB ID 4Q4K).....	35
Figure 2.5 Comparison of the active site residues of CsNMO (blue with first residue in label) and PaNMO (gray with second residue in label).	37
Figure 3.1 Conserved active site residues in PaNMO (PDB entry 4Q4K).....	45
Figure 3.2 UV-visible absorption spectra of wild-type and mutated PaNMO.....	50
Figure 3.3 Effect of pH on the steady-state kinetic parameters of wild-type PaNMO.....	52
Figure 3.4 Effect of pH on the UV-visible absorption spectrum of wild-type PaNMO.....	54
Figure 4.1 Stabilization of anionic and neutral flavin semiquinones in NMO.	68
Figure 4.2 Fluorescence emission of NMO in the oxidized (A) and neutral semiquinone (B) states. emission spectra as dashed curves. t pH 5.0 and 15 °C.	70

Figure 4.3 Fluorescence excitation of NMO in the oxidized (A) and neutral semiquinone (B) states.....	72
Figure 4.4 A. Simulated PCM TD-DFT UV-visible absorption spectrum (solid blue line) and emission (dashed blue line) spectra of LFH [•] . B. Simulated PCM TD-DFT UV-visible absorption spectrum (solid red line) of LF ^{•-} . C. The active site of PaNMO (PDB entry 4Q4K). D. A scheme showing the relative energies of ground and excited states given by PCM TD-DFT calculations. E. A scheme showing the relative energies of ground and excited states given by gas-phase TD-DFT calculations.....	74
Figure 5.1 The active site of choline oxidase wild-type with the reaction product glycine betaine bound (PDB entry 4MJW).....	89
Figure 5.2. Effect of Tris on the UV-visible absorption spectrum of the S101C enzyme.....	94
Figure 5.3 Effect of pH on the UV-visible absorption spectrum of the S101C enzyme with 20 mM Tris in 20 mM sodium phosphate, 20 mM sodium pyrophosphate, 15 °C.....	97
Figure 5.4 Effect of pH on the UV-visible absorption spectrum of the S101C enzyme in 20 mM sodium phosphate, 20 mM sodium pyrophosphate, 15 °C.....	98
Figure 5.5 Effect of pH on the UV-visible absorption spectrum of the wild-type enzyme in 20 mM sodium phosphate, 20 mM sodium pyrophosphate, 15 °C.....	99
Figure 5.6 Effect of pH on the UV-visible absorption spectrum of the S101A enzyme in 20 mM sodium phosphate, 20 mM sodium pyrophosphate, 15 °C.....	100
Figure 5.7 Effect of pH on the UV-visible absorption spectrum of the wild-type enzyme with 20 mM Tris, in 20 mM sodium phosphate, 20 mM sodium pyrophosphate, 15 °C.....	102
Figure 5.8 Effect of pH on the UV-visible absorption spectrum of the H99N enzyme in 20 mM sodium phosphate, 20 mM sodium pyrophosphate, 15 °C.....	103

Figure 5.9. Double reciprocal plot of the inhibition of the wild-type enzyme by Tris with choline as a substrate.	104
Figure 5.10 Glycine betaine titration of the S101C enzyme-Tris complex in 20 mM Tris-Cl, pH 8.0 and 25 °C.	105
Figure 5.11 Stopped-flow kinetics for formation of the C4a-S-cysteinyl-flavin in the S101C enzyme with Tris in 50 mM sodium phosphate pH 8.5 and 25 °C.	107
Figure 5.12 Proton inventories of k_{for} (\blacktriangledown) and k_{rev} (\triangle) of the reversible formation of the C4a-S-cysteinyl-flavin in the S101C enzyme in 50 mM sodium phosphate, pH 8.8 and 25 °C. Five replicates of each data point were performed.	109
Figure 6.1 The active site of choline oxidase wild-type (PDB 4MJW).	128
Figure 6.2 Fluorescence and absorption spectroscopy of FAD in free solution and choline oxidase.	131
Figure 6.3 Effect of pH on $\Delta\lambda$ ($\lambda_{\text{em}} - \lambda_{\text{ex}}$) of FAD in free solution and wild-type enzyme in 20 mM sodium pyrophosphate and 20 mM sodium phosphate at 15 °C.	133
Figure 6.4 Fluorescence and absorption spectroscopy of H466Q variant enzyme.	134
Figure 6.5 Fluorescence and absorption spectroscopy of S101A variant enzyme.	135

LIST OF SCHEMES

Scheme 1.1 Redox states of flavins.....	63
Scheme 3.1 Minimal reaction mechanism of <i>Pa</i> NMO with P3N and O ₂ as substrates.	44
Scheme 5.1 Ionization of the N3 atom of the flavin in the H99N enzyme (A), and in the wild-type, S101A, and S101C enzymes (B), and of the histidyl N1 atom of the 8 α -N ³ -histidyl-FAD in the wild-type, S101A, and S101C enzymes (B).	112
Scheme 5.2 Ionization of the histidyl N1 atom of H99, the flavin N3 atom of the 8 α -N ³ -histidyl-FAD, and Tris, in wild-type choline oxidase when Tris is present.....	113
Scheme 5.3 Stabilization of the C4a-S-cysteinyl-flavin in the S101C enzyme with Tris.....	116
Scheme 5.4 Minimal mechanism for the reversible formation of the C4a-S-cysteinyl-flavin in the S101C enzyme with protonated Tris in the pH range 8.0-9.0	117
Scheme 6.1 Schematic representation of excited state reaction in choline oxidase wild-type...	137

1 CHAPTER 1: INTRODUCTION

(This chapter has been published verbatim in Su, D., and Gadda, G. (2019), in Handbook of foodborne diseases. Boca Raton: Taylor & Francis.)

1.1 Chemical Properties of 3-NPA

3-NPA is a weak nitrocarbon acid with two ionization equilibria for the carboxylate and the α -carbon atom adjacent to the nitro group (Figure 1.1). A pK_a of 9.1 defines the equilibrium between the protonated and unprotonated α -carbon atom. The ionization of the α -carbon atom of 3-NPA, which results in the formation of P3N, is atypical in two aspects. First, it occurs with a pK_a value that is considerably lower than the pK_a values of ~50-60 typically observed for carbon atom ionizations in alkanes^{10,11}. Second, the deprotonation of the α -carbon atom occurs slowly and reaches equilibrium over several hours instead of occurring on the femto-picosecond timescale as commonly observed for O, N and S atoms¹². These processes have been extensively studied with nitroalkanes and are known as the principle of nonperfect synchronization^{12,13}. Nonperfect synchronization occurs when multiple physical-chemical processes, such as bond formation and cleavage, charge localization or delocalization, reactant solvation or desolvation, or changes in molecular orbital hybridization, are not synchronized in the transition state that defines the process^{12,13}. In the case of 3-NPA and other nitro compounds the presence of the nitro group delocalizes the electrons between the nitrogen and the deprotonated α -carbon atoms (Figure 1.1), resulting in a thermodynamic stabilization of the nitronate anion that is not synchronized with the ionization process. Hence, the pK_a values of nitro alkyl compounds are typically between 5.0 and 10.0¹¹, and the second-order rate constants for the deprotonation of nitroalkanes are between 2 and 6 $M^{-1}s^{-1}$ while those of the protonation of the conjugate base (nitronate anion) range from 15 to 75 $M^{-1}s^{-1}$ ^{11,14}.

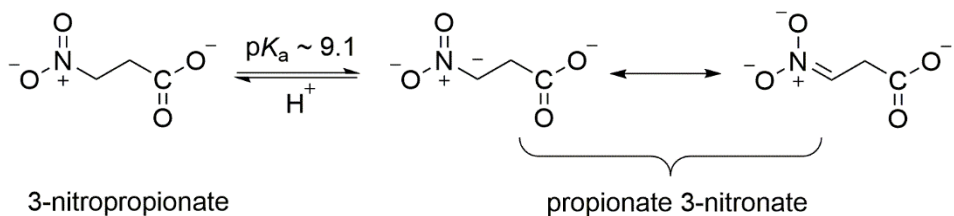


Figure 1.1 Ionization of 3-NPA (left) to P3N (right).

1.2 Natural Occurrence of 3-NPA

3-NPA was isolated for the first time in 1920 following the hydrolysis of the plant glucoside hiptagin (Figure 88.2) from the bark of *Hiptage madablota*¹. Other ester derivatives of 3-NPA have been identified afterwards in a wide range of plants and in leaf beetles; it also has been found in free form in fungi and plants^{1,10,15-23}.

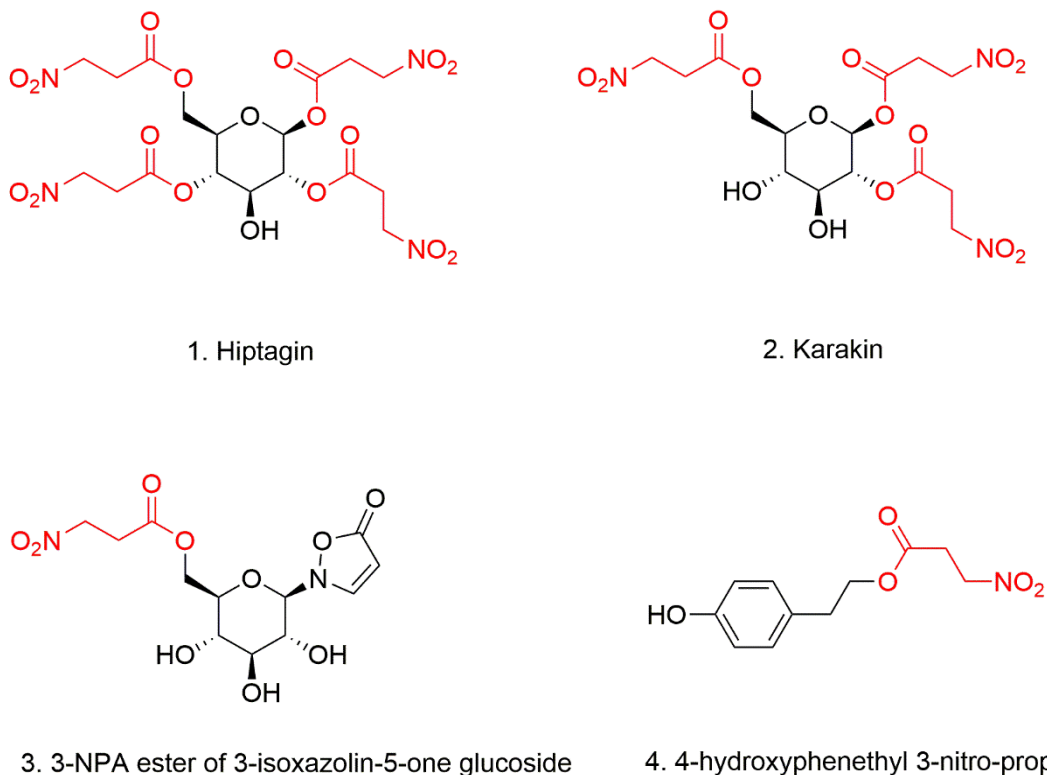


Figure 1.2 Chemical structures of select compounds containing 3-NPA moieties (in red).

In plants, 3-NPA and its ester derivatives have been found in Leguminosae (Fabaceae), Corynocarpaceae, Malpighiaceae and Violaceae^{1,18,24-31}. In the Leguminosae family 3-NPA is widely spread among more than 500 species from the genera *Astragalus*, *Coronilla*, *Hippocrepis*, *Indigofera*, *Lotus*, *Securigera* and *Scorpiurus*¹⁸. High concentrations of 3-NPA occur primarily in the plant shoots, where the compound can exceed 100 $\mu\text{mol g}^{-1}$ fresh weight, accounting for a significant portion (>7%) of the total soluble fixed nitrogen, but not in the roots¹⁸. Based on its known toxicity^{6,7,32} and tissue localization¹⁸ 3-NPA is proposed to serve as a defense mechanism against herbivores in plants. The presence of both 3-NPA and enzymatic activities that oxidize it, or its conjugate base P3N, in a number of legumes supports the notion that 3-NPA may be an intermediate in the nitrification process¹⁸. The introduction of the *Astragalus* species to revegetate areas of the Western United States previously depleted by overgrazing or mining has been associated with poisoning of livestock³³. Cases of poisoning by ingestion of plants containing 3-NPA have been widely documented in domestic livestock while anecdotal reports of human intoxication by ingestion of plants containing 3-NPA are confined to New Zealand and the Chatham Islands due to the consumption of the fruit kernel of the karaka tree (*Corynocarpus laevigatus*) by the Maori tribes^{5,7,27,32}. The fruit of the karaka contains karakin, a glucoside with three molecules of 3-NPA²⁷ (Figure 88.2).

3-NPA and its ester glucosides and glucose esters have been found in leaf beetles from the subfamily Chrysomelinae^{19,34-37}. A 3-NPA ester of 3-isoxazolin-5-one glucoside (Figure 88.2) has been detected in all life stages of *Chrysomela populi* and *Phaedon cochleariae*, being present as a major secondary metabolite in the eggs, the larval hemolymph, and the pupae and the adult hemolymph, as well as their defensive secretions^{19,34-37}. 3-NPA ester of 3-isoxazolin-5-one glucoside allows for the storage of high amounts of 3-NPA in leaf beetles as it was shown that it

is non-toxic to the organism in the hemolymph³⁴. Diverse esters of glucose containing up to three 3-NPA moieties have been identified by analysis of the adult secretions of the leaf beetle species *Plagioderia versicolora distincta*, *Gastrophysa atrocyanea*, *Chrysomela vigintipunctata costella* and *Gastrolina depressa*³⁸. The 3-NPA derivatives in Chrysomelinae leaf beetles are described as allomone secreted with other chemical aposematic repellent for self-defense¹⁹.

In fungi, the free form of 3-NPA has been identified in *Arthrinium*, *Aspergillus*, *Penicillium* genera as well as in the endophytic species *Diaporthe citri*, *Phomopsis* sp. usia5 and mfer5^{16,20,24,39,40}. The ester form 4-hydroxyphenethyl 3-nitro-propanoate (Figure 88.2) was also isolated from *Phomopsis* sp. PSU-D15⁴¹. The capability of endophytic fungi to produce 3-NPA gives rise to a debate as of whether 3-NPA in some plants is actually generated by symbiotic fungi¹⁶. The physiological role of 3-NPA in fungi remains unestablished. However, due to its potent antimycobacterial activity^{16,42}, 3-NPA may be utilized by fungi for colonization of ecological niches. The 3-NPA produced by endophytic fungi may be the source of protection against herbivores for their plant hosts^{16,42}. The naturally occurring 3-NPA from fungi accounts for most of the reported cases of human poisoning. Economically valuable fungi used in the food industry, e.g. *Aspergillus* sp. and *A. soyae*, were reported to introduce 3-NPA to miso, katsuobushi and cheese⁴³⁻⁴⁵. At least 884 cases of sugarcane poisoning have been documented in the Northern regions of China from 1972 to 1989⁵, with the 3-NPA produced by *Arthrinium* genus in improperly stored sugarcane being responsible for the mass poisonings⁴⁶.

1.3 Toxicity of 3-NPA

Acute toxicity studies in rats demonstrated a consistent LD₅₀ for 3-NPA administered either orally or intraperitoneally, ranging from 70 mg/kg to 80 mg/kg^{47,48}. The subcutaneous LD₅₀ determined was in a range from 20 mg/kg to 30 mg/kg⁴⁹. Bossi *et al.* administered 30 mg/kg (LD₅₀

dose) 3-NPA subcutaneously to different age groups of rats and observed that dose was the LD₅₀ in the age group of 11-14 weeks, but not lethal in the age groups of 3-6 weeks and 7-10 weeks⁵⁰. James *et al.* fed cattle with different doses of 3-NPA containing plants *Astragalus*. A single dose of dried *Astragalus* (200 mg NO₂/kg body weight) to a cow led to no effects while another cow exhibited foaming of the mouth and weakness after a single dose of 275 mg NO₂/kg body weight. A third cow died after a single dose of 350 mg NO₂/kg body weight. Upon a single dose of free synthetic 3-NPA (15 mg NO₂/kg body weight), cattle experienced a series of intoxication symptoms including incoordination, nervousness, weakness and eventually death⁶. Acute toxicity experiments with either free or diets of plants containing 3-NPA were also carried out in animal models sheep⁶, chicken⁵¹ and pigeons⁵². In all cases, 3-NPA was demonstrated to be lethal.

The intensive research on 3-NPA toxicity is primarily driven by the economic losses of 3-NPA poisoning on the agricultural industry in the Western regions of the United States, Canada and Northern Mexico^{5,7,32}. The impact of 3-NPA poisoning as the result of grazing on 3-NPA containing plants is severe. One case in New Mexico gave rise to 3% mortality and 20% morbidity in cattle foraging in affected pastures³². Most of the livestock losses are due to the consumption of milkvetch (*Astragalus* sp.), creeping indigo (*Indigofera endecaphylla*) and crownvetch (*Coronilla varia*). The long-term effects of 3-NPA consumption by humans through food prepared using fungi or unintentionally contaminated by fungi further justify the studies on the toxicity of 3-NPA^{23,43-45}.

Three intertwined modalities for the *in vivo* toxicity of 3-NPA can be considered: impairment of energy metabolism, oxidative stress, and excitotoxicity.

1.3.1 Impairment of Energy Metabolism by 3-NPA

At pH values relevant to physiology 3-NPA is in equilibrium with its conjugate base P3N (Figure 1.1). At pH 7.4 for instance, ~2% of the 3-NPA is in the nitronate, P3N form. P3N is an analog of succinate and acts as a potent irreversible inhibitor of mitochondrial succinate dehydrogenase. This inactivation is the primary biochemical basis for 3-NPA toxicity as it effectively shuts down energy production in all aerobes²⁻⁴. Succinate dehydrogenase catalyzes the oxidation of succinate to fumarate in the citric acid cycle and is the second complex that transfers electrons in the respiratory chain for oxidative phosphorylation in mitochondria. A time-dependent, irreversible inhibition of succinate oxidation was observed when P3N was added into isolated rat liver mitochondria incubated with succinate². The inhibition of succinate dehydrogenase was not observed upon the addition of 3-NPA, demonstrating that P3N is the inhibitory agent². The inhibited succinate dehydrogenase could not be reactivated by washing or centrifugation, suggesting irreversible inactivation of the enzyme². Alston *et al.* proposed an inhibitory mechanism involving the formation of an irreversible adduct between P3N and the N(5) atom of the enzyme cofactor bound to the enzyme², analogous to the oxidation of nitroethane with D-amino oxidase proceeding via a transient N(5) adduct with the flavin cofactor^{53,54}. However, a subsequent study on the purified enzyme from beef heart by Coles *et al.* demonstrated that the inactivation of succinate dehydrogenase does not occur via the formation of an irreversible flavin N(5) adduct, based on the features seen in the UV-visible absorption spectrum of the inactivated enzyme. An alternative mechanism explaining the available data proposes that 3-nitroacrylate is first produced by the flavin-dependent oxidation of P3N catalyzed by succinate dehydrogenase, followed by its reaction with a cysteine thiolate that inactivates the enzyme³. A crystallographic structure of succinate dehydrogenase from avian heart mitochondria was reported in 2006 in

complex with different inhibitors, including P3N⁴. The chemical modification on the flavin cofactor was not observed in the structure of the inactivated enzyme with P3N, consistent with the lack of a flavin N(5) adduct⁴. Instead, the crystal structure unveiled a cyclic adduct between the sidechain of arginine 297 and P3N⁴, but no mechanism was proposed. Hence, while the toxicity of 3-NPA, through its conjugate base P3N, is unequivocally due to the irreversible shut down of the citric acid cycle and the respiratory chain in mitochondria by the action of P3N on succinate dehydrogenase, the molecular mechanism is still unresolved.

1.3.2 Oxidative Stress Induced by 3-NPA

Oxidative stress due to increased generation of reactive oxygen species (ROS) is considered one of the mechanisms underlying 3-NPA toxicity in mitochondria. The oxidative stress associated with mitochondrial dysfunction has a central role in cognitive decline associated with aging⁵⁵ and neurodegenerative diseases, including Alzheimer's disease, Parkinson's disease, amyotrophic lateral sclerosis and Huntington's disease⁵⁶. Increases in ROS induced by 3-NPA have been reported in several studies. An increase of free radical signal was observed in rat liver from 15 min after oral administration of 80 mg/kg 3-NPA by electron paramagnetic resonance (EPR)⁵⁷. An increase in ROS was also detected by EPR in rat brains treated with 3-NPA⁵⁸. A concomitant increase in activities of antioxidant enzymes, e.g. catalase, glutathione peroxidase and superoxide dismutase, in rat hippocampus⁵⁹ and mice ovarian tissues treated with 3-NPA has been reported⁶⁰. Furthermore, systemic administration of 3-NPA introduces more striatal harm to glutathione peroxidase knock-out mice than in the wild-type mice, indicating that oxidative stress has an important role in 3-NPA toxicity⁶¹. Although 3-NPA induced oxidative stress is physiologically important, the mechanism of oxidative stress induction has not been fully established yet. Studies on the oxidation of P3N, as well as nitroethane, by flavin-dependent

enzymes, e.g. nitronate monooxygenase, P3N monooxygenase and glucose oxidase, demonstrate that the nitronate form of the organic substrate readily donates a single electron to the enzyme-bound flavin, producing a flavosemiquinone radical that can potentially reduce dioxygen to superoxide⁶²⁻⁶⁶. The resulting superoxide could subsequently initiate a free radical chain oxidation of the nitronate that propagates oxidative stress⁶⁷. However, further studies are required to corroborate the involvement of flavin-dependent enzymes in the mitochondrial generation of ROS induced by 3-NPA.

1.3.3 Excitotoxicity of 3-NPA

3-NPA belongs to a class of mitochondrial toxins that include cyanide, carbon monoxide, rotenone, manganese and 1-methyl-4-phenyl-1,2,3,6-tetrahydropyridine (MPTP), which cause neuropathology selectively in the basal ganglia upon peripheral exposure, despite a general impairment of energy metabolism throughout the entire body and brain⁶⁸. The neurotoxicity of 3-NPA has been extensively studied because the toxin induces pathological and clinical symptoms that closely resemble Huntington's disease^{8,9}. Basal ganglia damages and hippocampal lesions have been reported in rats and mice treated with 3-NPA^{8,69,70}. After chronic administration of 3-NPA baboons and macaques developed symptoms including orofacial and extremities dyskinesia, dystonia, and choreiform movements⁸. Lesions induced by 3-NPA treatment in primates were observed in the caudate and putamen by magnetic resonance imaging (MRI)⁸; furthermore, histologic evaluations revealed a series of Huntington's disease-like changes, e.g., a depletion of calbindin neurons, astrogliosis, sparing of NADPH-diaphorase neurons and growth-related proliferative changes in dendrites of spiny neurons⁸. Children accidentally poisoned by moldy sugarcane developed an acute encephalopathy followed by dystonia 11-60 days after ingestion, with bilateral hypodensities determined by computerized tomography scans in the putamen and to

a lesser extent in the globus pallidus^{8,71}. Knowledge and insights on the pathogenesis and cell biology associated with the phenotypes and neurotoxicity induced by 3-NPA have been accrued over the past twenty years and the field is currently active, and exemplifies well the intertwining of impairment of energy metabolism, oxidative stress, and excitotoxicity. Hindrance of energy metabolism in neurons treated with 3-NPA produces a partial depolarization of the neuronal cell membrane that arises from a lower intracellular concentration of ATP acting on ATP-sensitive ion pumps and channels⁷². Neuronal depolarization relieves the Mg²⁺ block on the N-methyl-D-aspartate receptor, a glutamate receptor and ion channel protein located in nerve cells^{8,73-76}, allowing for an influx of Ca²⁺ and Na⁺. The increase in the intracellular concentration of Ca²⁺ has two primary effects. On the one hand, it activates several cytosolic enzymes, including xanthine dehydrogenase, nitric oxide synthase and phospholipase A₂, which can generate ROS or other deleterious pathways, e.g., nitric oxide-mediated neurotoxicity^{77,78}, thereby promoting oxidative stress. On the other hand, because mitochondria are the main organelle sequestering Ca²⁺⁷⁹, during Ca²⁺ overload of the cytosol there is an accumulation of Ca²⁺ in the mitochondrial matrix that promotes Mitochondrial Permeability Transition (MPT)⁷⁹⁻⁸³. MPT leads to a spectrum of processes that decrease the biosynthesis of ATP, promote the generation of ROS in mitochondria⁷⁹, and release apoptogenic factors into the cytosol^{75,83-85}, which further exacerbate neuronal cell damage and stimulate apoptosis.

1.4 Biosynthesis of 3-NPA

1.4.1 Biosynthesis of 3-NPA in Fungi

Studies on the biosynthesis of 3-NPA were first carried out in fungi by the incorporation of ¹⁴C-, ¹⁵N- and ¹⁸O-labeled substrates in growing cultures of *Penicillium atrovenerum* followed by mass spectrometric and NMR analyses on 3-NPA and its derivatives. These studies

demonstrated that L-aspartate as well as metabolites associated with the citric acid cycle, e.g. acetate and pyruvate, could be precursors for 3-NPA⁸⁶⁻⁹⁰. By administering L-[4-¹⁴C]-aspartate in growth media, ¹⁴C was incorporated into the C-1 position of 3-NPA. NMR analyses of biosynthesized 3-NPA when [2-¹³C,¹⁵N]-DL-aspartate was present in the fungal growth media established that the C-N bond of aspartate is preserved in the biosynthesis⁸⁹. These studies supported the notion that both the amino group and the carbon skeleton of L-aspartate are the direct precursors for 3-NPA biosynthesis in *P. atrovenerum*. Additionally, cell-free extracts of *P. atrovenerum* contain a highly specific NADPH-dependent 3-nitropropanoate dehydrogenase that reduces 3-nitroacrylate to 3-NPA⁸⁸. Based on these results, Alston *et al.* proposed a mechanism for 3-NPA biosynthesis with a six-electron oxidation of an amino group to a nitro group and decarboxylation from the α -carbon atom of aspartate (Figure 1.3)⁹¹. In this mechanism, 3-nitroacrylate is the final intermediate yielding to 3-NPA by an NADPH-dependent enzymatic reduction⁹¹. However, further experiments using a combination of stable isotope methods conducted by Baxter *et al.* indicated a biosynthetic pathway for 3-NPA that involves a stepwise oxidation of L-aspartate to L-nitrosuccinate followed by the decarboxylation of the nitrosuccinate to 3-NPA (Figure 1.4)³⁹. Evidence in support of the proposed mechanism shown in Figure 88.4 came from the incorporation of ¹⁵N from DL-diethyl-[¹⁵N]-nitrosuccinate to 3-NPA and the lack of 3-nitropropanoate dehydrogenase activity during the first 82 h of penicillium growth, while 3-NPA could be detected from 48 h onwards³⁹.

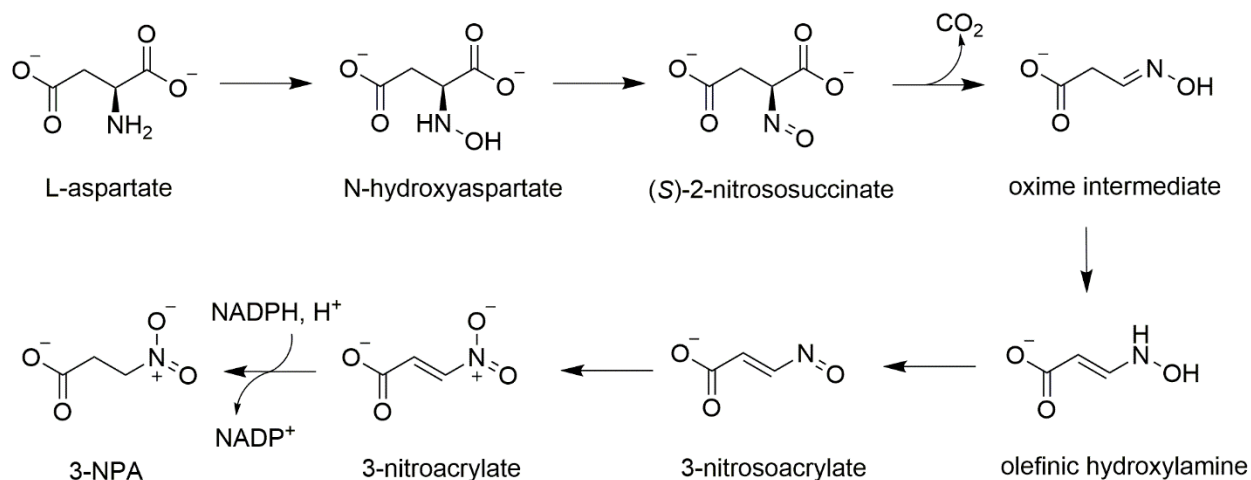


Figure 1.3 Proposed biosynthetic pathway for 3-NPA from aspartate in the fungus

P. atroveneretum.

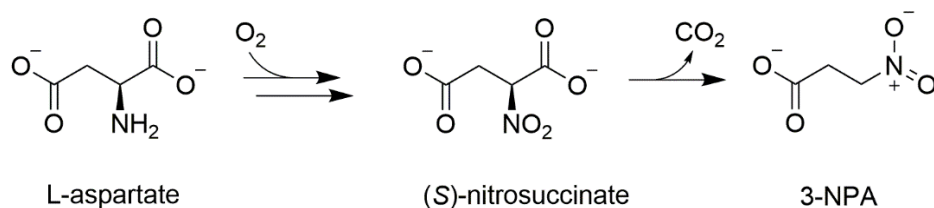


Figure 1.4 Alternative proposed biosynthetic pathway for 3-NPA from aspartate in the fungus *P. atroveneretum*.

1.4.2 Biosynthesis of 3-NPA in Plants

Studies on the biosynthesis of 3-NPA with cuttings and intact plants of *Indigofera spicata* suggested that higher plants may use different pathways than those used by fungi⁹². Indeed, no radioisotope incorporation was observed in 3-NPA when radiolabeled aspartate or any of the citric acid cycle intermediates were used in feeding experiments⁹². Based on experiments indicating increased production of 3-NPA in the presence of [2-¹⁴C]-malonate or the putative biosynthetic

intermediate [2-¹⁴C]-malonyl monohydroxamate were used both in root and stem feeding experiments⁹². ¹⁴C was incorporated into both the C-2 and C-3 positions of the 3-NPA product⁹², but to a low extent of $\leq 0.1\%$ ⁹². Thus, it was concluded that malonate and malonyl monohydroxamate do not serve as the direct precursors for the biosynthesis of 3-NPA in plants. An alternative direct biosynthetic pathway to produce 3-NPA from valine that includes β -alanine as an intermediate has been proposed and it awaits experimental validation in plants^{92,93}.

1.4.3 Biosynthesis of 3-NPA in Insects

Research on the biosynthesis of 3-NPA and its derivatives in leaf beetles was first carried out with the species *Chrysomela tremulae*^{37,94}. With the aim to understand the 3-NPA biosynthetic routes, *C. tremulae* adults were fed with leaves covered with [4-¹⁴C]-aspartate for a week, followed by radioactivity analysis on 3-isoxazolin-5-one glucoside and the 3-NPA ester of 3-isoxazolin-5-one glucoside (Figure 88.2), which are the major components found in the adult defensive secretion of the beetle³⁷. Radioactivity was detected in both glucosides, but not in the glucose moiety separated after acidic hydrolysis of 3-isoxazolin-5-one glucoside and the 3-NPA ester of 3-isoxazolin-5-one glucoside³⁷. Hence, it was concluded that aspartate serves as a joint precursor for both 3-NPA and the 3-isoxazolin-5-one moiety³⁷. However, later feeding experiments carried out on *Phaedon cochleariae* larvae reported random incorporation of fragments of [4-¹³C,¹⁵N]-aspartate into the 3-NPA ester of 3-isoxazolin-5-one glucoside by mass spectrometry⁹⁵. Since β -alanine had been previously proposed to be involved in 3-NPA biosynthesis in plants and it can be sequestered from valine via propanoate as an intermediate, *P. cochleariae* larvae were fed with [3-¹³C,¹⁵N]- β -alanine, [5-¹³C,¹⁵N]-valine or [3-¹³C]-propanoate. In all cases, the incorporation of an intact carbon skeleton of the administered precursors was established by mass spectrometry, with aspartate displaying a low incorporation of $\sim 0.02\%$ and β -alanine and propanoate of $\sim 2\%$ and

~17%, respectively⁹⁵. These data support the notion that the biosynthesis of 3-NPA in leaf beetles may occur through β -alanine or valine, through its conversion to propanoate and β -alanine, but not from aspartate.

1.5 Detoxification of 3-NPA

Due to the widespread distribution of 3-NPA, different protective and nutritional mechanisms have been evolved in various organisms that are exposed to the toxin. Enzymes that catalyze the oxidation of 3-NPA or its conjugate base P3N have been isolated and studied from fungi, plants, and bacteria^{21,22,42,63,96-98}. In all cases, a single flavin mononucleotide (FMN) is non-covalently bound to each protein subunit, irrespective of the oligomerization state of the enzyme.

Biochemical characterization of nitronate monooxygenase (NMO) from the fungi *Neurospora crassa* and *Cyberlindnera saturnus* has been carried out^{64,97,99,100}. These NMOs, which were previously classified until 2010 by the IUBMB as 2-nitropropane dioxygenase, have large k_{cat} (450-770 s⁻¹) and k_{cat}/K_m ($\sim 10^6$ M⁻¹s⁻¹) values with P3N as a substrate at pH 7.4, atmospheric oxygen and 30°C, consistent with a detoxifying role for the fungal enzyme⁴². In agreement with this conclusion, the K_m value for P3N (0.3 mM) in both enzymes lies in the physiological range of P3N concentrations found in fungi and plants²³. Indeed, the 3-NPA concentration in *Arthrinium* growing in sugarcane juice is 15 mM, corresponding to a P3N concentration of 0.3 mM at pH 7.4⁶¹. An enzyme that oxidizes 3-NPA was purified from *P. atrovenetum*, for which a stoichiometry of reaction was established as: 0.8 malonate semialdehyde, 0.4 nitrite and 0.7 nitrate produced for each 1.0 P3N and 0.9 oxygen consumed²¹. The nonintegral stoichiometry of the reaction, along with the known reactivity of superoxide with nitronates⁶⁷, is consistent that the oxidation of P3N in *P. atrovenetum* primarily occurring through a non-enzymatic free-radical chain reaction that is initiated by the formation and release of superoxide

in the active site of the enzyme reacting with P3N. A nonenzymatic oxidation of P3N has not been observed with the *N. crassa* and *C. saturnus* NMOs, for which no release of superoxide was established^{63,64}, consistent with the oxidation reactions catalyzed occurring exclusively in the active site of these enzymes.

An enzymatic oxidation of 3-NPA was reported in the leguminous plant *H. comosa*⁹⁸. The enzyme was named 3-NPA oxidase due to the detection of hydrogen peroxide and the preference for 3-NPA as a substrate (≥ 30 fold) with respect to its conjugate base P3N⁹⁸. Nitrate and nitrite were produced via a combination of enzymatic and non-enzymatic free-radical chain oxidation of the organic substrate as indicated by a nonintegral stoichiometry of hydrogen peroxide produced and 3-NPA consumed⁹⁸.

The NMO that is best characterized to date in its ability to oxidize P3N is the enzyme purified from *Pseudomonas aeruginosa* PAO1, for which kinetic, structural, and bioinformatics information is available. The enzyme is active on P3N with k_{cat} and $k_{\text{cat}}/K_{\text{m}}$ values of $1,300 \text{ s}^{-1}$ and $10^7 \text{ M}^{-1}\text{s}^{-1}$, respectively, but cannot oxidize 3-NPA. The X-ray crystallographic structure of the enzyme to a resolution of 1.44 \AA revealed a TIM barrel-fold and an FMN cofactor in the active site of the enzyme⁶². Based on the structural, biochemical and bioinformatics analysis of the bacterial NMO, four motifs in common with the biochemically characterized NMO from *C. saturnus* were identified, defining Class I NMO^{62,63}. A P3N monooxygenase (P3NMO) belonging to Class I NMO has also been isolated from *P. aeruginosa* strain JS189⁹⁶. By carrying out an oxygen-dependent oxidation of P3N into malonic semialdehyde, nitrate and nitrite, P3NMO allows the bacteria to exploit 3-NPA and P3N as a sole source of carbon and nitrogen⁹⁶. The four motifs of Class I NMO are conserved in 475 sequences of putative NMOs belonging primarily to bacteria and fungi, with only 2 from animals⁶². The widespread presence of NMO in bacteria and fungi

suggests the importance of the enzyme for the detoxification of P3N and possibly other physiological roles, such as the use of the toxin as a carbon and nitrogen source. An involvement of rumen bacteria as a protective mechanism for detoxification of P3N in cattle has been proposed based on the findings that 10 strains out of 33 tested of rumen bacteria showed the ability to degrade 3-NPA¹⁰¹. The detoxification of 3-NPA by rumen bacteria is proposed to occur through the oxidation of 3-NPA to nitrite, which is then reduced to ammonia¹⁰¹.

In insects that feed on leguminous plants, e.g. *Melanoplus* species and *Spodoptera littoralis*, it was shown that the detoxification of 3-NPA occurs through the formation of conjugates of 3-NPA with glycine, alanine, threonine, and serine¹⁰². The amino acid conjugates are then excreted via malpighian tubules of the insects¹⁰². In the case of leaf beetles, the mechanism for preventing self-poisoning by 3-NPA involves the formation of the 3-NPA ester of 3-isoxazolin-5-one glucoside (Figure 1.2)³⁷.

1.6 Specific Goals

This dissertation aims to characterize the spectroscopic and mechanistic properties of flavin-dependent Class I nitronate monooxygenase (NMO, E.C. 1.13.12.16) and choline oxidase (E.C.1.1.3.17) to gain insight on the chemical versatility of flavin.

Class I NMO catalyzes the oxidation of nitronates with molecular oxygen. The previous crystallographic study on *Pa*NMO establishes four conserved motifs and conserved residues in the active site of Class I NMO, i.e., Y109, Y299, Y303, and K307, with Y254 being conserved in ~70% of the amino acid sequences. It is speculated that one or more of these residues participated in binding the carboxylate group of P3N as a hydrogen bond donor. To elucidate the role of these residues, the individual replacement of the conserved active site tyrosine residue(s) with a phenylalanine or the lysine residue with methionine were prepared and purified. The steady-state

kinetics on the variant enzymes, and pH effects on the steady-state kinetic parameters and the UV-visible absorption spectrum of the wild-type enzyme were determined to establish which of the conserved amino acid residues in the active site of Class I NMO is important for binding the P3N substrate. The details will be described in Chapter 2 and 3.

A recent study on *Pa*NMO showed that the anaerobic mixing of the enzyme-bound flavin with P3N yielded anionic flavin semiquinone at pH 7.5. The small absorbance between 550 nm and 700 nm suggested that there might be small amounts of FMNH[•] as well. The stabilization of both neutral and anionic flavin semiquinones in *Pa*NMO was investigated by anaerobic reduction of *Pa*NMO with its substrate P3N using UV-visible absorption spectroscopy. The fluorescence emission and excitation properties of the enzyme-bound flavin semiquinone in its neutral and anionic states were determined and interpreted with the aid of time-dependent density functional theory (TD-DFT) calculations. The details will be discussed in Chapter 4.

Choline oxidase catalyzes two-step, flavin-dependent oxidation of choline to glycine betaine, with betaine aldehyde as an intermediate. In the crystallographic structure of choline oxidase, S101 and H466 were located ~ 4 Å from the flavin C4a atom on flexible peptide loops, which is similar to light-responsive LOV domain where a flavin C4a adduct is formed with the proximal cysteine upon excitation. Choline oxidase thus serves in this study as a model system to study the charge or photo-induced flavin C4a adduct. A reversible C4a-S-cysteinyl-flavin linkage in choline oxidase was engineered by mutagenesis, rapid kinetics, and mechanistic probes such as pH, kinetic isotope effects and proton inventories. A transient C4a-N-histidyl-flavin linkage was observed with the aid of fluorescence excitation spectroscopy. The mechanistic rationale will be presented in Chapter 5 and 6.

1.7 References

- [1] Gorter K. Hiptagin, a new glucoside from *Hiptage madablota*. Bull Jard Bot Buitenz 1920;2:187.
- [2] Alston TA, Mela L, Bright HJ. 3-Nitropropionate, the toxic substance of *Indigofera*, is a suicide inactivator of succinate dehydrogenase. Proc Natl Acad Sci U S A 1977;74:3767-71.
- [3] Coles CJ, Edmondson DE, Singer TP. Inactivation of succinate dehydrogenase by 3-nitropropionate. J Biol Chem 1979;254:5161-7.
- [4] Huang LS, Sun G, Cobessi D, et al. 3-nitropropionic acid is a suicide inhibitor of mitochondrial respiration that, upon oxidation by complex II, forms a covalent adduct with a catalytic base arginine in the active site of the enzyme. J Biol Chem 2006;281:5965-72.
- [5] Hamilton BF, Gould DH, Gustine DL. History of 3-nitropropionic acid. In Mitochondrial Inhibitors and Neurodegenerative Disorders Comptemporary Neuroscience. Totowa, New Jersey: Humana Press; 2000.
- [6] James LF, Hartley WJ, Williams MC, Van Kampen KR. Field and experimental studies in cattle and sheep poisoned by nitro-bearing *Astragalus* or their toxins. Am J Vet Res 1980;41:377-82.
- [7] Mathews FP. Poisoning in sheep and goats by sacahuiste (*Nolina texana*) buds and blooms. J Am Vet Med Assoc 1940;97:125-34.
- [8] Brouillet E, Hantraye P, Ferrante RJ, et al. Chronic mitochondrial energy impairment produces selective striatal degeneration and abnormal choreiform movements in primates. Proc Natl Acad Sci U S A 1995;92:7105-9.
- [9] Burdock GA, Carabin IG, Soni MG. Safety assessment of β -nitropropionic acid: a monograph in support of an acceptable daily intake in humans. Food Chem 2001;75:1-27.
- [10] Bush MT, Touster O, Brockman JE. The production of beta-nitropropionic acid by a strain of *Aspergillus flavus*. J Biol Chem 1951;188:685-93.
- [11] Nielsen AT. Nitronic acids and esters. In the Chemistry of the Nitro and Nitroso Groups. New York: Interscience Publishers; 1969.
- [12] Bernasconi CF. Intrinsic barriers of reaction and the principle of non-perfect synchronization. Acc Chem Res 1987;20:301-8.
- [13] Bernasconi CF. The principle of non-perfect synchronization. New York: Academic Press Inc.; 1992.
- [14] Goodall DM, Long FA. Protonation of nitroalkane anions by acetic acid in mixed water-deuterium oxide solvents. J Am Chem Soc 1968;90 (2):238-43.
- [15] Carter CL, Mc CW. Hiptagenic acid identified as beta-nitropropionic acid. Nature 1949;164:575.
- [16] Chomcheon P, Wiyakrutta S, Sriubolmas N, Ngamrojanavanich N, Isarangkul D, Kittakoop P. 3-Nitropropionic acid (3-NPA), a potent antimycobacterial agent from endophytic fungi: is 3-NPA in some plants produced by endophytes? J Nat Prod 2005;68:1103-5.
- [17] Flores AC, Pamphile JA, Sarragiotto MH, Clemente E. Production of 3-nitropropionic acid by endophytic fungus *Phomopsis longicolla* isolated from *Trichilia elegans* A. JUSS ssp. *elegans* and evaluation of biological activity. World J Microbiol Biotechnol 2013;29:923-32.
- [18] Hipkin CR, Simpson DJ, Wainwright SJ, Salem MA. Nitrification by plants that also fix nitrogen. Nature 2004;430:98-101.
- [19] Pauls G, Becker T, Rahfeld P, et al. Two defensive lines in juvenile leaf beetles; Esters of 3-nitropropionic acid in the hemolymph and aposematic warning. J Chem Ecol 2016;42:240-8.

- [20] Polonio JC, Ribeiro MA, Rhoden SA, Sarragiotto MH, Azevedo JL, Pamphile JA. 3-Nitropropionic acid production by the endophytic *Diaporthe citri*: Molecular taxonomy, chemical characterization, and quantification under pH variation. *Fungal Biol* 2016;120:1600-8.
- [21] Porter DJ, Bright HJ. Propionate 3-nitronate oxidase from *Penicillium atrovenerum* is a flavoprotein which initiates the autoxidation of its substrate by O₂. *J Biol Chem* 1987;262:14428-34.
- [22] Somanthan R, Rivero I.A, Beltran RG. Nitropropanoic acid from five *Astragalus* species. *Rev Latinoamer Quim* 1990;21:101-7.
- [23] Wei DL, Chang S C, Lin SC, Doong M L, Jong SC. Production of 3-nitropropionic acid by *Arthrimum* species. *Curr Microbiol* 1994;28:1-5.
- [24] Anderson RC, Majak W, Rassmussen MA, et al. Toxicity and metabolism of the conjugates of 3-nitropropanol and 3-nitropropionic acid in forages poisonous to livestock. *J Agric Food Chem* 2005;53:2344-50.
- [25] Simpson DJ, Wainwright SJ, and Hipkin CR. Presence of 3-nitropropionic acid, in widely distributed pasture legumes in Britain. *Vet Rec* 1999;145:169-71.
- [26] Benn M, Bai Y, Majak, W. Aliphatic nitro-compounds in *Astragalus canadensis*. *Phytochemistry* 1995;40:1629-31.
- [27] Majak W, Benn M. Additional esters of 3-nitropropanoic acid and glucose from fruit of the New Zealand karaka tree, *Corynocarpus laevigatus*. *Phytochemistry* 1994;35:901-3.
- [28] Gnanasunderam C, Sutherland ORW. Hiptagin and other aliphatic nitro esters in *Lotus pedunculatus*. *Phytochemistry* 1986;25:409-10.
- [29] Qiu L Liang Y, Tang GH, et al. Two new flavonols, including one flavan dimer, from the roots of *Indigofera stachyodes*. *Phytochem Lett* 2013;6:368-71.
- [30] Benn MH, Majak W, Aplin R. A nitropropanoyl isoxazolinone derivative in two species of *Astragalus*. *Biochem Sys Ecol* 1997;25:467-8.
- [31] Salem MA, Williams JM, Wainwright SJ, Hipkin CR. Nitroaliphatic compounds in *Hippocrepis comosa* and other legumes in the European flora. *Phytochemistry* 1995;40:89-91.
- [32] Williams MC, James LF, Bond BO. Emory milkvetch (*Astragalus emoryanus* var *emoryanus*) poisoning in chicks, sheep, and cattle. *Am J Vet Res* 1979;40:403-6.
- [33] Williams MC, Davis AM. Nitro compounds in introduced *Astragalus* species. *J Range Manage* 1982;35:113-5.
- [34] Pasteels JM, Daloze D, Rowell-Rahier M. Chemical defence in chrysomelid eggs and neonate larvae. *Physiol Entomol* 1986;11:29-37.
- [35] Pasteels JMaR-R, M. Defensive glands and secretions as taxonomical tools in the Chrysomelinae. *Entomography* 1989;6:423-32.
- [36] Pasteels JM, Braekman JC, Daloze D, Ottinger R. Chemical defence in chrysomelid larvae and adults. *Tetrahedron* 1982;38:1891-7.
- [37] Randoux T, Braekman JC, Daloze D, Pasteels JM. De novo biosynthesis of delta-isoxazolin-5-one and 3-nitropropanoic acid derivatives in *Chrysomela tremulae*. *Naturwissenschaften* 1991;78:313-4.
- [38] Sugeno W, Matsuda K. Adult secretions of four Japanese Chrysomelinae (Coleoptera: Chrysomelidae). *Appl Entomol Zool* 2002;37:191-7.
- [39] Baxter RL, Hanley AB, Chan HWS, et al. Fungal biosynthesis of 3-nitropropanoic acid. *J Chem Soc, Perkin Trans 1* 1992:2495-502.

- [40] Andolfi A, Boari A, Evidente M, et al. Gulypyrones A and B and phomentrioloxins B and C produced by *Diaporthe gulyae*, a potential mycoherbicide for saffron thistle (*Carthamus lanatus*). *J Nat Prod* 2015;78:623-9.
- [41] Rukachaisirikul V, Sommart U, Phongpaichit S, Sakayaroj J, Kirtikara K. Metabolites from the endophytic fungus *Phomopsis* sp. PSU-D15. *Phytochemistry* 2008;69:783-7.
- [42] Francis K, Nishino SF, Spain JC, Gadda G. A novel activity for fungal nitronate monooxygenase: Detoxification of the metabolic inhibitor propionate-3-nitronate. *Arch Biochem Biophys* 2012;521:84-9.
- [43] Iwasaki T, Kosikowski FV. Production of β -nitropropionic acid in foods. *J Food Sci* 1973;38:1162-5.
- [44] Kinoshita R, Ishiko T, Sugiyama S, Seto T, Igarasi S, Goetz IE. Mycotoxins in fermented food. *Cancer Res* 1968;28:2296-311.
- [45] Orth R. Mycotoxins of *Aspergillus oryzae* strains used in the food industry as starters and enzyme producing molds. *Ann Nutr Aliment* 1977;31:617-24.
- [46] Liu X, Luo X, Hu W. Studies on the epidemiology and etiology of moldy sugarcane poisoning in China. *Biomed Environ Sci* 1992;5:161-77.
- [47] Pass MA, Muir AD, Majak W, Yost GS. Effect of alcohol and aldehyde dehydrogenase inhibitors on the toxicity of 3-nitropropanol in rats. *Toxicol Appl Pharmacol* 1985;78:310-5.
- [48] Majak W, Pass MA, Madryga FJ. Toxicity of miserotoxin and its aglycone (3-nitropropanol) to rats. *Toxicol Lett* 1983;19:171-8.
- [49] Gould DH, Wilson MP, Hamar DW. Brain enzyme and clinical alterations induced in rats and mice by nitroaliphatic toxicants. *Toxicol Lett* 1985;27:83-9.
- [50] Bossi SR, Simpson JR, Isacson O. Age dependence of striatal neuronal death caused by mitochondrial dysfunction. *Neuroreport* 1993;4:73-6.
- [51] Cooke AR. The toxic constituent of *Indigofera endecaphylla*. *Arch Biochem Biophys* 1955;55:114-20.
- [52] Bell ME. Toxicology of karaka kernel, karakin, and beta-nitropropionic acid. *New Zealand J Sci* 1974;17:327-34.
- [53] Porter DJT, Voet JG, Bright HJ. Nitromethane: a novel substrate for D-amino acid oxidase. *J Biol Chem* 1972;247:1951-3.
- [54] Porter DJT, Voet JG, Bright HJ. Direct evidence for carbanions and covalent N5-flavin-carbanion adducts as catalytic intermediates in the oxidation of nitroethane by D-amino acid oxidase. *J Biol Chem* 1973;248:4400-16.
- [55] Lu T, Pan Y, Kao S-Y, et al. Gene regulation and DNA damage in the ageing human brain. *Nature* 2004;429:883-91.
- [56] Lin MT, Beal MF. Mitochondrial dysfunction and oxidative stress in neurodegenerative diseases. *Nature* 2006;443:787-95.
- [57] Fu YT, He FS, Zhang SL, Zhang JS. Lipid peroxidation in rats intoxicated with 3-nitropropionic acid. *Toxicon* 1995;33:327-31.
- [58] Fontaine MA, Geddes JW, Banks A, Butterfield DA. Effect of exogenous and endogenous antioxidants on 3-nitropropionic acid-induced in vivo oxidative stress and striatal lesions: insights into Huntington's disease. *J Neurochem* 2000;75:1709-15.
- [59] Binienda Z, Simmons C, Hussain S, Slikker Jr W, Ali SF. Effect of acute exposure to 3-nitropropionic acid on activities of endogenous antioxidants in the rat brain. *Neurosci Lett* 1998;251:173-6.

- [60] Zhang JQ, Shen M, Zhu CC, et al. 3-Nitropropionic acid induces ovarian oxidative stress and impairs follicle in mouse. *PLoS One* 2014;9:e86589.
- [61] Klivenyi P, Andreassen OA, Ferrante RJ, et al. Mice deficient in cellular glutathione peroxidase show increased vulnerability to malonate, 3-nitropropionic acid, and 1-methyl-4-phenyl-1,2,5,6-tetrahydropyridine. *J Neurosci* 2000;20:1-7.
- [62] Salvi F, Agniswamy J, Yuan H, et al. The combined structural and kinetic characterization of a bacterial nitronate monooxygenase from *Pseudomonas aeruginosa* PAO1 establishes NMO class I and II. *J Biol Chem* 2014;289:23764-75.
- [63] Smitherman C, Gadda G. Evidence for a transient peroxy-nitro acid in the reaction catalyzed by nitronate monooxygenase with propionate 3-nitronate. *Biochemistry* 2013;52:2694-704.
- [64] Gadda G, Francis K. Nitronate monooxygenase, a model for anionic flavin semiquinone intermediates in oxidative catalysis. *Arch Biochem Biophys* 2010;493:53-61.
- [65] Porter DJ, Bright HJ. Mechanism of oxidation of nitroethane by glucose oxidase. *J Biol Chem* 1977;252:4361-70.
- [66] Kido T, Soda K. Oxidation of anionic nitroalkanes by flavoenzymes, and participation of superoxide anion in the catalysis. *Arch Biochem Biophys* 1984;234:468-75.
- [67] Kuo CF, Fridovich I. Free-radical chain oxidation of 2-nitropropane initiated and propagated by superoxide. *Biochem J* 1986;237:505-10.
- [68] Alexi T, Hughes PE, Faull RLM, Williams CE. 3 - Nitropropionic acid's lethal triplet: cooperative pathways of neurodegeneration. *Neuroreport* 1998;9:R57-R64.
- [69] Sato S, Gobbel GT, Honkaniemi J, et al. Apoptosis in the striatum of rats following intraperitoneal injection of 3-nitropropionic acid. *Brain Res* 1997;745:343-7.
- [70] Beal MF, Brouillet E, Jenkins BG, et al. Neurochemical and histologic characterization of striatal excitotoxic lesions produced by the mitochondrial toxin 3-nitropropionic acid. *J Neurosci* 1993;13:4181-92.
- [71] Ludolph AC, He F, Spencer PS, Hammerstad J, Sabri M. 3-Nitropropionic acid-exogenous animal neurotoxin and possible human striatal toxin. *Can J Neurol Sci* 1991;18:492-8.
- [72] Riepe M, Hori N, Ludolph AC, Carpenter DO, Spencer PS, Allen CN. Inhibition of energy metabolism by 3-nitropropionic acid activates ATP-sensitive potassium channels. *Brain Res* 1992;586:61-6.
- [73] Novelli A, Reilly JA, Lysko PG, Henneberry RC. Glutamate becomes neurotoxic via the N-methyl-D-aspartate receptor when intracellular energy levels are reduced. *Brain Res* 1988;451:205-12.
- [74] Zeevalk GD, Nicklas WJ. Chemically induced hypoglycemia and anoxia: relationship to glutamate receptor-mediated toxicity in retina. *J Pharmacol Exp Ther* 1990;253:1285-92.
- [75] Milnerwood AJ, Gladding CM, Pouladi MA, et al. Early increase in extrasynaptic NMDA receptor signaling and expression contributes to phenotype onset in Huntington's disease mice. *Neuron* 2010;65:178-90.
- [76] Blandini F, Porter RH, Greenamyre JT. Glutamate and Parkinson's disease. *Mol Neurobiol* 1996;12:73-94.
- [77] Rego AC, Oliveira CR. Mitochondrial dysfunction and reactive oxygen species in excitotoxicity and apoptosis: implications for the pathogenesis of neurodegenerative diseases. *Neurochem Res* 2003;28:1563-74.
- [78] Sattler R, Tymianski M. Molecular mechanisms of calcium-dependent excitotoxicity. *J Mol Med* 2000;78:3-13.

- [79] Maciel EN, Vercesi AE, Castilho RF. Oxidative stress in Ca(2+)-induced membrane permeability transition in brain mitochondria. *J Neurochem* 2001;79:1237-45.
- [80] Gunter TE, Pfeiffer DR. Mechanisms by which mitochondria transport calcium. *Am J Physiol* 1990;258:C755-86.
- [81] Smaili SS, Hsu Y-T, Youle RJ, Russell JT. Mitochondria in Ca²⁺ signaling and apoptosis. *J Bioenerg Biomembr* 2000;32:35-46.
- [82] Kowaltowski AJ, Castilho RF, Vercesi AE. Mitochondrial permeability transition and oxidative stress. *FEBS Letters* 2001;495:12-5.
- [83] Zoratti M, Szabo I. The mitochondrial permeability transition. *Biochim Biophys Acta* 1995;1241:139-76.
- [84] Green DR, Reed JC. Mitochondria and apoptosis. *Science* 1998;281:1309-12.
- [85] Kroemer G, Dallaporta B, Resche-Rigon M. The mitochondrial death/life regulator in apoptosis and necrosis. *Annu Rev Physiol* 1998;60:619-42.
- [86] Hylin JW, Matsumoto H. The biosynthesis of 3-nitropropanoic acid by *Penicillium atrovenerum*. *Arch Biochem Biophys* 1961;93:542-5.
- [87] Shaw PD. Biosynthesis of nitro compounds. III. The enzymatic reduction of β -nitroacrylic acid to β -nitropropionic acid. *Biochemistry* 1967;6:2253-60.
- [88] Shaw PD, McCloskey JA. Biosynthesis of nitro compounds. II. Studies on potential precursors for the nitro group of β -nitropropionic acid. *Biochemistry* 1967;6:2247-53.
- [89] Baxter RL, Abbot EM, Greenwood SL, McFarlane IJ. Conservation of the carbon-nitrogen bond of aspartic acid in the biosynthesis of 3-nitropropanoic acid. *J Chem Soc, Chem Commun* 1985:564-6.
- [90] Birkinshaw JH, Dryland AML. Studies in the biochemistry of micro-organisms. 116. Biosynthesis of β -nitropropionic acid by the mould *Penicillium atrovenerum* G. Smith. *Biochem J* 1964;93:478-87.
- [91] Alston TA, Porter DJT, Bright HJ. The bioorganic chemistry of the nitroalkyl group. *Bioorg Chem* 1985;13:375-403.
- [92] Candlish E, La Croix LJ, Unrau AM. Biosynthesis of 3-nitropropionic acid in creeping indigo (*Indigofera spicata*). *Biochemistry* 1969;8:182-6.
- [93] Becker T, Pasteels J, Weigel C, Dahse HM, Voigt K, Boland W. A tale of four kingdoms - isoxazolin-5-one- and 3-nitropropanoic acid-derived natural products. *Nat Prod Rep* 2017;34:343-60.
- [94] Laurent P, Braekman J-C, Daloze D, Pasteels J. Biosynthesis of defensive compounds from beetles and ants. *Eur J Org Chem* 2003;2003:2733-43.
- [95] Becker T, Ploss K, Boland W. Biosynthesis of isoxazolin-5-one and 3-nitropropanoic acid containing glucosides in juvenile *Chrysomelina*. *Org Biomol Chem* 2016;14:6274-80.
- [96] Nishino SF, Shin KA, Payne RB, Spain JC. Growth of bacteria on 3-nitropropionic acid as a sole source of carbon, nitrogen, and energy. *Appl Environ Microbiol* 2010;76:3590-8.
- [97] Mijatovic S, Gadda G. Oxidation of alkyl nitronates catalyzed by 2-nitropropane dioxygenase from *Hansenula mrakii*. *Arch Biochem Biophys* 2008;473:61-8.
- [98] Hipkin CR, Salem MA, Simpson D, Wainwright SJ. 3-nitropropionic acid oxidase from horseshoe vetch (*Hippocrepis comosa*): a novel plant enzyme. *Biochem J* 1999;340 (Pt 2):491-5.
- [99] Francis K, Gadda G. The nonoxidative conversion of nitroethane to ethylnitronate in *Neurospora crassa* 2-nitropropane dioxygenase is catalyzed by histidine 196. *Biochemistry* 2008;47:9136-44.

- [100] Francis K, Gadda G. Kinetic evidence for an anion binding pocket in the active site of nitronate monooxygenase. *Bioorg Chem* 2009;37:167-72.
- [101] Majak W, Cheng KJ. Identification of rumen bacteria that anaerobically degrade aliphatic nitrotoxins. *Can J Microbiol* 1981;27:646-50.
- [102] Novoselov A, Becker T, Pauls G, von Reuss SH, Boland W. *Spodoptera littoralis* detoxifies neurotoxic 3-nitropropanoic acid by conjugation with amino acids. *Insect Biochem Mol Biol* 2015;63:97-103.

2 CHAPTER 2: CRYSTAL STRUCTURE OF YEAST NITRONATE MONOOXYGENASE FROM *CYBERLINDNERA SATURNUS*

(This chapter has been published verbatim in Agniswamy, J., Reis, R.A.G., Wang, Y.F., Smitherman, C., Su, D., Weber, I., and Gadda, G. (2018) *Proteins* 86: 599-605. The author's contribution involves determination of steady-state kinetic parameters of NMOs in the presence of PEG and structural comparison of two NMOs.)

2.1 Abstract

Nitronate monooxygenase (NMO) is an FMN-dependent enzyme that oxidizes the neurotoxin propionate 3-nitronate (P3N) and represents the best-known system for P3N detoxification in different organisms. The crystal structure of the first eukaryotic Class I NMO from *Cyberlindnera saturnus* (*Cs*NMO) has been solved at 1.65 Å resolution and refined to an R-factor of 14.0%. The three-dimensional structures of yeast *Cs*NMO and bacterial *Pa*NMO are highly conserved with the exception of three additional loops on the surface in the *Cs*NMO enzyme and differences in four active sites residues. A PEG molecule was identified in the structure and formed extensive interactions with *Cs*NMO, suggesting a specific binding site; however, 8% PEG showed no significant effect on the enzyme activity. This new crystal structure of a eukaryotic NMO provides insight into the function of this class of enzymes.

2.2 Introduction

Propionate 3-nitronate (P3N) is a toxic nitro acid compound commonly found in ester glucosides in legumes¹, fungi²⁻⁶, and leaf beetles⁷⁻⁹. Upon hydrolysis by glucosidases P3N is released from the esters and exists in a pH-dependent equilibrium with 3-nitropropionic acid (3-NPA)^{2, 10}. The toxin acts as a potent irreversible inhibitor of mitochondrial succinate dehydrogenase¹¹⁻¹³. Inhibition of succinate dehydrogenase, which is a key enzyme of both the Krebs cycle and the oxidative phosphorylation pathway, compromises the energetic metabolism

in cells and leads to a variety of neurological disorders in livestock and humans and even death at sufficiently high concentrations¹⁴. Based on the observation that P3N is found in plant shoots and leaves but not in roots, the compound has been proposed to act as a defensive mechanism against herbivores¹. In small amounts (i.e., 20 mg/kg), P3N is used in laboratories to poison mitochondria in animal models, such as rats¹⁵, macaques and baboons¹⁶, to induce symptoms that mimic Huntington's disease for the development and testing of potential treatments^{11-15, 17-20}.

Several P3N-producing bacteria, fungi, and plants, have developed enzymes that metabolize P3N as a self-protection mechanism¹⁴. The most well-known system for P3N detoxification is represented by nitronate monooxygenases (NMO, E.C. 1.13.12.16). NMOs are FMN-dependent enzymes that quickly and efficiently catalyze the oxidation of P3N, with k_{cat} values $\geq 800 \text{ s}^{-1}$ and $k_{\text{cat}}/K_{\text{m}}$ values $\geq 10^6 \text{ M}^{-1}\text{s}^{-1}$ at atmospheric oxygen and pH 7.5^{14, 21-23}. NMOs also oxidize alkyl nitronates of various lengths, although with lower catalytic efficiency as compared to P3N²⁰⁻²³. Two classes of NMOs were recently established based on a bioinformatics, mechanistic, and structural study on the NMO from the prokaryote *Pseudomonas aeruginosa* (*Pa*NMO)²². Class I NMOs, are defined by the presence of four consensus structural motifs and contain approximately 450 NMO gene products from primarily bacteria and fungi, and two from animals²². Enzymes in Class I oxidize exclusively P3N and its nitronate analogues, but not 3-NPA and the nitroalkane analogues²². Class II NMOs, a smaller group consisting of ten fungal gene products²², contain only parts of the motifs identified in Class I NMO. Class II oxidizes both nitronates and nitroalkanes²⁴, although the latter with lower efficiency. Biochemical studies on Class II NMO are limited to the *Neurospora crassa* enzyme using nitronates and nitroalkane analogues^{21, 22}. In regards to Class I NMOs, mechanistic studies with P3N as a substrate are available for the eukaryotic *Cs*NMO from the yeast *Cyberlindnera saturnus*. The enzyme

mechanism has been investigated using steady-state kinetics, solvent viscosity effects, pH effects, rapid reaction kinetics, and time-resolved absorption spectroscopy²³. The enzymatic mechanism is initiated by a single electron transfer from P3N to the enzyme-bound flavin, yielding an enzyme-bound flavosemiquinone, which is then oxidized by dioxygen to form superoxide. The superoxide and P3N radical react in the active site of the enzyme to form 3-peroxy-3-nitro-propanoate, which subsequently decays to products. Alternatively, the peroxy-nitro acid can arise from the reaction of radical P3N with the superoxide formed in the reduction of dioxygen by the flavosemiquinone²³. While there is no three-dimensional structure currently available for the eukaryotic *CsNMO*, a structure of the prokaryotic Class I *PaNMO* to a resolution of 1.44 Å has been recently solved²². However, due to an amino acid sequence identity of 34% shared by the *CsNMO* and *PaNMO* enzymes, correlations of the available structural and mechanistic data are limited and should be exerted with caution because the two enzymes may have significant structural differences.

In the present study, the crystal structure of *CsNMO* was solved to 1.65 Å resolution, demonstrating an overall fold similar to that of bacterial *PaNMO*, conservation of most of the active site residues and some differences in surface loops. The structure of *CsNMO* revealed a PEG molecule neatly bound on the surface of the enzyme. The new structural information for the fungal NMO can be combined with the detailed enzymatic characterization to build a full picture at a molecular level of NMO function.

2.3 Materials and Methods

Materials. 3-Nitropropionic acid was from Sigma-Aldrich (St. Louis, MO). Similar to primary and secondary nitroalkanes, the α -carbon atom of 3-nitropropionic acid has a pK_a value of 9.1 and undergoes slow deprotonation with a strong base². P3N, the conjugate base of 3-nitropropionic acid, was thus prepared in water by incubating the nitro compound with a 2.2 molar

excess of KOH for 24 h at 4 °C, as previously described²³. Addition of KOH was slow to avoid sample boiling and possible decomposition of P3N, which was then used within a week. Crystallography trays, cover slips, and supplies used for the crystallization of the enzyme were purchased from Hampton Research (Aliso Viejo, CA). All other reagents were of the highest purity commercially available.

Recombinant Protein Production. Recombinant CsNMO from *C. saturnus* was obtained through expression and purification methods previously described²⁵.

Crystallization. The recombinant CsNMO was dialyzed against 50 mM potassium pyrophosphate, pH 7.4, and concentrated to 5 mg mL⁻¹. The enzyme concentration was estimated based on the molar extinction coefficient of the enzyme-bound FMN²⁵. Crystals were grown at room temperature in hanging drops using 2:2 μL protein to reservoir, equilibrated against 500 μL reservoir solution. Yellow crystals were obtained in presence of 21% (w/v) PEG 3350, 70 mM sodium citrate at pH 4.0 and 100 mM ammonium acetate within 5 days.

Data Collection and Processing. The crystals were cryo-cooled in the mother liquor with 25% (v/v) glycerol. X-ray diffraction data were collected at 100 K on beamline X4A of the National Synchrotron Light Source at Brookhaven National Laboratory. The data were collected for 262° with an oscillation angle of 1° per frame. The X-ray data were integrated and scaled with HKL2000²⁶. The crystal was solved in space group $P2_1$ with unit cell dimensions of $a = 44.82$, $b = 68.43$, $c = 58.37$ Å. The Matthews coefficient calculated with the CCP4i suite²⁷ suggested one monomer in the asymmetric unit.

Structure Determination. The structure of yeast CsNMO was solved by molecular replacement employing PHASER^{28, 29} and using the coordinates of bacterial PaNMO (PDB ID: 4Q4K)²², which has a sequence identity of 34% with CsNMO, as the initial search model.

Successful structure solution of CsNMO by molecular replacement was obtained by pruning the six N-terminal residues and the five C-terminal residues of PaNMO, and substituting serine for the dissimilar amino acids in the bacterial PaNMO sequence compared with the CsNMO sequence. The CsNMO structure model was constructed from the molecular replacement phases using the Arp/wArp^{30, 31} program, which fitted 90% of the sequence into the electron density map. The model was subjected to several rounds of refinement in REFMAC³² with manual map inspection and model building performed in COOT³³. Solvent molecules were inserted at stereochemically reasonable positions in peaks of $2F_o-F_c$ and F_o-F_c maps contoured at 1 and 3 sigma (σ) levels, respectively. The final R_{work} and R_{free} values were 14.0 % and 17.9 % for the refined structure. All structural figures were produced using PyMol (www.pymol.org). Refined atomic coordinates and experimental structure factors have been deposited in the Protein Data Bank (PDB entry 6BKA).

Effect of PEG 3350 on the Apparent Steady-state Kinetic Parameters of Yeast CsNMO with P3N. Enzymatic assays were carried out using a computer-interfaced Oxy-32 oxygen-monitoring system (Hansatech Instruments, Inc., Norfolk, England) by monitoring the initial rates of oxygen consumption. Apparent steady-state kinetic parameters of CsNMO with P3N as substrate (0.03-0.80 mM) were measured in the absence of PEG 3350 and in presence of 8% PEG 3350 in 50 mM sodium phosphate, pH 7.5 and 30 °C, at atmospheric oxygen (i.e., 0.23 mM O₂). Solution of PEG 3350 was prepared in water just prior to use. Initial rates of the reactions were calculated based on the concentration of enzyme-bound flavin using previously determined extinction coefficients: $\epsilon_{446nm} = 13,100 \text{ M}^{-1}\text{s}^{-1}$ for CsNMO²⁵. The enzyme was allowed to incubate in the oxygen electrode vessel with PEG 3350 for 30 s prior to the start of the enzymatic reaction by addition of P3N to the reaction mixture. Apparent steady-state kinetic data were fit with Sigmaplot (Systat. Software Inc. Richmond, CA, USA) software.

2.4 Results and Discussion

Overall Structure of Yeast CsNMO. Yeast CsNMO was crystallized in the monoclinic space group $P2_1$ with one molecule per asymmetric unit. The structure was refined to 1.65 Å with an R_{factor} of 14.0% and R_{free} value of 17.9%. The data collection and refinement statistics are reported in Table 1. The overall structure of CsNMO contained an FMN-binding domain (residues 1-79, 122-271 and 356-374), and a separate substrate-binding domain (residues 80-121 and 272-355) (Figure 2.1A). An FMN was present in the FMN-binding domain of CsNMO (Figure 2.1A). The N- and C-termini of the enzyme are positioned on the same side of FMN binding domain and are separated by 20.7 Å. The FMN-binding domain adopted a TIM barrel-fold, while the substrate-binding domain had 3 helices connected by loops (Figure 2.1A). The active site of CsNMO was located at a cleft formed by the FMN-binding domain and the substrate-binding domain. Residues M23, A24, N77, F79, Y119, H147, H197, Y321, Y325, and L348, line the active site surrounding the isoalloxazine ring of FMN (Figure 2.2).

Table 2.1 X-ray Diffraction Data Collection and Refinement Statistics

Data Collection	
Wavelength (Å)	1.1
Space group	P2 ₁
Unit cell parameters (Å, deg)	a = 44.82, b = 68.43, c = 58.37, β = 106.3
Number of molecules per asymmetric unit	1
Resolution range (Å)	50.0 – 1.65 (1.71-1.65) ^a
Total observations	198467
Unique reflections	39464
Completeness (%)	96.0 (72.6)
$\langle I/\sigma(I) \rangle$	18.3 (2.6)
R _{merge} (%)	7.8 (47.8)
Wilson B-factor (Å ²)	11
Refinement	
Refinement resolution range	50 – 1.65
R _{cryst} (%)	14.0
R _{free} (%)	17.9
RMS deviations from ideality	
Bond lengths (Å)	0.021
Angles (°)	2.1
Number of atoms	
Protein	3100
Water	273
Average B-factor (Å ²)	
Protein	18.3
Water	25.9
FMN	10.8
Glycerol	31.7
PEG	34.3
Ramachandran analyses	
Outliers (%)	0
Favored regions (%)	96
Allowed regions (%)	4

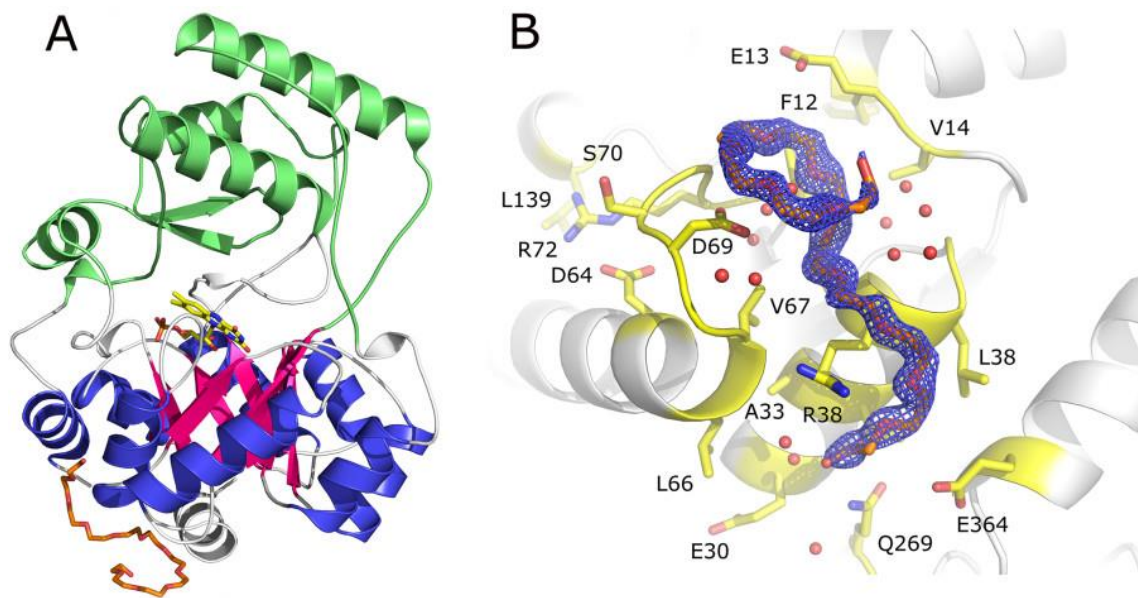


Figure 2.1 Structure of yeast CsNMO (PDB ID 6BKA). (A) Cartoon representation of the overall structure. A central barrel composed of eight parallel β strands illustrated in pink is surrounded by eight α -helices illustrated in blue. Stick representation of the prosthetic FMN group and PEG, carbon atoms are colored in yellow and orange, respectively. (B) PEG 3350 binding site in CsNMO (PDB ID 6BKA). Residues interacting with PEG in the binding pocket of CsNMO. Carbon atoms are colored in orange for PEG and in yellow for residues of CsNMO, and the water molecules interacting with PEG are shown as red spheres. The $2F_o-F_c$ electron density map of PEG contoured at 1.3σ is shown in blue.

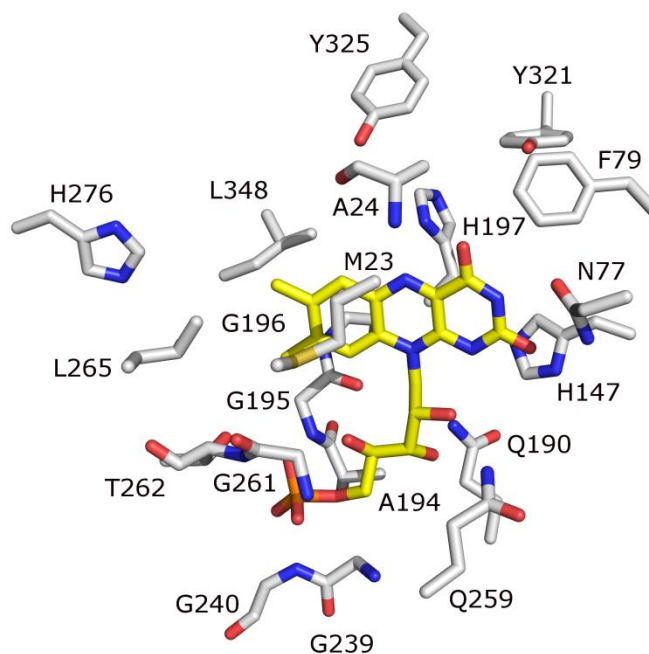


Figure 2.2 Close-up view of the FMN binding-site showing the residues around FMN. Protein side chains are displayed in sticks with carbon atoms colored in gray.

FMN Binding Site and Active Site Interactions. The phosphate group of FMN in *CsNMO* was buried deep within the FMN-binding domain and formed hydrogen bonds with the main chain amide groups of G240, G261, and T262 (Figure 2.2). In addition, the phosphate group of FMN also formed a hydrogen bond with the side chain hydroxyl group of T262 (Figure 2.2). The ribityl group of the cofactor was held in place by hydrogen bonds between the N ϵ 2 atom of Q190 and the O3' atom of FMN and the N ϵ 2 atom of Q259 and the O2' atom of FMN. The *si* face of the isoalloxazine ring was exposed to the substrate-binding cavity, whereas the *re* face formed a van der Waals contact with the C α atom of M23 (Figure 2.2). The isoalloxazine ring exhibited a butterfly bend of 169° along the C6-N5-C4 atoms. The N5 and O4 atoms of FMN had van der Waals contacts with the main chain amide group of A24 (Figure 2.2). H147 was located 3.9 Å from the N1 atom of the cofactor. The O2 and N3 atoms of FMN formed hydrogen bonds with the

side chain of N77, and the O4 atom participated in a hydrogen bond to the main chain amide of A24. L265 (5.3 Å) and H276 (7.7 Å) made the closest contacts with the C7 and C8 atoms of the isoalloxazine ring (Figure 2.2).

PEG-binding Site and Effect of PEG 3350 on Apparent Steady-state Kinetics. An extended PEG molecule from the crystallization solution was observed lying between a surface loop composed of residues 67-73 and a crevice composed of two helices in the FMN-binding domain of *CsNMO* (Figure 2.1B). The PEG molecule was separated by 21.6 Å from the FMN when measured at the closest distance, which was between the O1 atom of the PEG and the N5 atom of the flavin. The PEG polymer bound to the enzyme was composed of 11 ethylene units (Figure 2.1B). Six of the eleven ethylene units formed a helical turn around a central water molecule held in place through hydrogen bonding with the side chain of D69 (Figure 2.1B). The conformation of the protein loop defining the PEG-binding site was anchored by an ion pair of R72 and D64 and hydrogen bonding between the guanidinium group of R72 and the carbonyl oxygen atom of L139. The PEG molecule also formed additional interactions with side chain atoms of T34, R37, and D69. The PEG curls around the side chain of R37 forming a hydrogen bond with the guanidinium head of R37, while the side chains of T34, D69 and backbone carbonyl oxygen of R37 contacted PEG via water-mediated hydrogen bonds. In addition, the PEG molecule formed several van der Waals contacts with E13, T34, R37, D69, E364 while L38, V67, and I73 provide hydrophobic patches conducive for interactions with aliphatic segments of the bound PEG. The PEG molecule was bound at the interface between four symmetry-related subunits of *CsNMO*, as shown in Figure 2.3. In spite of the extensive interactions of PEG with one subunit of *CsNMO*, it has only four van der Waals contacts with symmetry-related subunits of the enzyme, suggesting that PEG binding is unlikely to be an artifact of crystal packing contacts. The steady state kinetics

parameters of CsNMO with P3N as a substrate were measured in the presence and absence of 8 % PEG, and showed similar $^{app}k_{cat}$ values of $610 \pm 50 \text{ s}^{-1}$ and $620 \pm 10 \text{ s}^{-1}$, and $^{app}K_m$ values of $70 \pm 20 \text{ }\mu\text{M}$ and $50 \pm 10 \text{ }\mu\text{M}$, respectively. Although PEG had no significant effect on enzyme catalysis, the observation of 12 ethylene units interacting with the enzyme suggest the presence of a putative binding site for an unknown molecule of similar structure. Polyethylene glycols used as precipitants during crystallization have been previously observed bound to substrate/ligand binding sites and allosteric sites of proteins. In the recently solved crystal structure of muscarinic acetylcholine M4 receptor, PEG 300, which was used as a precipitant in concentrations above 1M, was observed bound at the allosteric site of the inactive-state receptor³⁴. In attempts to derive the crystal structure of human type 5 17β -hydroxysteroid dehydrogenase in complex with its inhibitor EM1404, PEG 4000 used as precipitant was found bound at the substrate binding site³⁵. Similarly, in the crystal structure of odorant binding protein, AgamOBP1 from *A. gambiae mosquito*, PEG 8000 was found bound at a long binding site whose real ligand was unknown³⁶. Subsequent research led to the identification of indole as the ligand for AgamOBP1³⁷.

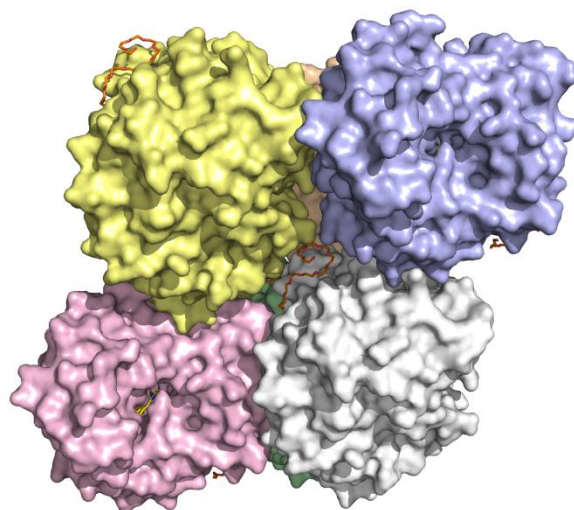


Figure 2.3 CsNMO crystal packing around PEG molecule.

Comparison of CsNMO with PaNMO. Previous studies have shown that yeast *CsNMO* and bacterial *PaNMO* are similar in terms of kinetic properties. When the steady-state kinetic parameters are compared, no differences on the $k_{\text{cat}}/K_{\text{P3N}}$ and $k_{\text{cat}}/K_{\text{oxygen}}$ values are observed (Table 2.2)^{22, 23}. The k_{cat} value for *CsNMO* is only 2-fold slower than the k_{cat} value for *PaNMO* (Table 2.2)^{22, 23}. Regarding the structural comparison, *CsNMO* and *PaNMO* can be superposed with a root mean square difference (RMSD) of 1.6 Å on 339 equivalent C α atoms using secondary structure matching³⁸ in CCP4i^{27, 39}. Hence, the overall structures of the two NMOs are similar despite an increase in length of 23 amino acids in *CsNMO*, i.e., 378 vs. 355 amino acids. The N-terminus of *CsNMO*, specifically, had a three-residue extension in comparison to *PaNMO*. Five other additions of two or more residues in surface loops of the FMN-binding domain of *CsNMO*, with the largest insertions of 3 to 7 amino acids occurring in the loops formed by residues 67-73, 124-131, and 224-234 (Figure 2.4). A PEG molecule is observed to be bound at one of these amino acids insertion sites in the FMN binding domain, the loop formed by residues 67-73. This loop

adopts a different conformation from the corresponding loop in *Pa*NMO and moves out by ~ 4.8 Å, facilitating the formation of the PEG binding groove (Figure 2.1B).

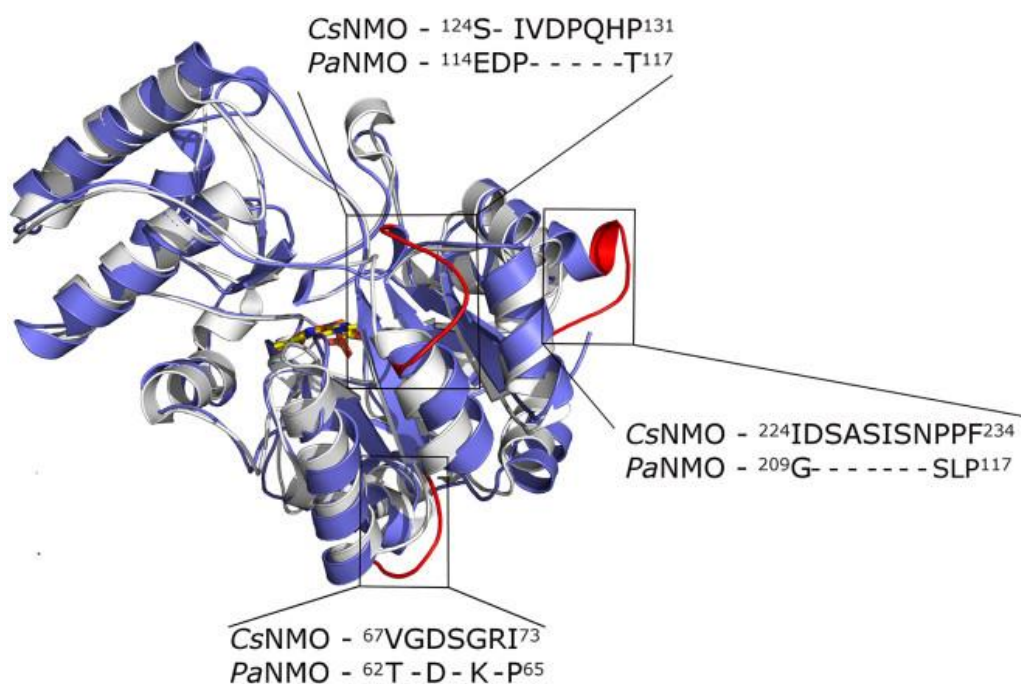


Figure 2.4 Comparison of the three-dimensional structure of CsNMO (light-blue, PDB ID 6BKA) with *Pa*NMO (gray, PDB ID 4Q4K). The boxes show the three surface loops highlighted in red in CsNMO that differ in the two enzymes, with loop 67-73 of CsNMO being the site of PEG binding to the enzyme. The amino acid sequences of the three loops are shown in boxes.

Table 2.2 Comparison of Steady-State Kinetic Parameters of CsNMO and PaNMO

Kinect Parameter	CsNMO^a	PaNMO^b
$k_{\text{cat}}, \text{s}^{-1}$	800 ± 100	1450 ± 10
$k_{\text{cat}} / K_{\text{P3N}}, \text{M}^{-1} \text{s}^{-1}$	$(10 \pm 1) \times 10^6$	$(10.8 \pm 0.2) \times 10^6$
$k_{\text{cat}} / K_{\text{oxygen}}, \text{M}^{-1} \text{s}^{-1}$	$(15 \pm 5) \times 10^6$	$(19.0 \pm 0.3) \times 10^6$

^aSteady-state parameters were measured at varying concentrations of both P3N and oxygen at 30°C. ^aNo pH effects on the steady-state kinetic parameters between pH 5.5 and 10.5 were observed (from ref 23). ^bThe assay was performed at pH 7.5 (from ref 22).

Residues M23, A24, N77, F79, H147, H197, L265, H276, Y321, Y325, and L348, line the active site surrounding the isoalloxazine ring of FMN, corresponding to residues M20, L21, N69, F71, H133, H183, V243, Y254, Y299, Y303, and W325 in bacterial *PaNMO*²² (Figure 2.5). The interaction of the phosphate and ribityl groups of FMN in *CsNMO* is identical to that of *PaNMO* but striking differences are observed in the residues interacting with the isoalloxazine head of FMN. Although the FMN of *CsNMO* has a slight bent along the C6-N5-C4, the angle is less acute than seen for FMN in *PaNMO*, i.e., 169° and 156°, respectively.

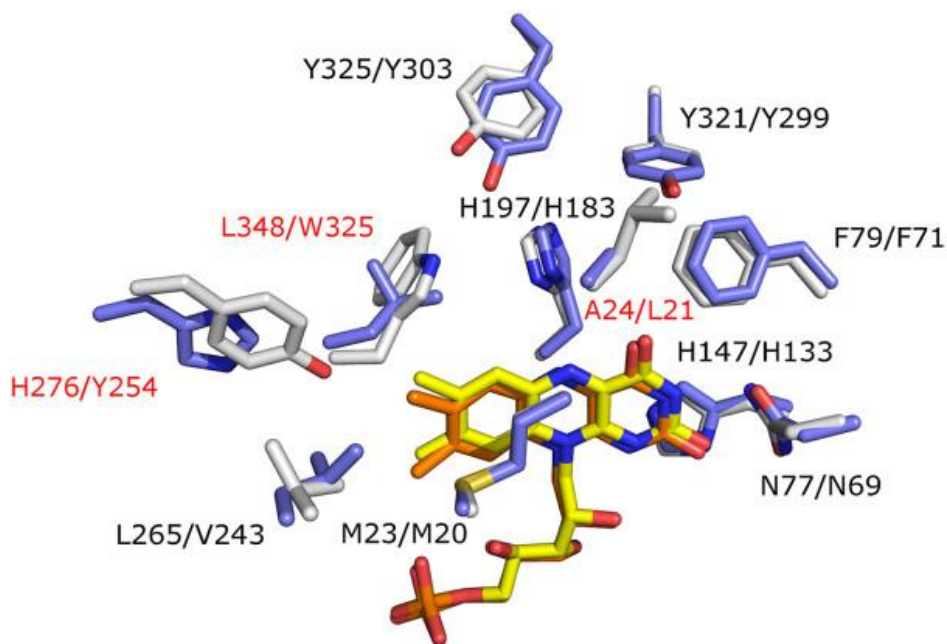


Figure 2.5 Comparison of the active site residues of *CsNMO* (blue with first residue in label) and *PaNMO* (gray with second residue in label). The significant changes are labeled in red.

As observed in *PaNMO*, the H147 in *CsNMO* is located 4 Å from the N1 atom of the cofactor. The presence of histidine in this location differs from about 20 other FMN-binding TIM barrel proteins where an arginine or lysine is present at 3 Å distance. The pH profile of the steady state kinetic parameters of *CsNMO* exhibits two orders of magnitude higher $k_{\text{cat}}/K_{\text{m}}$ and k_{cat} at acidic pH over alkaline pH with ethynitronate²³ which suggests the presence of positive charge in the active site. H147 in the proximity of the N1 atom is envisaged to enhance the catalysis in *CsNMO*. The O2 and N3 atoms of FMN form hydrogen bonding interactions with the side chain of N77. The O4 atom of FMN is hydrogen bonded to the main chain amide of A24. The interactions of O2, N3 and O4 of FMN in *CsNMO* are identical to those observed for *PaNMO*. However, the O4 of FMN in *CsNMO* is more accessible than in *CsNMO* due to the proximity of A24 instead of leucine in *PaNMO*. Except for A24, the interactions at the pyrimidine moiety of the isoalloxazine group of FMN in *CsNMO* are like those of *PaNMO*, however, major differences in interactions occur at the dimethylbenzene moiety of the flavin. The C7 atom of FMN in *PaNMO* has a C-

H...O (3.1Å) interaction with the side chain hydroxyl group of Y254 in *Pa*NMO. However, the corresponding residue in *Cs*NMO is H276, which has no contact with the C7 atom of FMN with the shortest interatomic distance of 7.7 Å (Figure 2.5). The C7 atom of FMN also interacts with hydrophobic residues W325 and V23 in *Pa*NMO, while these residues are replaced with the smaller residues L348 and A26 in *Cs*NMO. These substitutions result in loss of interactions and increased space around the C7 atom of FMN *Cs*NMO.

2.5 Conclusion

In the current study, the crystal structure of the first eukaryotic Class I NMO from the yeast *C. saturnus* has been resolved. Despite extensive characterization of the catalytic behavior of *Cs*NMO with P3N as a substrate, no three-dimensional structure was available previously for this enzyme. The new crystal structure gives information about the particularities of the eukaryotic enzyme that can be combined with the detailed enzymatic characterization available, allowing insights into functional difference between eukaryotic and prokaryotic NMOs.

The three-dimensional structures of yeast *Cs*NMO and bacterial *Pa*NMO are highly conserved. Three additional surface loops and differences in several active site residues in the *Cs*NMO enzyme may lead to functional differences between the eukaryotic and prokaryotic enzymes in Class I NMOs. A PEG molecule was identified on the surface of the yeast *Cs*NMO enzyme structure, suggesting the presence of a putative binding site for an unknown molecule of similar structure. No effect was observed in terms of the steady state kinetics parameters of *Cs*NMO in the presence of 8% of PEG. Further studies are needed to determine if this putative binding site is specific to yeast *Cs*NMO or occurs in other eukaryotic NMOs.

2.6 Acknowledgement

We thank Allen M. Orville for assistance with X-ray data collection at X12B, Brookhaven National Laboratory.

2.7 References

- [1] Hipkin, C. R., Simpson, D. J., Wainwright, S. J., and Salem, M. A. (2004) Nitrification by plants that also fix nitrogen, *Nature* 430, 98-101.
- [2] Bush, M. T., Touster, O., and Brockman, J. E. (1951) The production of beta-nitropropionic acid by a strain of *Aspergillus flavus*, *J Biol Chem* 188, 685-693.
- [3] Chomcheon, P., Wiyakrutta, S., Sriubolmas, N., Ngamrojanavanich, N., Isarangkul, D., and Kittakoop, P. (2005) 3-Nitropropionic acid (3-NPA), a potent antimycobacterial agent from endophytic fungi: is 3-NPA in some plants produced by endophytes?, *J Nat Prod* 68, 1103-1105.
- [4] Flores, A. C., Pamphile, J. A., Sarragiotto, M. H., and Clemente, E. (2013) Production of 3-nitropropionic acid by endophytic fungus *Phomopsis longicolla* isolated from *Trichilia elegans* A. JUSS ssp. *elegans* and evaluation of biological activity, *World J Microbiol Biotechnol* 29, 923-932.
- [5] Polonio, J. C., Ribeiro, M. A., Rhoden, S. A., Sarragiotto, M. H., Azevedo, J. L., and Pamphile, J. A. (2016) 3-Nitropropionic acid production by the endophytic *Diaporthe citri*: Molecular taxonomy, chemical characterization, and quantification under pH variation, *Fungal Biol* 120, 1600-1608.
- [6] Porter, D. J., and Bright, H. J. (1987) Propionate-3-nitronate oxidase from *Penicillium atrovenetum* is a flavoprotein which initiates the autoxidation of its substrate by O₂, *J Biol Chem* 262, 14428-14434.
- [7] Pauls, G., Becker, T., Rahfeld, P., Gretscher, R. R., Paetz, C., Pasteels, J., von Reuss, S. H., Burse, A., and Boland, W. (2016) Two Defensive Lines in Juvenile Leaf Beetles; Esters of 3-nitropropionic Acid in the Hemolymph and Aposematic Warning, *J Chem Ecol* 42, 240-248.
- [8] Rowell-Rahier, M., and Pasteels, J. M. (1986) Economics of chemical defense in chrysomelinae, *J Chem Ecol* 12, 1189-1203.
- [9] Randoux, T., Braekman, J. C., Daloze, D., and Pasteels, J. M. (1991) De novo biosynthesis of Delta(3)-Isoxazolin-5-one and 3-Nitropropanoic acid derivatives in *Chrysomela tremulae*, *Naturwissenschaften* 78, 313-314.
- [10] Smith, P. A. S. (1969) The Chemistry of the Nitro and Nitroso Groups. Part I. Edited by Henry Feuer, *Journal of the American Chemical Society* 91, 7789-7790.
- [11] Alston, T. A., Mela, L., and Bright, H. J. (1977) 3-Nitropropionate, the toxic substance of *Indigofera*, is a suicide inactivator of succinate dehydrogenase, *Proc Natl Acad Sci U S A* 74, 3767-3771.
- [12] Coles, C. J., Edmondson, D. E., and Singer, T. P. (1979) Inactivation of succinate dehydrogenase by 3-nitropropionate, *J Biol Chem* 254, 5161-5167.
- [13] Huang, L. S., Sun, G., Cobessi, D., Wang, A. C., Shen, J. T., Tung, E. Y., Anderson, V. E., and Berry, E. A. (2006) 3-nitropropionic acid is a suicide inhibitor of mitochondrial respiration that, upon oxidation by complex II, forms a covalent adduct with a catalytic base arginine in the active site of the enzyme, *J Biol Chem* 281, 5965-5972.

- [14] Francis, K., Smitherman, C., Nishino, S. F., Spain, J. C., and Gadda, G. (2013) The biochemistry of the metabolic poison propionate 3-nitronate and its conjugate acid, 3-nitropropionate, *IUBMB Life* 65, 759-768.
- [15] Beal, M. F., Brouillet, E., Jenkins, B. G., Ferrante, R. J., Kowall, N. W., Miller, J. M., Storey, E., Srivastava, R., Rosen, B. R., and Hyman, B. T. (1993) Neurochemical and histologic characterization of striatal excitotoxic lesions produced by the mitochondrial toxin 3-nitropropionic acid, *J Neurosci* 13, 4181-4192.
- [16] Brouillet, E., Hantraye, P., Ferrante, R. J., Dolan, R., Leroy-Willig, A., Kowall, N. W., and Beal, M. F. (1995) Chronic mitochondrial energy impairment produces selective striatal degeneration and abnormal choreiform movements in primates, *Proc Natl Acad Sci U S A* 92, 7105-7109.
- [17] Guyot, M. C., Hantraye, P., Dolan, R., Palfi, S., Maziere, M., and Brouillet, E. (1997) Quantifiable bradykinesia, gait abnormalities and Huntington's disease-like striatal lesions in rats chronically treated with 3-nitropropionic acid, *Neuroscience* 79, 45-56.
- [18] Tsang, T. M., Haselden, J. N., and Holmes, E. (2009) Metabonomic characterization of the 3-nitropropionic acid rat model of Huntington's disease, *Neurochem Res* 34, 1261-1271.
- [19] Parry, R., Nishino, S., and Spain, J. (2011) Naturally-occurring nitro compounds, *Nat Prod Rep* 28, 152-167.
- [20] Francis, K., Nishino, S. F., Spain, J. C., and Gadda, G. (2012) A novel activity for fungal nitronate monooxygenase: detoxification of the metabolic inhibitor propionate-3-nitronate, *Arch Biochem Biophys* 521, 84-89.
- [21] Gadda, G., and Francis, K. (2010) Nitronate monooxygenase, a model for anionic flavin semiquinone intermediates in oxidative catalysis, *Arch Biochem Biophys* 493, 53-61.
- [22] Salvi, F., Agniswamy, J., Yuan, H., Vercammen, K., Pelicaen, R., Cornelis, P., Spain, J. C., Weber, I. T., and Gadda, G. (2014) The combined structural and kinetic characterization of a bacterial nitronate monooxygenase from *Pseudomonas aeruginosa* PAO1 establishes NMO class I and II, *J Biol Chem* 289, 23764-23775.
- [23] Smitherman, C., and Gadda, G. (2013) Evidence for a transient peroxy-nitro acid in the reaction catalyzed by nitronate monooxygenase with propionate 3-nitronate, *Biochemistry* 52, 2694-2704.
- [24] Francis, K., and Gadda, G. (2006) Probing the chemical steps of nitroalkane oxidation catalyzed by 2-nitropropane dioxygenase with solvent viscosity, pH, and substrate kinetic isotope effects, *Biochemistry* 45, 13889-13898.
- [25] Mijatovic, S., and Gadda, G. (2008) Oxidation of alkyl nitronates catalyzed by 2-nitropropane dioxygenase from *Hansenula mrakii*, *Arch Biochem Biophys* 473, 61-68.
- [26] Otwinowski, Z., and Minor, W. (1997) Processing of X-ray diffraction data collected in oscillation mode, *Methods Enzymol* 276, 307-326.
- [27] Winn, M. D., Ballard, C. C., Cowtan, K. D., Dodson, E. J., Emsley, P., Evans, P. R., Keegan, R. M., Krissinel, E. B., Leslie, A. G., McCoy, A., McNicholas, S. J., Murshudov, G. N., Pannu, N. S., Potterton, E. A., Powell, H. R., Read, R. J., Vagin, A., and Wilson, K. S. (2011) Overview of the CCP4 suite and current developments, *Acta Crystallogr D Biol Crystallogr* 67, 235-242.
- [28] McCoy, A. J., Grosse-Kunstleve, R. W., Storoni, L. C., and Read, R. J. (2005) Likelihood-enhanced fast translation functions, *Acta Crystallogr D Biol Crystallogr* 61, 458-464.
- [29] Storoni, L. C., McCoy, A. J., and Read, R. J. (2004) Likelihood-enhanced fast rotation functions, *Acta Crystallogr D Biol Crystallogr* 60, 432-438.

- [30] Perrakis, A., Harkiolaki, M., Wilson, K. S., and Lamzin, V. S. (2001) ARP/wARP and molecular replacement, *Acta Crystallogr D Biol Crystallogr* 57, 1445-1450.
- [31] Perrakis, A., Morris, R., and Lamzin, V. S. (1999) Automated protein model building combined with iterative structure refinement, *Nat Struct Biol* 6, 458-463.
- [32] Murshudov, G. N., Vagin, A. A., and Dodson, E. J. (1997) Refinement of macromolecular structures by the maximum-likelihood method, *Acta Crystallogr D Biol Crystallogr* 53, 240-255.
- [33] Emsley, P., and Cowtan, K. (2004) Coot: model-building tools for molecular graphics, *Acta Crystallogr D Biol Crystallogr* 60, 2126-2132.
- [34] Thal, D. M., Sun, B., Feng, D., Nawaratne, V., Leach, K., Felder, C. C., Bures, M. G., Evans, D. A., Weis, W. I., Bachhawat, P., Kobilka, T. S., Sexton, P. M., Kobilka, B. K., and Christopoulos, A. (2016) Crystal structures of the M1 and M4 muscarinic acetylcholine receptors, *Nature* 531, 335-340.
- [35] Qiu, W., Zhou, M., Mazumdar, M., Azzi, A., Ghanmi, D., Luu-The, V., Labrie, F., and Lin, S. X. (2007) Structure-based inhibitor design for an enzyme that binds different steroids: a potent inhibitor for human type 5 β -hydroxysteroid dehydrogenase, *J Biol Chem* 282, 8368-8379.
- [36] Wogulis, M., Morgan, T., Ishida, Y., Leal, W. S., and Wilson, D. K. (2006) The crystal structure of an odorant binding protein from *Anopheles gambiae*: evidence for a common ligand release mechanism, *Biochem Biophys Res Commun* 339, 157-164.
- [37] Biessmann, H., Andronopoulou, E., Biessmann, M. R., Douris, V., Dimitratos, S. D., Eliopoulos, E., Guerin, P. M., Iatrou, K., Justice, R. W., Krober, T., Marinotti, O., Tsitoura, P., Woods, D. F., and Walter, M. F. (2010) The *Anopheles gambiae* odorant binding protein 1 (AgamOBP1) mediates indole recognition in the antennae of female mosquitoes, *PLoS One* 5, e9471.
- [38] Krissinel, E., and Henrick, K. (2004) Secondary-structure matching (SSM), a new tool for fast protein structure alignment in three dimensions, *Acta Crystallogr D Biol Crystallogr* 60, 2256-2268.
- [39] Potterton, E., Briggs, P., Turkenburg, M., and Dodson, E. (2003) A graphical user interface to the CCP4 program suite, *Acta Crystallogr D Biol Crystallogr* 59, 1131-1137.

3 CHAPTER 3: CHARACTERIZATION OF CONSERVED ACTIVE SITE RESIDUES IN CLASS I NITRONATE MONOOXYGENASE

(This chapter has been published verbatim in Su, D., Aguilon, C., and Gadda, G. (2019) *Archives and Biochemistry and Biophysics*. The author's contribution involves the preparation and purification of the variant enzymes, and determination of steady-state parameters.)

3.1 Abstract

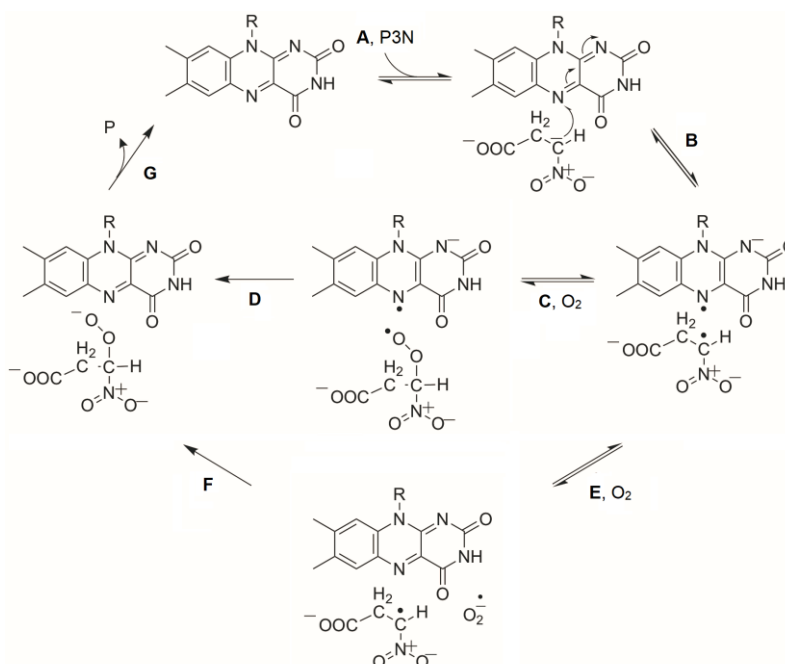
Propionate 3-nitronate (P3N) is a natural toxin that irreversibly inhibits mitochondrial succinate dehydrogenase. P3N poisoning leads to a variety of neurological disorders and even death. Nitronate monooxygenase (NMO) from *Pseudomonas aeruginosa* PAO1 was the first NMO characterized in bacteria and serves as a paradigm for Class I NMO. Here, we hypothesized that the carboxylate group of P3N might form a hydrogen bond with one or more of the four tyrosine or a lysine residues that are conserved in the active site of the enzyme. In the wild-type enzyme, the k_{cat} value was pH independent between pH 6.0 and 11.0, while the $k_{\text{cat}}/K_{\text{P3N}}$ value decreased at high pH, suggesting that a protonated group with a $\text{p}K_{\text{a}}$ value of 9.5 is required for binding the anionic substrate. A pH titration of the UV-visible absorption spectrum of the enzyme showed an increased absorbance at 297 nm with increasing pH, defining a $\text{p}K_{\text{a}}$ value of 9.5 and a $\Delta\epsilon_{297 \text{ nm}}$ of $2.4 \text{ M}^{-1}\text{cm}^{-1}$, consistent with a tyrosine being important for substrate binding. The N3 atom of the oxidized flavin, instead, did not ionize likely because its $\text{p}K_{\text{a}}$ was perturbed by the ionization of a tyrosine in the active site of the enzyme. The Y109F, Y254F, Y299F, Y303F, and K307M, substitutions had small effects (i.e., <3.5-fold) on the steady-state kinetic parameters of the enzyme. With all mutated enzymes, the $k_{\text{cat}}/K_{\text{P3N}}$ value was less than 2.5-fold different from the wild-type enzyme, suggesting that none of the residues is solely important for substrate binding.

3.2 Introduction

Nitronate monooxygenase (NMO, E.C. 1.13.12.16) is an FMN-dependent enzyme that uses molecular oxygen to oxidize propionate 3-nitronate (P3N)¹⁻⁴. P3N exists in equilibrium with 3-nitropropionic acid (3-NPA), which in plants^{5, 6}, fungi^{7, 8}, and insects^{9, 10}, is stored in a number of glycosidic esters and is released upon acidic hydrolysis^{6, 11}. P3N is a potent inhibitor of mitochondrial succinate dehydrogenase, resulting in ATP depletion and heightened oxidative stress^{11, 12}. Livestock and human intoxication by P3N manifest in foaming of the mouth, respiratory distress, neurological impairment, and often times death^{1, 13, 14}. Two classes of NMOs have been established using a combination of biochemical and structural analyses, and bioinformatics². Class I NMO includes ~500 enzymes from bacteria, fungi, and two animals, including a biochemically characterized prokaryotic NMO from *Pseudomonas aeruginosa* PAO1 (*Pa*NMO) and a eukaryotic NMO from *Cyberlindnera saturnus* (*Cs*NMO)^{2, 4}. Class II NMO comprises ~10 enzymes², and includes a biochemically characterized eukaryotic NMO from *Neurospora crassa* (*Nc*NMO)^{1, 15, 16}.

The enzymatic oxidation of P3N in Class I NMO begins with substrate binding (Step A in Scheme 3.1), followed by a single electron transfer from P3N to the enzyme-bound FMN (Step B), forming a P3N radical species and a flavin semiquinone^{2, 3}. *Pa*NMO is the only enzyme for which thermodynamic stabilization of both neutral and anionic semiquinones with a ratio that is pH-dependent has been demonstrated to date¹⁷. The P3N radical is proposed to react directly with molecular oxygen to generate a 3-peroxy-3-nitropropanoate radical (Step C). A subsequent electron transfer from the flavin semiquinone to the 3-peroxy-3-nitropropanoate radical gives 3-peroxy-3-nitropropanoate (Step D), which would decay to the products. Alternatively, the flavin semiquinone would donate an electron to molecular oxygen yielding superoxide anion (Step E),

which subsequently reacts with P3N radical to form 3-peroxy-3-nitropropanoate (Step F). Consistent with the reductive and oxidative half-reactions involving single electron transfers, the steady-state kinetic parameters $k_{\text{cat}}/K_{\text{P3N}}$ and $k_{\text{cat}}/K_{\text{O}_2}$ are unusually large for a flavin-dependent monooxygenase, with values in the 10^6 - 10^7 $\text{M}^{-1}\text{s}^{-1}$ range^{2, 3}. Enzyme turnover at saturating concentrations of P3N and oxygen is also fast with a k_{cat} value of $1,300$ s^{-1} at pH 7.5 and 30 $^\circ\text{C}$ ².³ The crystallographic structures of *Pa*NMO and *Cs*NMO have been solved previously to resolutions ≤ 1.65 Å ^{2, 4}, demonstrating a collection of fully conserved residues in the active site of the prokaryotic and eukaryotic enzymes. While the available structures provide a platform to hypothesize roles for active site residues, no mutagenesis studies have been reported to establish which amino acid residues participate in substrate binding and catalysis.



Scheme 3.1 Minimal reaction mechanism of PaNMO with P3N and O₂ as substrates.

In the active site of Class I NMO there are three fully conserved tyrosine residues, Y109, Y299, and Y303 (numbering for *Pa*NMO) (Figure 3.1). A fourth tyrosine is conserved in ~70% of the amino acid sequences, being replaced with a histidine in ~25% of the sequences and phenylalanine and tryptophan in the remaining cases. Another fully conserved residue in Class I NMO is K307, which is located at the entrance of the active site. It is conceivable that at least one or more of these residues participate as a hydrogen bond donor for binding the carboxylate group of the P3N substrate. Thus, we hypothesize that the individual replacement of a conserved active site tyrosine residue(s) with a phenylalanine or the lysine residue with methionine would negatively impact substrate binding. In this study, we have used mutagenesis, steady-state kinetics on the mutant enzymes, and pH effects on the steady-state kinetic parameters and the UV-visible absorption spectrum of the wild-type enzyme to establish which, if any, of the conserved amino acid residues in the active site of Class I NMO is important for binding the P3N substrate.

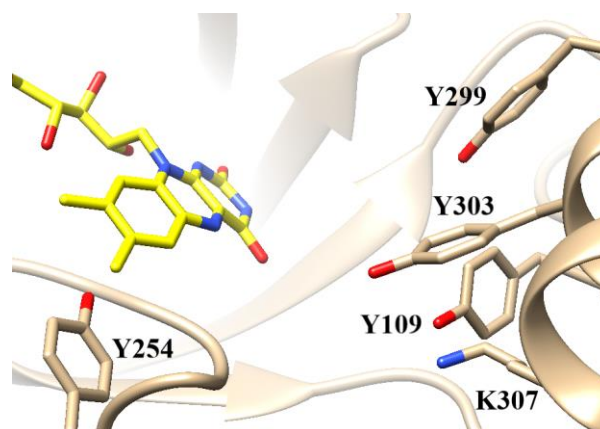


Figure 3.1 Conserved active site residues in *Pa*NMO (PDB entry 4Q4K). The carbon atoms of the FMN cofactor are shown as yellow sticks, whereas those of select protein residues are displayed as tan sticks; nitrogen and oxygen atoms are colored in blue and red, respectively.

3.3 Materials and Methods

Site-Directed Mutagenesis and Purification of PaNMO Variants. The genes for nitronate monooxygenase variants Y109F, Y254F, Y299F, Y303F, and K307M were prepared using the pET20b(+) plasmid harboring the wild-type gene PA4202 as a template and mutagenic primers containing the corresponding site mutation. Upon mutagenesis, the mutant genes were sequenced at Macrogen Inc (Rockville, MD). Plasmids were purified using kits from Qiagen Inc. (Valencia, CA). The constructs containing the correct mutation were transformed by heat shock into *Escherichia coli* strain Rosetta(DE3)pLysS competent cells for protein expression¹⁸. The expression and purification of NMO mutant enzymes Y109F, Y254F, Y299F, Y303F, and K307M, followed the protocol of wild-type enzyme as previously described².

Enzymatic Assays. 3-Nitropropionic acid was from Sigma-Aldrich (St. Louis, MO). Similar to primary and secondary nitroalkanes, the α -carbon atom of 3-nitropropionic acid has a pK_a value of 9.1 and undergoes slow deprotonation with a strong base¹⁹. P3N, the conjugate base of 3-nitropropionic acid, was thus prepared in water by incubating the nitro compound with a 2.2 molar excess of KOH for 24 h at 4 °C, as previously described^{2,3}. Addition of KOH was slow to avoid sample boiling and possible decomposition of P3N, which was then used within a week²⁰.

Enzymatic activity was measured by monitoring initial rates of oxygen consumption using a computer-interfaced Oxy-32 oxygen-monitoring system (Hansatech Instruments, Inc., Norfolk, England). The steady-state kinetic parameters for wild-type and variant enzymes were obtained by varying concentrations of P3N and oxygen. The experiment was carried out in the presence of 50 mM potassium phosphate at pH 8.0 and 30 °C. The assay reaction mixture was equilibrated with an O₂/N₂ gas mixture to reach a desired oxygen concentration for at least 5 min before initiating the reaction with the addition of enzyme then P3N. Since the second-order rate constants for

protonation of the nitronates are in the range $15\text{-}75\text{ M}^{-1}\text{s}^{-1}$ ^{21, 22}, enzymatic activity assays were initiated with the addition of the nitronate to the reaction mixture to ensure that a negligible amount of the neutral species of the nitronate was present during the time required to acquire initial rates of reaction (typically ~ 30 s). The pH dependence of the steady-state kinetic parameters of the wild-type enzyme were determined in 50 mM sodium pyrophosphate in the pH range between 6.0 and 11.0, with the exception of pH 8.0 where 50 mM sodium phosphate was used.

UV-visible Absorption Spectroscopy. UV-visible absorption spectra were recorded using an Agilent Technologies model HP 8453 PC diode-array spectrophotometer (Santa Clara, CA). The extinction coefficients of the enzyme-bound FMN for the variant enzymes were determined by heat denaturation ²³. The enzymes were passed through a PD-10 desalting column equilibrated with 50 mM potassium phosphate at pH 7.0, before heat denaturation at 100 °C for 30 or 40 min. The denatured protein was removed by centrifugation at $20,000 \times g$, and the concentration of released FMN was measured using a molar extinction coefficient $\epsilon_{450\text{ nm}}$ of $12,200\text{ M}^{-1}\text{ cm}^{-1}$ for free FMN ²⁴. The total protein concentration was determined by using the Bradford assay with bovine serum albumin as standard ²⁵. For the pH dependence of the UV-visible absorption spectrum, the wild-type enzyme was passed through a PD-10 desalting column equilibrated with 20 mM sodium phosphate and 20 mM sodium pyrophosphate, pH 7.8. A 2-mL enzyme solution with a concentration of enzyme-bound FMN of $10\text{ }\mu\text{M}$ was used to record the absorption spectra. Serial additions of 1-10 μL of 1 M NaOH were placed into the enzyme solution with a $10\text{ }\mu\text{L}$ syringe while stirring until the pH was incrementally changed to ~ 10.4 . After each careful and slow addition of the base the enzyme solution was let equilibrate until no changes in the pH value and absorbance were observed, which typically required 2-3 min.

Data Analysis. Steady-state kinetic data were fit using KaleidaGraph software (Synergy Software, Reading, PA) or Enzfitter (Biosoft, Cambridge, UK) software. When initial rates of reaction were determined at varying concentrations of P3N and oxygen, the kinetic data were fit to Eqs 1 and 2. Eq 1 is for a sequential steady-state kinetic mechanism where v_o represents the initial velocity, e is the concentration of the enzyme, k_{cat} is the first-order macroscopic rate constant for enzyme turnover at saturating concentration of both P3N and oxygen, K_{P3N} and K_{O_2} are the Michaelis constants for P3N and oxygen, respectively, and K_{ia} is a kinetic constant that accounts for the intersecting line pattern in the double reciprocal plot. Eq 2 represents a sequential steady-state kinetic mechanism of the type described by Eq 1 when K_{ia} is not significantly different from zero. Data for each variant enzyme were fit to both equations and the equation providing the best fit (R^2) was used to determine the kinetic parameters.

The pH dependence of the k_{cat}/K_{P3N} value for the wild-type enzyme was determined with Eq 3, which describes a pH profile with a limiting value (C) at low pH and a slope of -1 at high pH.

The pH dependence of the UV-visible absorption spectrum of the wild-type enzyme was fit to Eq 4, which describes a curve with one pK_a value and two limiting values at high pH (A) and low pH (B).

$$\frac{v_o}{e} = \frac{k_{cat} [P3N][O_2]}{K_{P3N}[O_2] + K_{O_2}[P3N] + [P3N][O_2] + K_{ia}K_{O_2}} \quad (1)$$

$$\frac{v_o}{e} = \frac{k_{cat} [P3N][O_2]}{K_{P3N}[O_2] + K_{O_2}[P3N] + [P3N][O_2]} \quad (2)$$

$$\log(k_{cat}/K_{P3N}) = \log\left(\frac{C}{1+10^{(pH-pK_a)}}\right) \quad (3)$$

$$Y = \frac{A+B \times 10^{(pK_a-pH)}}{1+10^{(pK_a-pH)}} \quad (4)$$

3.4 Results

Purification and Spectral Properties of PaNMO Variants. The mutated enzymes Y109F, Y254F, Y299F, Y303F, and K307M, were purified to high levels following the same protocol previously used for the wild-type enzyme ². The UV-visible absorption spectra of the variant enzymes showed the characteristic features of oxidized flavoproteins with maximal absorbance at ~370 nm and ~443 nm (Figure 3.2). All variant enzymes showed <10% differences in the absorption intensity at ~443 nm, and up to a 23%-increase in the absorption intensity at ~370 nm compared to the wild-type enzyme (Table 3.1). These changes agree well with an increase in the hydrophobicity of the protein environment surrounding the flavin introduced in the enzyme by the replacement of tyrosine and lysine with phenylalanine and methionine, respectively ²⁶. In all cases the FMN/protein stoichiometry was low, but comparable with that of the wild-type enzyme purified from heterologous expression in *E. coli* (Table 3.1).

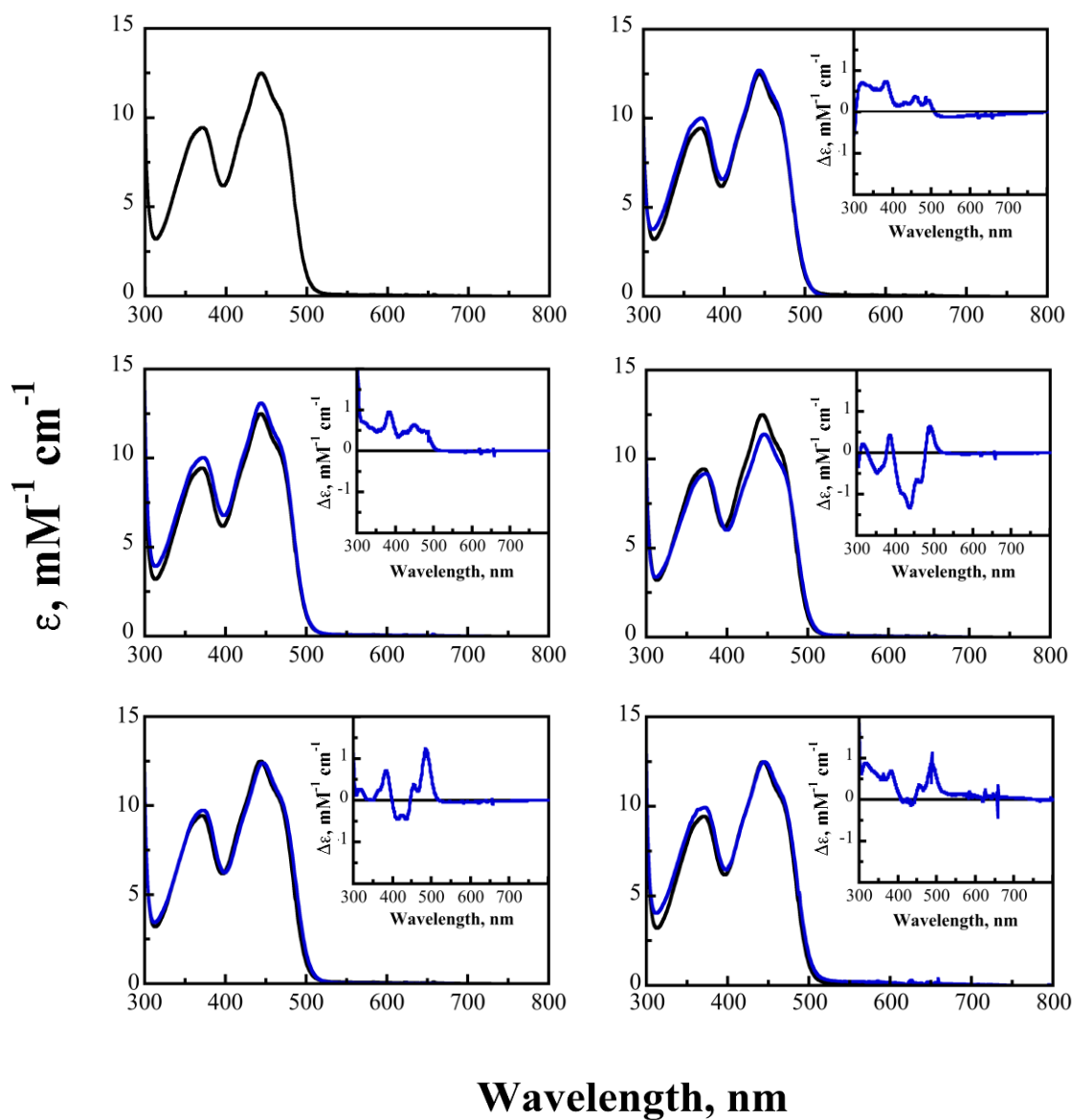


Figure 3.2 UV-visible absorption spectra of wild-type and mutated *PaNMO*. The UV-visible absorption spectra were recorded in 50 mM potassium phosphate, pH 8.0. Enzymes: wild-type (A), Y109F (B), Y254F (C), Y299F (D), Y303F (E), and K307M (F). Insets show the difference absorption spectra of variant enzyme minus the wild-type enzyme.

Table 3.1 UV-Visible Absorption Maxima and FMN/Protein Stoichiometry of Wild-Type and Mutated *Pa*NMO

	WT	Y109F	Y254F	Y299F	Y303F	K307M
^a λ_{\max} , nm	370, 443	371, 443	371, 443	372, 445	372, 446	370, 445
^a ϵ (mM ⁻¹ cm ⁻¹)	8.4, 12.5	10, 12.7	10.3, 13.1	9.1, 11.4	9.7, 12.4	10, 12.5
^b FMN/protein	0.25	0.21	0.17	0.16	0.16	0.14

^aSpectra were recorded in 50 mM potassium phosphate, pH 8.0 and 15 °C.

^bMolar ratio.

pH-Profiles of Steady-state Kinetic Parameters for Wild-type PaNMO. The pH dependence of the steady-state kinetic parameters of the wild-type enzyme was determined to establish possible ionizations of active site residues involved in substrate binding and the half-reactions catalyzed by the enzyme. To this end, initial rates of reaction were determined with an oxygen electrode at varying concentrations of both P3N and oxygen in the pH range from 6.0 to 11.0, as illustrated in the example of Figure 3.3A. At all pH values tested, the best fit of the steady-state kinetic data was obtained with Eq 2, consistent with a value for the K_{ia} constant being negligible when compared to the K_{P3N} and K_{O_2} values (Table 3.2). As shown in Figure 3.3B, the k_{cat} value was independent of pH with an average value of 1200 (± 200) s⁻¹, consistent with no ionizable groups being involved in kinetic steps that determine the overall turnover of the enzyme saturated with both substrates. The k_{cat}/K_{P3N} had a maximal value of 4.5×10^6 ($\pm 1 \times 10^6$) M⁻¹s⁻¹ up to pH 9.0 and decreased at higher pH values yielding a pK_a value of 9.5 (± 0.1), consistent with the requirement for a group to be protonated in the reductive half-reaction catalyzed by the enzyme (Figure 3.3B). In contrast, the k_{cat}/K_{O_2} value was pH-independent with an average value of 4.4×10^6 ($\pm 2.7 \times 10^6$) M⁻¹s⁻¹, consistent with absence of ionizable groups being relevant in the oxidative

half-reaction catalyzed by the enzyme (Figure 3.3B). The steady-state kinetic parameters of *Pa*NMO in the pH-independent region were comparable with those previously reported for eukaryotic *Cs*NMO, showing pH-independent values for $k_{\text{cat}} = 1,450 (\pm 10) \text{ s}^{-1}$, $k_{\text{cat}}/K_{\text{P3N}} = 10.8 \times 10^6 (\pm 0.2 \times 10^6) \text{ M}^{-1}\text{s}^{-1}$, and $k_{\text{cat}}/K_{\text{O}_2} = 19.0 \times 10^6 (\pm 0.3 \times 10^6) \text{ M}^{-1}\text{s}^{-1}$.

Table 3.2 Effects of pH on Steady-State Kinetic Parameters of Wild-Type *Pa*NMO

pH	$k_{\text{cat}}/K_{\text{P3N}}, \text{M}^{-1}\text{s}^{-1}$	$k_{\text{cat}}/K_{\text{O}_2}, \text{M}^{-1}\text{s}^{-1}$	$k_{\text{cat}}, \text{s}^{-1}$	$K_{\text{P3N}}, \text{mM}$	$K_{\text{O}_2}, \text{mM}$
6.0	$3.7 (\pm 0.5) \times 10^6$	$4.2 (\pm 0.6) \times 10^6$	1500 (± 20)	0.41 (± 0.01)	0.36 (± 0.01)
7.0	$4.2 (\pm 0.3) \times 10^6$	$5.2 (\pm 0.6) \times 10^6$	1300 (± 50)	0.31 (± 0.02)	0.25 (± 0.02)
8.0	$5.7 (\pm 0.5) \times 10^6$	$10.0 (\pm 1.2) \times 10^6$	1200 (± 100)	0.21 (± 0.01)	0.12 (± 0.01)
9.0	$3.0 (\pm 0.4) \times 10^6$	$3.0 (\pm 0.4) \times 10^6$	1100 (± 100)	0.37 (± 0.04)	0.37 (± 0.04)
10.0	$9.9 (\pm 0.1) \times 10^5$	$4.1 (\pm 0.2) \times 10^6$	820 (± 100)	0.83 (± 0.01)	0.20 (± 0.01)
10.5	$4.3 (\pm 1.9) \times 10^5$	$1.7 (\pm 0.9) \times 10^6$	1300 (± 400)	3.0 (± 1.0)	0.77 (± 0.36)
11.0	$1.2 (\pm 0.1) \times 10^5$	$2.8 (\pm 0.1) \times 10^6$	1200 (± 20)	9.7 (± 0.4)	0.43 (± 0.02)

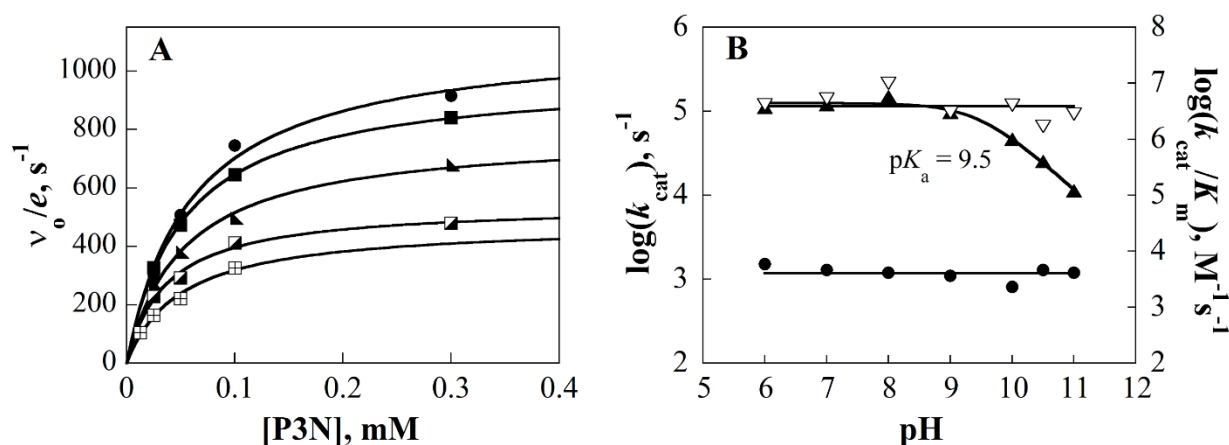


Figure 3.3 Effect of pH on the steady-state kinetic parameters of wild-type *Pa*NMO. (A) Initial rates of reaction with varying [P3N] and [oxygen] determined in 50 mM potassium phosphate, pH 8.0 and 30 °C. [Oxygen] were 28 (\square), 50 (\triangle), 88 (\blacktriangle), 145 (\blacksquare), and 241 (\bullet) μM . (B) pH-Profiles of the k_{cat} (\bullet), $k_{\text{cat}}/K_{\text{P3N}}$ (\blacktriangle), and $k_{\text{cat}}/K_{\text{O}_2}$ (∇) values. Data for the $k_{\text{cat}}/K_{\text{P3N}}$ value were fit Eq 3.

pH Effects on the UV-Visible Absorption Spectrum of Wild-Type *Pa*NMO. The N3 atom of flavin in the oxidized state or the side chain of one of the active site tyrosine residues could be

responsible for the pK_a of 9.5 seen in the pH-profile of the k_{cat}/K_{P3N} value. In either case the active site would acquire a negative charge that would hinder binding of the anionic substrate P3N, resulting in a decrease of the k_{cat}/K_{P3N} value. Both ionizations of flavin and tyrosine are associated with large spectral changes in the UV-visible absorption spectrum, with deprotonation of flavin yielding changes at ~ 490 nm^{27, 28} and tyrosine at ~ 300 nm^{29, 30}. Thus, the determination of the pH effects on the UV-visible absorption spectrum of wild-type *Pa*NMO is an effective tool to establish the nature of the group responsible for the pH effect on the observed k_{cat}/K_{P3N} value. As shown in Figure 3.4A, large spectral changes were seen in the near UV-region of the electromagnetic spectrum of the enzyme when the pH was incrementally raised from 7.8 to 10.4, whereas the visible region of the spectrum was not affected. The maximal spectral changes were centered at 297 nm as seen when the UV-visible absorption spectrum at pH 7.8 was used as a reference and the difference spectra were computed (Figure 3.4B). A plot of the $\Delta\epsilon_{297\text{ nm}}$ versus pH yielded a maximal spectral change $\Delta\epsilon_{297\text{ nm}}$ of $2.4 (\pm 0.1) \text{ M}^{-1}\text{cm}^{-1}$, consistent with deprotonation of a tyrosine residue²⁹. A pK_a value of $9.5 (\pm 0.1)$ could be determined, in perfect agreement with the pK_a value determined kinetically on the k_{cat}/K_{P3N} value.

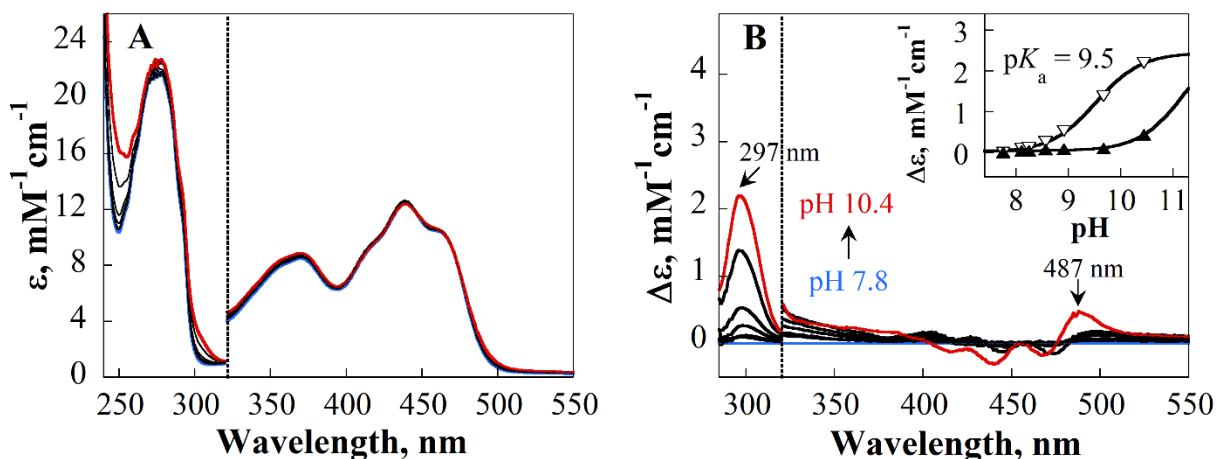


Figure 3.4 Effect of pH on the UV-visible absorption spectrum of wild-type *PaNMO* (A) Enzyme in the range from pH 7.8 (blue) to pH 10.4 (red). (B) Difference UV-visible absorption spectra between the species seen at higher pH values minus the species at pH 7.8. Inset: plot of the $\Delta\epsilon_{297\text{ nm}}$ (∇) and $\Delta\epsilon_{487\text{ nm}}$ (\blacktriangle) as a function of the pH; the curves are the fit of the data to Eq 4. The extinction coefficients for the protein absorption band at ≤ 320 nm were normalized with respect to the flavin absorption bands at ≥ 320 nm based on the experimentally determined FMN/enzyme stoichiometry of 0.25.

Steady-state Kinetic Parameters of *PaNMO* Variant Enzymes at pH 8.0. To characterize the effect of each mutation on substrate binding and catalysis during the oxidation of P3N catalyzed by *PaNMO*, the steady-state kinetic parameters of the variant enzymes were measured and compared to the wild-type enzyme. To avoid artifactual conclusions stemming from pH effects, pH 8.0 was chosen because the kinetic parameters of the wild-type enzyme determined in this study were pH-independent (Figure 3.3B). As for the case of the wild-type enzyme, the best fit of the kinetic data for the Y254F, Y303F, and K307M enzymes was obtained with Eq 2. Small, but not negligible, K_{ia} values were instead determined with the Y109F and Y299F enzymes (Table 3.3). With all variant enzymes, the k_{cat} values differed from the wild-type *PaNMO* by less than 1.5-fold, the k_{cat}/K_{P3N} values by less than 2.5-fold, and the k_{cat}/K_{O_2} values by less than 3-fold.

Table 3.3 *Steady-State Kinetic Parameters of Wild-Type and Mutated PaNMO at pH 8.0*

enzyme	$k_{\text{cat}}/K_{\text{P3N}}, \text{M}^{-1}\text{s}^{-1}$	$k_{\text{cat}}/K_{\text{O}_2}, \text{M}^{-1}\text{s}^{-1}$	$k_{\text{cat}}, \text{s}^{-1}$	$K_{\text{P3N}}, \text{mM}$	$K_{\text{O}_2}, \text{mM}$	K_{ia}, mM
WT	$5.7 (\pm 0.5) \times 10^6$	$10 (\pm 1) \times 10^6$	1200 (± 100)	0.21 (± 0.01)	0.12 (± 0.01)	-
Y109F	$14.0 (\pm 1.0) \times 10^6$	$14 (\pm 1) \times 10^6$	1400 (± 60)	0.10 (± 0.01)	0.10 (± 0.01)	0.02 (± 0.01)
Y299F	$8.6 (\pm 0.6) \times 10^6$	$32 (\pm 8) \times 10^6$	1300 (± 20)	0.15 (± 0.01)	0.04 (± 0.01)	0.10 (± 0.02)
Y303F	$8.8 (\pm 0.8) \times 10^6$	$14 (\pm 2) \times 10^6$	970 (± 10)	0.11 (± 0.01)	0.07 (± 0.01)	-
Y254F	$6.4 (\pm 0.4) \times 10^6$	$26 (\pm 6) \times 10^6$	1020 (± 10)	0.16 (± 0.01)	0.04 (± 0.01)	-
K307M	$2.4 (\pm 0.3) \times 10^6$	$13 (\pm 2) \times 10^6$	1900 (± 100)	0.8 (± 0.08)	0.15 (± 0.02)	-

3.5 Discussion

The active site of *PaNMO* contains a lysine and four tyrosine residues that are fully or highly conserved among ~500 sequences belonging to Class I NMO, suggesting that one or more of these residues may be important for substrate binding or catalysis. The mutagenesis and kinetic study presented here provides evidence demonstrating that the substrate can bind to the active site only when the side chains of the tyrosine residues are in the protonated rather than anionic state, but none of the conserved residues is solely essential for substrate binding. Furthermore, the reductive and oxidative half-reactions catalyzed by the enzyme are not affected by the individual substitution of the conserved tyrosine residues with phenylalanine or lysine with methionine, for which evidence is provided below.

The side chains of the tyrosine residues in the active site of *PaNMO* must be protonated for binding of the negatively charged P3N substrate. Evidence for this conclusion comes from the pH-profiles of the steady-state kinetic parameters and the UV-visible absorption spectrum of the wild-type enzyme. The group with a $\text{p}K_{\text{a}}$ value of 9.5 seen in the pH-profile of the $k_{\text{cat}}/K_{\text{P3N}}$ value must participate in substrate binding because the pH-profile of the k_{cat} value did not show ionization of any group between pH 6.0 and 11.0. This conclusion stems from the fact that while both kinetic parameters report on the kinetic step of flavin reduction from P3N, the $k_{\text{cat}}/K_{\text{P3N}}$ value also includes the reversible step of substrate binding yielding a Michaelis complex competent for

catalysis³¹. The participation of a tyrosine residue as being the group responsible for the pK_a of 9.5 comes from the pH-profile of the UV-visible absorption spectrum of the enzyme, showing an increase in absorbance in the 297 nm region of the electromagnetic spectrum that is indicative of the presence of tyrosinate at high pH values. The $\Delta\epsilon_{297\text{ nm}}$ value of $2.4\text{ M}^{-1}\text{cm}^{-1}$ seen in *Pa*NMO is consistent with deprotonation of a single tyrosine residue, as previously established for tyrosine in solution with a $\Delta\epsilon_{295\text{ nm}}$ value of $2.8\text{ mM}^{-1}\text{cm}^{-1}$ and in the active site of a ketosteroid isomerase D40N mutant with a $\Delta\epsilon_{295\text{ nm}}$ value of $2.6\text{ mM}^{-1}\text{cm}^{-1}$ ²⁹. We have made no attempts to determine which tyrosine residue is responsible for the pH effects seen in *Pa*NMO because in the confined space of the enzyme active site any of the four tyrosine residues would deprotonate irrespective of which single tyrosine to phenylalanine mutation would be tested. To our knowledge this is the first instance in which deprotonation of an active site tyrosine residue rather than the N3 atom of the oxidized flavin has been reported in a flavin-dependent enzyme. Many flavin-dependent enzymes have one or more tyrosine residues in the active site³²⁻³⁷. Because the absorption changes in the near-UV region of the electromagnetic spectrum attributable to tyrosine ionization are small with reference to the strong protein absorbance and the focus is typically on the visible region associated with the flavin, tyrosine ionizations may have been overlooked in previous studies.

The reductive half-reaction in which the enzyme-bound FMN is reduced to the semiquinone state through a single electron transfer from the P3N substrate is not affected by the individual replacement of any of the tyrosine residues with phenylalanine or the lysine with methionine. Evidence to support this conclusion comes from the comparison of the $k_{\text{cat}}/K_{\text{P3N}}$ values determined with P3N and oxygen as substrates for the wild-type and the mutant enzymes at pH 8.0. With the Y254F, Y299F, Y303F, and K307M, the $k_{\text{cat}}/K_{\text{P3N}}$ value was ≤ 2.5 -fold than in the wild-type enzyme. In contrast, replacement of Y109 with phenylalanine yielded a 2.5-fold increase

in the $k_{\text{cat}}/K_{\text{P3N}}$ value. When one considers the energetics associated with the changes in the $k_{\text{cat}}/K_{\text{P3N}}$ value, the mutant enzymes differ from the wild-type by ~ 0.1 kJ/mol or less, consistent with negligible contributions of the side chains of the lysine and tyrosine residues towards the capture of P3N into an enzyme-substrate complex that proceeds to catalysis. These data, in turn, indicate that none of the conserved lysine or tyrosine residues in the active site of the enzyme are essential for either substrate binding or the electron transfer reaction yielding the reduction of the flavin by P3N.

The oxidative half-reaction in which the enzyme-bound FMN is oxidized is not affected by the individual replacement of any of the tyrosine residues with phenylalanine or the lysine with methionine. This conclusion stems from the comparison of the $k_{\text{cat}}/K_{\text{O}_2}$ values determined with P3N and oxygen as substrates for the wild-type and the mutant enzymes at pH 8.0. With all mutant enzymes the $k_{\text{cat}}/K_{\text{O}_2}$ value is between 1.3- and 3.2-fold larger than in the wild-type enzyme, with values between $1.4 \times 10^7 \text{ M}^{-1}\text{s}^{-1}$ and $3.2 \times 10^7 \text{ M}^{-1}\text{s}^{-1}$. As for the case of the reductive half-reaction, the corresponding energetic contribution associated with the individual replacement of lysine with methionine or tyrosine with phenylalanine in the active site of the enzyme is negligible, with at the most the electron transfer that results in flavin oxidation being favored by a mere 0.2 kJ/mol in the mutant enzymes as compared to wild-type *PaNMO*.

3.5 Conclusion

In summary, the results presented in this study demonstrate that the tyrosine residues in the active site of *PaNMO* must be in the protonated form to allow binding of the anionic P3N substrate and catalysis. However, the replacement of any of the four tyrosine residues, i.e., Y109, Y254, Y299, and Y303, with phenylalanine or K307 with methionine does not affect substrate binding or the electron transfer reactions yielding the flavin-mediated oxidation of P3N with oxygen. Thus,

the compelling question of why these residues are conserved among ~500 proteins in the active site of Class I NMO remains unattended. One can speculate that because substrate oxidation in NMO does not involve a hydride transfer between NAD(P)H and the enzyme-bound flavin, the geometry and special arrangement of the reactive centers in the enzyme-substrate complex to allow electron transfer from P3N and flavin is less critical than in other flavin-dependent monooxygenases. Thus, having multiple hydroxyl groups in the active site would ensure P3N binding. Alternatively, it is possible that NMO might catalyze other biochemical reactions, besides the very efficient oxidation of P3N, and that the tyrosine and lysine residues have been conserved in the active site due to an unknown selective pressure. This study also offers the first example of a flavin-dependent enzyme in which tyrosine/tyrosinate equilibrium has been demonstrated spectroscopically in the active site of the enzyme, rather than the classical ionization of the N3 atom of the flavin at high pH values.

3.6 References

- [1] Francis, K., Gadda, G., The nonoxidative conversion of nitroethane to ethylnitronate in *Neurospora crassa* 2-nitropropane dioxygenase is catalyzed by histidine 196. *Biochemistry* 2008;47:9136-44.
- [2] Salvi, F., Agniswamy, J., Yuan, H., Vercammen, K., Pelicaen, R., Cornelis, P., Spain, J.C., Weber, I.T., Gadda, G., The combined structural and kinetic characterization of a bacterial nitronate monooxygenase from *Pseudomonas aeruginosa* PAO1 establishes NMO class I and II. *J. Biol. Chem.* 2014;289:23764-75.
- [3] Smitherman, C., Gadda, G., Evidence for a Transient Peroxynitro Acid in the Reaction Catalyzed by Nitronate Monooxygenase with Propionate 3-Nitronate. *Biochemistry* 2013;52:2694-704.
- [4] Agniswamy, J., Reis, R.A.G., Wang, Y.F., Smitherman, C., Su, D., Weber, I.T., Gadda, G., Crystal structure of yeast nitronate monooxygenase from *Cyberlindnera saturnus*. *Proteins* 2018;86:599-605.
- [5] Gorter, K., Hiptagin, a new glucoside from *Hiptage madablota*. *Bull. Jard. Bot. Buitenz.* 1920;2:187.
- [6] Hipkin, C.R., Simpson, D.J., Wainwright, S.J., Salem, M.A., Nitrification by plants that also fix nitrogen. *Nature* 2004;430:98.
- [7] Chomcheon, P., Wiyakrutta, S., Sriubolmas, N., Ngamrojanavanich, N., Isarangkul, D., Kittakoop, P., 3-Nitropropionic acid (3-NPA), a potent antimycobacterial agent from

- endophytic fungi: is 3-NPA in some plants produced by endophytes? *J. Nat. Prod.* 2005;68:1103-5.
- [8] Andolfi, A., Boari, A., Evidente, M., Cimmino, A., Vurro, M., Ash, G., Evidente, A., Gulpyrones A and B and Phomentrioloxins B and C Produced by *Diaporthe gulyae*, a Potential Mycoherbicide for Saffron Thistle (*Carthamus lanatus*). *J. Nat. Prod.* 2015;78:623-9.
- [9] Pasteels, J.M., Braekman, J.C., Daloz, D., Ottinger, R., Chemical defence in chrysomelid larvae and adults. *Tetrahedron* 1982;38:1891-7.
- [10] Randoux, T., Braekman, J.C., Daloz, D., Pasteels, J.M., De novo biosynthesis of Delta(3)-Isoxazolin-5-one and 3-Nitropropanoic acid derivatives in *Chrysomela tremulae*. *Naturwissenschaften* 1991;78:313-4.
- [11] Francis, K., Smitherman, C., Nishino, S.F., Spain, J.C., Gadda, G., The biochemistry of the metabolic poison propionate 3-nitronate and its conjugate acid, 3-nitropropionate. *IUBMB Life* 2013;65:759-68.
- [12] Brouillet, E., Jacquard, C., Bizat, N., Blum, D., 3-Nitropropionic acid: a mitochondrial toxin to uncover physiopathological mechanisms underlying striatal degeneration in Huntington's disease. *J. Neurochem.* 2005;95:1521-40.
- [13] Su, D., Gadda, G., 3-Nitropropionate in *Handbook of foodborne diseases*. Boca Raton: Taylor & Francis; 2019.
- [14] James, L.F., Hartley, W.J., Williams, M.C., Van Kampen, K.R., Field and experimental studies in cattle and sheep poisoned by nitro-bearing *Astragalus* or their toxins. *Am. J. Vet. Res.* 1980;41:377-82.
- [15] Francis, K., Nishino, S.F., Spain, J.C., Gadda, G., A novel activity for fungal nitronate monooxygenase: Detoxification of the metabolic inhibitor propionate-3-nitronate. *Arch. Biochem. Biophys.* 2012;521:84-9.
- [16] Francis, K., Russell, B., Gadda, G., Involvement of a flavosemiquinone in the enzymatic oxidation of nitroalkanes catalyzed by 2-nitropropane dioxygenase. *J. Biol. Chem.* 2005;280:5195-204.
- [17] Su, D., Kabir, M.P., Orozco-Gonzalez, Y., Gozem, S., Gadda, G., Fluorescence Properties of Flavin Semiquinone Radicals in Nitronate Monooxygenase. *ChemBioChem* 2019
- [18] Inoue, H., Nojima, H., Okayama, H., High efficiency transformation of *Escherichia coli* with plasmids. *Gene* 1990;96:23-8.
- [19] Bush, M.T., Touster, O., Brockman, J.E., The production of beta-nitropropionic acid by a strain of *Aspergillus flavus*. *J. Biol. Chem.* 1951;188:685-93.
- [20] Lewis, R.J., *Sax's Dangerous Properties of Industrial Materials*. 9th ed. New York: Van Nostrand Reinhold; 1996.
- [21] Goodall, D.M., Long, F.A., Protonation of nitroalkane anions by acetic acid in mixed water-deuterium oxide solvents. *J. Am. Chem. Soc.* 1968;90:238-43.
- [22] Nielsen, A.T., Nitronic acids and esters. In *the Chemistry of the Nitro and Nitroso Groups*. . New York: Interscience Publishers; 1969.
- [23] Aliverti, A., Curti, B., Vanoni, M.A., Identifying and quantitating FAD and FMN in simple and in iron-sulfur-containing flavoproteins. *Methods in molecular biology* (Clifton, NJ) 1999;131:9-23.
- [24] Whitby, L.G., A new method for preparing flavin-adenine dinucleotide. *Biochem. J.* 1953;54:437-42.
- [25] Bradford, M.M., A rapid and sensitive method for the quantitation of microgram quantities of protein utilizing the principle of protein-dye binding. *Anal. Biochem.* 1976;72:248-54.

- [26] Orozco-Gonzalez, Y., Kabir, M.P., Gozem, S., Electrostatic Spectral Tuning Maps for Biological Chromophores. *J. Phys. Chem.B* 2019.
- [27] Su, D., Yuan, H., Gadda, G., A Reversible, Charge-Induced Intramolecular C4a-S-Cysteinyl-Flavin in Choline Oxidase Variant S101C. *Biochemistry* 2017;56:6677-90.
- [28] Macheroux, P., Massey, V., Thiele, D.J., Volokita, M., Expression of spinach glycolate oxidase in *Saccharomyces cerevisiae*: purification and characterization. *Biochemistry* 1991;30:4612-9.
- [29] Schwans, J.P., Sunden, F., Gonzalez, A., Tsai, Y., Herschlag, D., Uncovering the determinants of a highly perturbed tyrosine pKa in the active site of ketosteroid isomerase. *Biochemistry* 2013;52:7840-55.
- [30] Latovitzki, N., Halper, J.P., Beychok, S., Spectrophotometric Titration of Tyrosine Residues in Human Lysozyme. *J. Biol. Chem.* 1971;246:1457-60.
- [31] Cleland, W.W., The kinetics of enzyme-catalyzed reactions with two or more substrates or products: I. Nomenclature and rate equations. *Biochim.Biophys. Acta. - Specialized Section on Enzymological Subjects* 1963;67:104-37.
- [32] Murray, M.S., Holmes, R.P., Lowther, W.T., Active site and loop 4 movements within human glycolate oxidase: implications for substrate specificity and drug design. *Biochemistry* 2008;47:2439-49.
- [33] Wohlfahrt, G., Witt, S., Hendle, J., Schomburg, D., Kalisz, H.M., Hecht, H.J., 1.8 and 1.9 Å resolution structures of the *Penicillium amagasakiense* and *Aspergillus niger* glucose oxidases as a basis for modelling substrate complexes. *Acta. Crystallogra. D* 1999;55:969-77.
- [34] Xia, Z.X., Mathews, F.S., Molecular structure of flavocytochrome b2 at 2.4 Å resolution. *J. Mol. Biol.* 1990;212:837-63.
- [35] Fu, G., Yuan, H., Li, C., Lu, C.D., Gadda, G., Weber, I.T., Conformational changes and substrate recognition in *Pseudomonas aeruginosa* D-arginine dehydrogenase. *Biochemistry* 2010;49:8535-45.
- [36] Sobrado, P., Fitzpatrick, P.F., Identification of Tyr413 as an active site residue in the flavoprotein tryptophan 2-monooxygenase and analysis of its contribution to catalysis. *Biochemistry* 2003;42:13833-8.
- [37] Schreuder, H.A., van der Laan, J.M., Hol, W.G.J., Drenth, J., Crystal structure of p-hydroxybenzoate hydroxylase complexed with its reaction product 3,4-dihydroxybenzoate. *Journal of Molecular Biology* 1988;199:637-48.

4 CHAPTER 4: FLUORESCENCE PROPERTIES OF FLAVIN SEMIQUINONE RADICALS IN NITRONATE MONOOXYGENASE

(This chapter has been published verbatim in Su, D., Kabir, M.P., Orozco-Gonzalez, Y., Gozem, S., and Gadda, G. (2019), *Chembiochem* 20: 1646-1652. The author's contribution involves the enzyme purification and spectroscopic characterization.)

4.1 Abstract

Fluorescent cofactors like flavins can be exploited to probe their local environment with spatial and temporal resolution. While the fluorescence properties of oxidized and two-electron reduced states of flavins have been studied extensively, this is not the case for the one-electron reduced state. Both the neutral and anionic semiquinones have proven particularly challenging to examine, as they are unstable in solution and are transient, short-lived species in many catalytic cycles. Here, we report that nitronate monooxygenase from *Pseudomonas aeruginosa* PAO1 (NMO) is capable of stabilizing both semiquinone forms anaerobically for hours, enabling us to study their spectroscopy in a constant protein environment. We find that in the active site of NMO the anionic semiquinone exhibits no fluorescence while the neutral semiquinone radical shows a relatively strong fluorescence, with a behavior that violates Kasha-Vavilov's rule. The fluorescence properties are discussed in the context of TD-DFT calculations, which reveal low-lying dark states in both systems.

4.2 Introduction

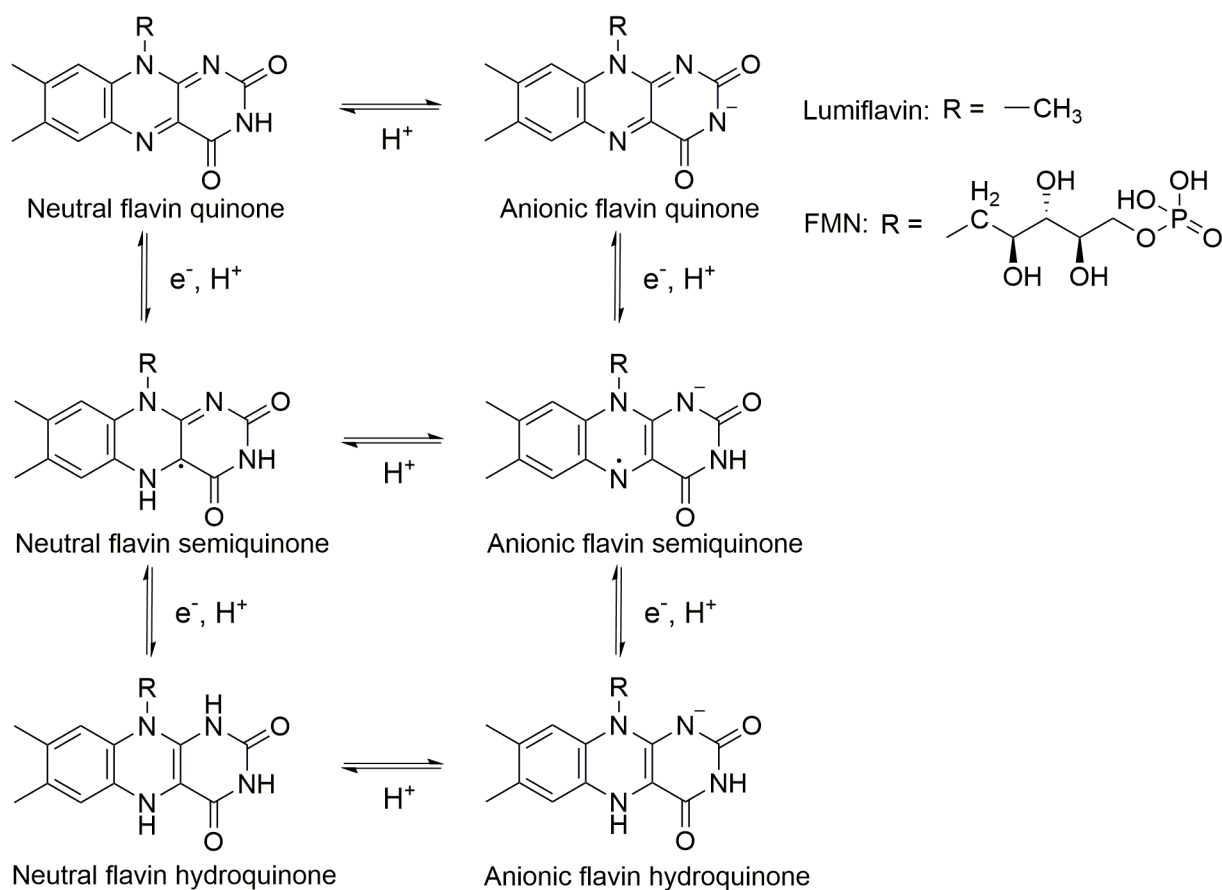
Studies of flavins and flavoproteins have a long history dating back to 1933 with the discovery of Old Yellow Enzyme by Warburg and Christian and the identification of its cofactor as FMN in 1935 by Theorell.^{1, 2} The relatively recent discovery in 1993 of flavin-dependent photoreceptors has drawn renewed interest in the photophysics and photochemistry of flavins.³⁻⁶ Flavin-dependent light-responsive proteins and enzymes, notably DNA photolyases,

cryptochromes, light-oxygen-voltage (LOV) and blue-light sensing using FAD (BLUF) domains, participate in many critical biological processes, including DNA repair, photoregulation of circadian rhythms, and gene expression.^{4, 6-10}

Flavins adopt three different redox states: oxidized quinone, one-electron reduced semiquinone, and two-electron reduced hydroquinone. In each redox state, a flavin can exist in multiple protonation states depending on the pH, with anionic and neutral species being biochemically relevant at the pH values between 3 and 12 at which most proteins are stable and functional (Scheme 4.1). The photophysics and photochemistry of oxidized flavins¹¹⁻¹³ and hydroquinones¹⁴⁻¹⁶ have been studied both in solution and in numerous proteins. The oxidized flavin is fluorescent in solution, but nearby electron donors can act as quenchers,^{8, 17-19} a feature responsible for the lowered fluorescence intensity typically observed in flavoproteins.^{20, 21} Hydroquinone usually displays weak fluorescence in solution, but upon confinement in a rigid protein environment, or at low temperature, it shows enhanced fluorescence.^{14, 22} In contrast, the understanding of the photophysics and photochemistry of flavin semiquinones has lagged because they are not stable in solution²³ and are transient, short-lived species in many catalytic cycles.

Flavin semiquinones are essential intermediates in the photocycle of light-responsive flavoproteins. An electron transfer from the excited reduced FAD (FADH^-) to the damaged DNA yields a neutral FAD semiquinone (FADH^\bullet), initiating the catalytic repair of pyrimidine dimers in DNA photolyase.^{8, 24, 25} A photoinduced proton-coupled electron transfer reduces the oxidized FAD to FADH^\bullet in plant cryptochromes, initiating signal transduction in the plant photocycle.^{26, 27} Photoreduction to generate the anionic FAD semiquinone ($\text{FAD}^{\bullet -}$) occurs in animal Type 1 cryptochrome.^{17, 28} In analogy with cryptochromes, LOV and BLUF domains function by photoinduced electron transfer (PET) to oxidized flavins, generating flavin semiquinones in their

photocycles.^{29, 30} Despite flavin semiquinones participate in the photocycle of flavin-dependent photoreceptors and enzymes, we have limited knowledge of the fluorescence properties of the excited state of flavin semiquinones. To date, there are only two reports on the emission spectra of FMNH^{\bullet} in flavodoxin from *Desulfovibrio vulgaris*, FADH^{\bullet} in DNA photolyase, and $\text{FAD}^{\bullet -}$ in insect Type 1 cryptochrome from *Anopheles gambiae* and *Antheraea pernyi*.^{31, 32}



Scheme 4.1 Redox states of flavins.

The lack of a single protein system capable of thermodynamically stabilizing both the anionic and neutral forms of flavin semiquinone is a fundamental problem that prevents the direct comparison of the photophysical properties of the flavin semiquinone in different ionized states

due to the effects exerted by the surrounding protein environment.^{32, 33} Glucose oxidase is the only known case in which both neutral and anionic flavin semiquinones can be transiently formed by photoreduction.³⁴⁻³⁷ However, the rapid disproportionation of the neutral flavin semiquinone at low pH^{35, 36} prevents its photophysical characterization due to contamination with oxidized FAD and hydroquinone.

A recent study on nitronate monooxygenase (NMO; E.C. 1.13.12.16) from *Pseudomonas aeruginosa* PAO1 showed that the anaerobic mixing of the enzyme-bound flavin with propionate 3-nitronate (P3N) yielded $\text{FAD}^{\bullet -}$ at pH 7.5 (34). P3N is a potent toxin that irreversibly inhibits mitochondrial succinate dehydrogenase.^{38, 39} Mechanisms underlying the toxicity of P3N involve impairment of energy metabolism, oxidative stress, and excitotoxicity,^{38, 40} and have been reviewed recently.⁴¹

In this study, we demonstrated that the enzyme stabilizes the neutral form of flavin semiquinone. A pH titration of the UV-visible absorption spectrum of the one-electron reduced form of NMO allowed for the determination of the $\text{p}K_{\text{a}}$ value for the ionization of the flavin semiquinone in the active site of the enzyme. The fluorescence emission and excitation properties of the enzyme-bound flavin semiquinone in its neutral and anionic states were determined, and time-dependent density functional theory (TD-DFT) calculations were used to obtain insights on the absorption and fluorescence properties of flavin semiquinone. There have been a number of computational studies that model the spectra of flavins in the gas phase,⁴²⁻⁵⁰ solution,^{42-47, 51-54} or in proteins.⁵⁵⁻⁵⁷ Most of these studies have modeled the spectroscopy of flavin in the oxidized state, or in just a few cases also the reduced state. However, far fewer computational studies have investigated the semiquinone flavin.⁵⁸ These studies have been limited to the lowest excited state.

4.3 Materials and Methods

Materials. 3-Nitropropionic acid was purchased from Sigma-Aldrich (St. Louis, MO). *Escherichia coli* strain Rosetta(DE3)pLysS was from Novagen (La Jolla, CA). Recombinant NMO from *P. aeruginosa* PAO1 was expressed and purified as described in a previous study. P3N was prepared in water by incubating 3-nitropropionic acid with a 2.2 molar excess KOH for 24 h, at 4 °C, as previously described.

Experimental Methods. Anaerobic reduction of NMO with P3N was recorded with an Agilent Technologies diode-array spectrophotometer Model HP8453 PC equipped with a thermostated water bath at 15 °C. Just prior to use, NMO was gel-filtered into 20 mM piperazine, 0.1 M NaCl for pH 5.5, or 20 mM sodium pyrophosphate, 0.1 M NaCl, 10% glycerol in the pH range from 6.0 to 8.9 by desalting chromatography through a PD-10 column. At pH 5.0, 20 mM piperazine, 0.1 M NaCl with 20% glycerol was used to stabilize NMO. The concentration of oxidized NMO was calculated by the enzyme-bound flavin with an experimentally determined $\epsilon_{443\text{ nm}} = 12,500 \text{ M}^{-1}\text{cm}^{-1}$. Samples were made anaerobic by at least 20 cycles of flushing with ultra-pure argon and applying vacuum in an anaerobic cuvette with two side arms; 20 μM NMO was loaded in the cuvette together with 1 μM glucose oxidase; 1 mM P3N was loaded into one of the side arms while 5 mM glucose was added into the other one. Glucose was mixed with the NMO/glucose oxidase mixture before P3N to ensure the complete removal of traces of oxygen. UV-visible absorption spectra were recorded until no further changes were observed.

Fluorescence characterization of NMO in different redox states was carried out in a Shimadzu model RF-5301 PC spectrofluorophotometer at 15 °C. FMNH[•]/FMN^{•-} were prepared by mixing 5 μM final concentration of NMO with 1 mM P3N in 20 mM piperazine, 0.1 M NaCl, 20% glycerol at pH 5.0 and 10.0, respectively, after removal of oxygen in an anaerobic fluorescence

cuvette. UV-visible absorption spectra of FMNH[•]/ FMN^{•-} were recorded before the fluorescence characterization to determine the complete reduction of the enzyme bound flavin to the semiquinone state. The fluorescence emission spectra of 5 μM oxidized enzyme were recorded in the same condition. The same buffer solution with 1mM P3N without NMO after the removal of oxygen was used as the blank and subtracted from emission and excitation spectra of NMO. The excitation spectra of different flavin redox states were recorded when the emission was set at peaks of emission spectra.

Computational Methods. All DFT and TD-DFT energy calculations and optimizations in this work were performed using the B3LYP functional and cc-pVTZ basis set. TD-B3LYP has been shown in multiple computational studies to accurately reproduce the spectra of oxidized LF. In fact, the LFH[•] and FL^{•-} spectra computed using TD-B3LYP in this work also reproduce the experimental spectral features very well. Therefore, it is our method of choice due to the reasonable computational cost in the modeling of vertical and adiabatic energies in a system the size of flavin. Calculations were performed using a PCM solvent model with a dielectric constant, ϵ , of 6 to simulate the weak field of the protein. Calculations on LFH[•] were also repeated in the gas phase and in PCM solvents for argon, cyclohexane, ethanol, and water to study the effect of changing the solvent environment. Adiabatic energies were computed for each state by optimizing the geometry on that state and computing the energy difference between the minima of the excited states and that of the ground state. The adiabatic energies reported in Table 2 also include zero-point vibrational energy corrections. Franck-Condon factors (i.e., accounting for the vibronic excitations by computing overlaps in the ground and excited state vibrational wave functions) were computed using ezSpectrum. The vibronic peaks were then broadened using Gaussian functions with a full width at half maximum of 0.25 eV. The relative peak heights depend on the

relative oscillator strengths of the different transitions and were not scaled otherwise. Electronic structure calculations in this work were performed with Gaussian 16 on SDSC Comet and GSU ACoRE supercomputers.

Data Analysis. KaleidaGraph software (Synergy Software, Reading, PA) was used to fit the data. The pH effect on the UV-visible absorption spectrum of NMO in the semiquinone state was determined with equation 1, which describes a curve with one pK_a value and plateaus at both low and high pH values.

$$Y = \frac{A}{1+10^{(pH-pK_a)}} + \frac{B}{1+10^{(pK_a-pH)}} \quad (1)$$

4.4 Results and Discussion

Mixing NMO and 1 mM P3N anaerobically at pH 5.0 yielded FMNH^{*}, as indicated by the broad absorbance between 550 nm and 700 nm (Figure 4.1A). The extinction coefficients of the enzyme-bound FMNH^{*} determined at 333 nm (10,200 M⁻¹cm⁻¹), 488 nm (3,600 M⁻¹cm⁻¹), and 584 nm (4,900 M⁻¹cm⁻¹) were comparable to those typically reported for the neutral flavin semiquinone bound to other proteins (Figure 4.1A).^{73, 74} In a previous study, the anaerobic reduction of NMO with P3N at pH 7.5 yielded FMN^{* -} (Figure 4.1A).⁵⁹ Thus, NMO can stabilize both anionic and neutral flavin semiquinones in its active site. As a reference, 10 μM PaNMO was mixed anaerobically with 5 mg sodium borohydride in 200 mM piperzaine, pH 10.0 and 15 °C. Flavin was fully reduced to the anionic 1,5-hydroquinone as indicated by the depletion of the absorbance at 439 nm peak and the development of 345 nm maximum, with extinction coefficient of 5.1 mM⁻¹cm⁻¹ (Figure 4.1A)^{75, 76}.

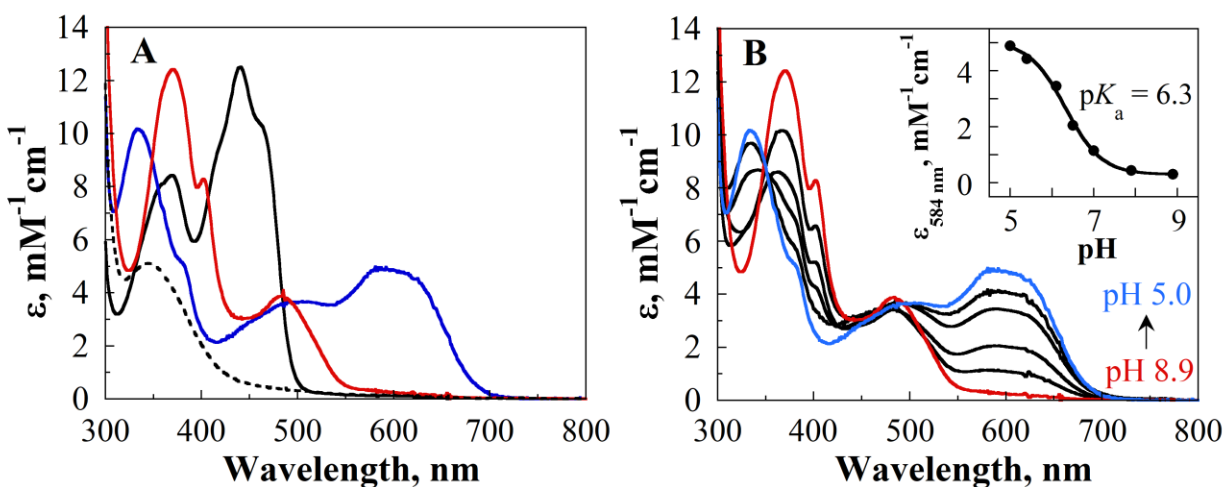


Figure 4.1 Stabilization of anionic and neutral flavin semiquinones in NMO. (A) The UV-visible absorption spectrum of the oxidized enzyme (black curve) was recorded in 20 mM piperazine, 0.1 M NaCl, at pH 10.0 and 15 °C; those of the enzyme in the neutral (blue curve) and anionic (red curve) semiquinone states in 20 mM piperazine, 0.1 M NaCl, 20% glycerol at pH 5.0 and 10.0, respectively, after anaerobic reduction with 1 mM P3N at 15 °C; that of the enzyme in the hydroquinone state (dashed curve) in 200 mM piperazine, pH 10.0, after anaerobic reduction with 5 mg sodium borohydride at 15 °C. (B) Anaerobic reduction of NMO with 1 mM P3N at pH 5.0, 5.4, 6.1, 6.5, 7.0, 7.9 and 8.9, 15 °C, with the inset showing the dependence of the $\epsilon_{584\text{ nm}}$ value as a function of pH; the curve is the fit of the data to equation 1.

To establish the pK_a value for the equilibration of the neutral and anionic flavin semiquinones in the active site of NMO, the enzyme was reduced anaerobically with 1 mM P3N in the pH range from 5.0 to 8.9 at 15 °C. As shown in Figure 4.1B, there was a progressive decrease in the absorbance between 550 and 700 nm and the appearance of distinct peaks at 370 nm, 402 nm, and 485 nm with increased pH values, consistent with a pH-dependent equilibration of the neutral and anionic flavin semiquinones in the active site of NMO.^{35, 36} A pK_a value of 6.3 ± 0.1 was calculated for the equilibration of $\text{FMNH}^{\cdot}/\text{FMN}^{\cdot -}$ bound to NMO by plotting the absorbance at 584 nm versus pH and fitting the data to equation 1. At all pH values tested, the flavin semiquinone was stable over at least 8 h, consistent with thermodynamic stabilization of both anionic and neutral flavin semiquinones in the active site of the enzyme. The pK_a value of 6.3 in

NMO agrees reasonably well with the pK_a value of ~ 8.3 kinetically determined for flavin semiquinone in aqueous solution using potentiometry and pulse radiolysis^{61, 77, 78} and ~ 7.3 in the active site of glucose oxidase using kinetic determinations of the second order rate constant for semiquinone oxidation with molecular oxygen.^{35, 36}

The emission and excitation spectra of the enzyme-bound flavin (5 μM) in the oxidized and semiquinone state were measured at 15 °C at pH 5.0 and 10.0. The emission intensity of oxidized FMN (2 μM) in bulk solution was also acquired and used to normalize the relative emission intensity of each flavin species when bound to the enzyme. Oxidized FMN in bulk solution had a maximal emission wavelength at 531 nm at both low and high pH, but the fluorescence intensity was ~ 2.5 -times smaller at high pH (Table 4.1) likely due to $\sim 50\%$ of the flavin being anionic at pH 10.0 because the N3 atom of FMN with a pK_a value of ~ 10.0 is partially ionized and the anionic species has lower fluorescence quantum yield.^{12, 79} A high emission intensity concomitant with a 7 nm hypsochromic shift at pH 10.0 compared to pH 5.0 was also observed for the FMN bound to NMO (Figure 2A, Table 4.1). Irrespective of the pH, the fluorescence intensity of FMN in the enzyme active site was ≥ 120 -times smaller than free FMN (Table 4.1), presumably due to quenching of the oxidized flavin in the active site of NMO by photoinduced electron transfer (PET) from a nearby aromatic residue. NMO contains four tyrosines, two phenylalanines, and one tryptophan⁵⁹ in the active site that could potentially quench the fluorescence of the flavin.

Table 4.1 Fluorescence properties of FMN in bulk solution and bound to NMO at 15 °C^a

	pH	Excitation peaks (nm)	Emission peaks (nm)	Relative intensity ^b
Free oxidized FMN	5.0	379, 463	531	2400
	10.0	378, 459	531	920
Oxidized FMN in PaNMO	5.0	380, 464	530	20
	10.0	373, 463	523	2
Neutral semiquinone in PaNMO	5.0	574, 586	628	280

^a Conditions: anaerobically in 20 mM piperazine, 0.1 M NaCl with 20% glycerol.

^b Intensity at the emission peaks are reported. Intensity of 2 μ M free oxidized FMN was experimentally measured and converted to the intensity corresponding to 5 μ M free oxidized FMN due to the instrument limit. Intensity of enzyme-bound FMN in different redox states was determined with 5 μ M NMO.

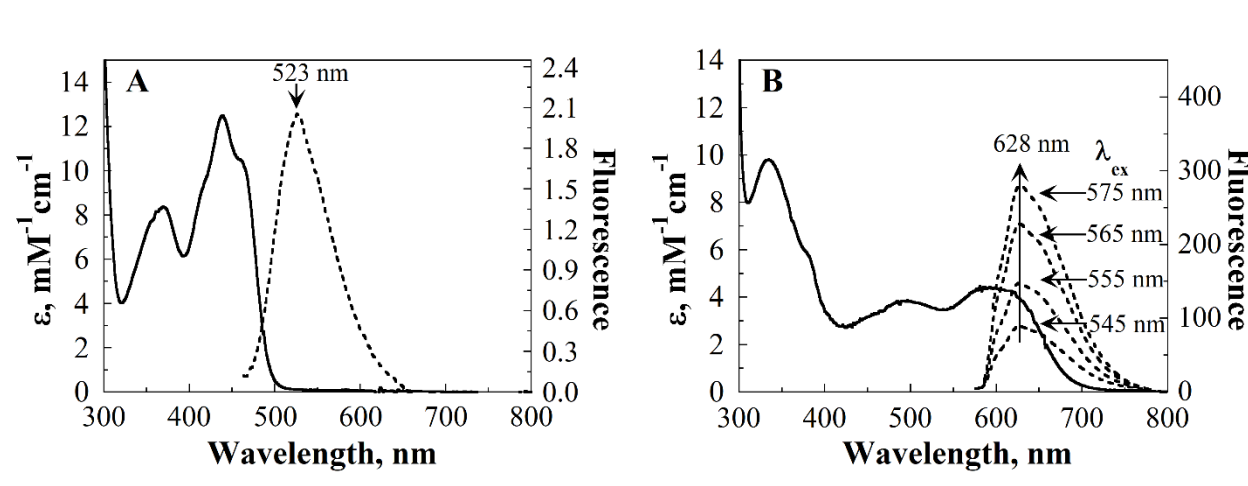


Figure 4.2 Fluorescence emission of NMO in the oxidized (A) and neutral semiquinone (B) states. UV-visible absorption spectra are shown as solid curves, and fluorescence emission spectra as dashed curves. The spectra of the oxidized NMO were recorded in 20 mM piperazine, 0.1 M NaCl, 20% glycerol at pH 10.0 and 15 °C; those for the neutral semiquinone in 20 mM piperazine, 0.1 M NaCl, 20% glycerol at pH 5.0 and 15 °C. The arrows and wavelengths in panel B refer to the λ_{ex} used to excite the enzyme-bound FMN.

As shown in Figure 4.2B, FMN^{•-} in NMO had maximal fluorescence emission at 628 nm when excited at 575 nm, with an intensity of ~12% that of oxidized FMN in bulk solution at pH 5.0 (Table 4.1). Thus, the flavin bound to NMO was ~15-times more fluorescent as a neutral semiquinone than in the oxidized state. The higher fluorescence intensity of the neutral semiquinone as compared to the oxidized flavin is consistent with a higher excited-state reduction

potential of FMNH[•] compared to FMN, which would make a PET from a nearby aromatic residue more difficult to the semiquinone than the oxidized state. This makes the FMNH[•] radical one of only a few families of fluorescent radical species.⁸⁰ The intensity of fluorescence emission of FMNH[•] in NMO decreased when the excitation wavelength was reduced from 575 nm to 545 nm (Figure 4.2B), and there was no fluorescence emission upon exciting at wavelengths ≤ 488 nm. Note that FMNH[•] is similar in chemical structure to 4a-hydroxy FMN (FMNH₂OH), the putative fluorophore of bacterial luciferase that exhibits strong emission as well.^{81, 82} FMNH₂OH has an -OH substituent instead of the radical center at the 4a carbon of FMNH[•]. However, the two molecules have different electronic structure, as demonstrated by their very different absorption and emission spectra.⁸³

The FMN⁻ bound to NMO at pH 10.0 did not emit fluorescence irrespective of the wavelength at which the flavin was excited, i.e., 370 nm, 402 nm, and 485 nm. The only other study of the fluorescence properties of a protein-bound anionic flavin semiquinone reported weak fluorescence at 525 nm upon excitation at 450 nm of the FAD in insect Type 1 cryptochrome.^{31, 32} Fluorescence processes of flavin in the oxidized state typically yield excitation at 450 nm and emission at 525-535 nm, suggesting that small traces of oxidized flavin may have been present in the cryptochrome sample.⁸⁴⁻⁸⁷ Alternatively, a more dynamic protein environment surrounding the flavin anionic semiquinone in NMO than in Type 1 cryptochrome may explain the lack of fluorescence emission in NMO.^{32, 33}

The excitation spectrum of FMNH[•] in NMO featured a single sharp band between 500 nm and 610 nm instead of mimicking the general shape of the UV-visible absorption spectrum of FMNH[•] (Figure 4.3A), as expected.^{88, 89} This phenomenon was not observed with the oxidized flavin of NMO, for which the excitation spectrum resembles the shape of the UV-visible

absorption spectrum (Figure 4.3B). Thus, the fluorescence of FMNH^{*} bound to NMO violates the Kasha-Vavilov rule, which assumes that internal conversion between excited states are faster than any competing excited-state processes.⁸⁸⁻⁹⁰ Some known exceptions to the Kasha-Vavilov rule, such as blue shifts of emission spectra when excited to higher excited states, occur when the rates of emission decay from high excited states are comparable or faster than internal conversion to the lowest excited state.⁹¹

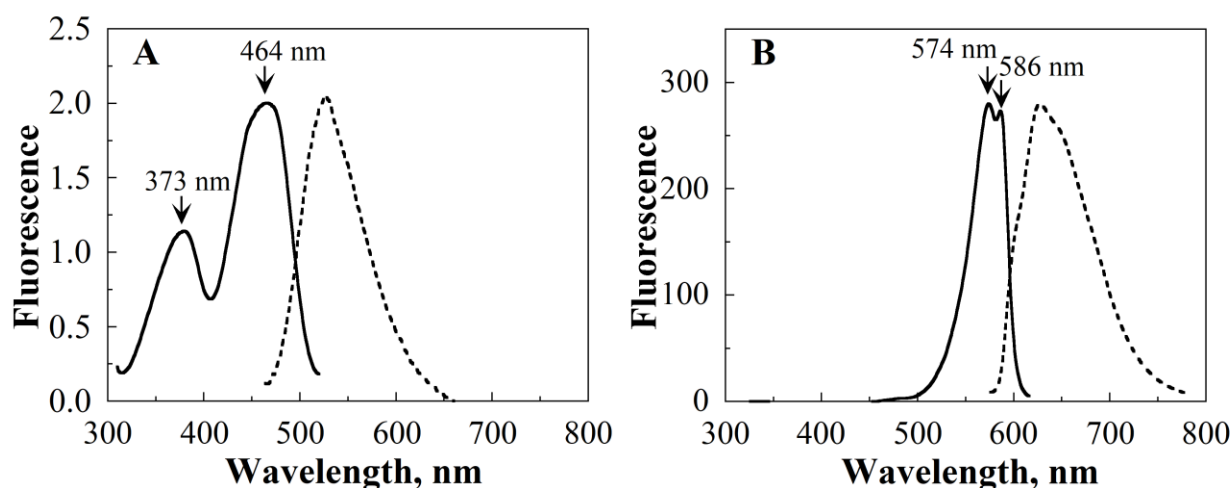


Figure 4.3 Fluorescence excitation of NMO in the oxidized (A) and neutral semiquinone (B) states. The excitation spectra are shown as solid curves, the emission spectra as dashed curves. The spectra of the oxidized NMO were recorded in 20 mM piperazine, 0.1 M NaCl, 20% glycerol at pH 10.0 and 15 °C; those for the neutral semiquinone in 20 mM piperazine, 0.1 M NaCl, 20% glycerol at pH 5.0 and 15 °C.

To gain insight on the unusual fluorescence properties of the flavin semiquinone in NMO (*vide supra*), we performed TD-DFT calculations. Since the π -electron conjugation responsible for fluorescence emission and absorbance localizes exclusively on the isoalloxazine ring, we used lumiflavin as a computational model (LFH^{*}, Scheme 1) instead of FMN to minimize computational cost. A polarizable continuum model (PCM) with a ϵ value of 6 was used to crudely mimic the weak dielectric field of a general protein environment.⁶⁸ Figure 4.4A shows the UV-visible

absorption spectrum of LFH^{*} computed with TD-DFT/PCM. The comparison of the absorption spectra of the calculated LFH^{*} and the experimental FMNH^{*} bound to the enzyme shows good agreement (Figure 4.4A), implying minimal perturbation of the electronic character of the excited states of the flavin by the protein environment around the flavin. The computed absorption spectrum is based on adiabatic excitation energies and includes vibronic excitations computed using Franck-Condon factors. We found that neither the vertical nor adiabatic computed excitation energies are representative of the UV-visible absorption spectrum. Our results are in keeping with a previous computational study on oxidized lumiflavin,^{56, 65} reinforcing the importance of incorporating vibronic excitations to reproduce the experimental absorption spectrum.

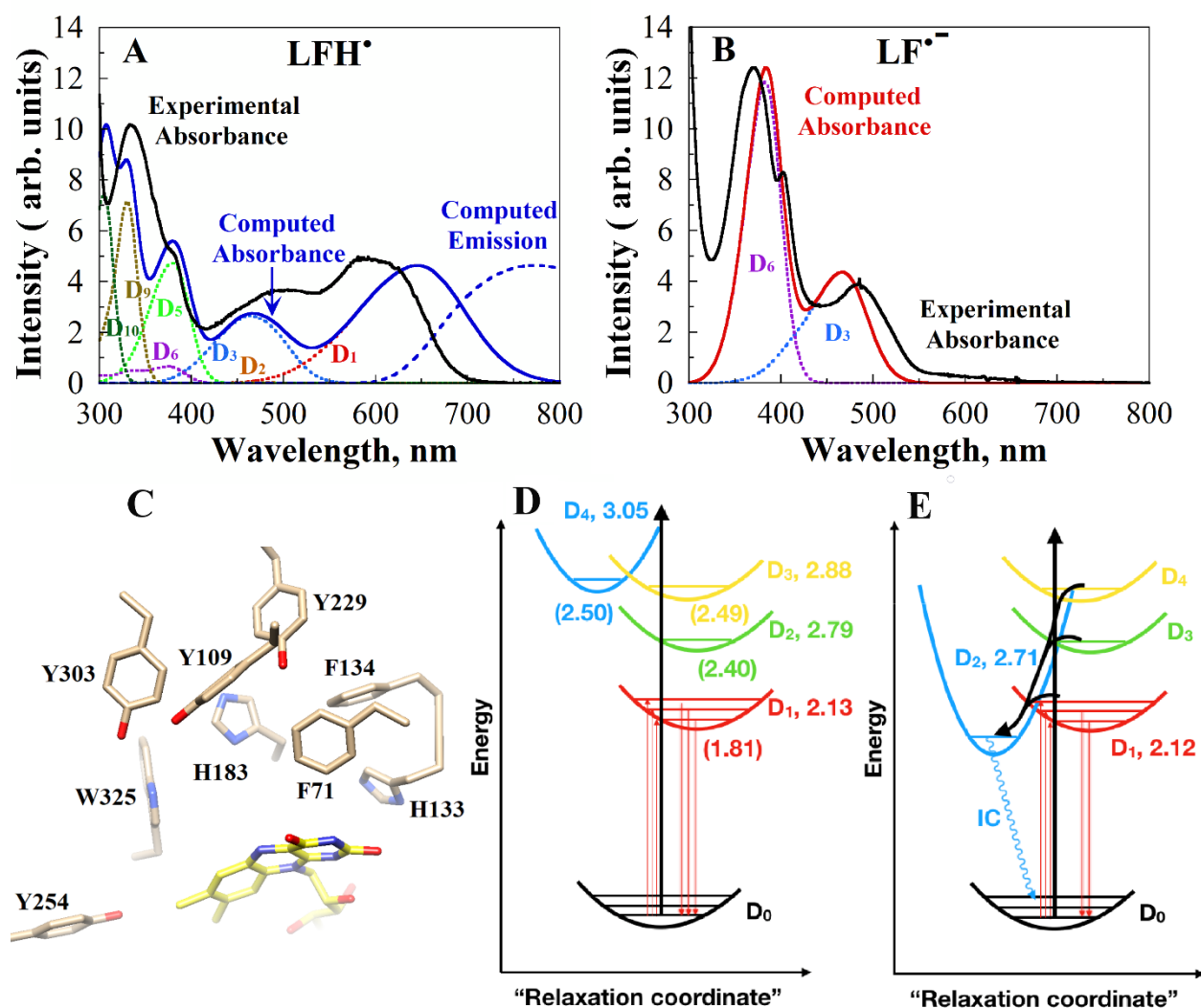


Figure 4.4 A. Simulated PCM TD-DFT UV-visible absorption spectrum (solid blue line) and emission (dashed blue line) spectra of LFH^{*}, shown in comparison to the experimental FMNH^{*} UV-visible absorption spectrum in PaNMO (solid black line). B. Simulated PCM TD-DFT UV-visible absorption spectrum (solid red line) of LF^{*-}, shown in comparison to the experimental FMN⁻ UV-visible absorption spectrum in PaNMO (solid black line). C. The active site of PaNMO (PDB entry 4Q4K). The carbon atoms of the FMN cofactor are shown as yellow sticks, whereas those of select protein residues are displayed as tan sticks; nitrogen and oxygen atoms are colored in blue and red, respectively. D. A scheme showing the relative energies of ground and excited states given by PCM TD-DFT calculations. E. A scheme showing the relative energies of ground and excited states given by gas-phase TD-DFT calculations. The gas-phase calculations support a possible mechanism that can explain the violation of the Kasha-Vavilov rule in FMNH^{*}. Computed vertical excitation energies (and adiabatic excitation energies in parentheses) are labeled for each state in units of eV.

The first vertical excited state of the neutral semiquinone (D_1) is a bright $\pi\pi^*$ state and is responsible for the absorbance in the 550-700 nm region of the spectrum and the emission at 628 nm (Figure 4.4A, Table 4.2). The D_2 and D_3 states are also $\pi\pi^*$ states, but with a weaker absorbance and contribute to the absorption feature in the 450-550 nm region of the spectrum. The fourth excited state (D_4) is a dark $n_o\pi^*$ state and does not contribute to the absorption spectrum (Table 4.2). D_4 lies close in energy to and overlaps with the bright D_2 and D_3 states in the TD-DFT/PCM calculation carried out with a ϵ value of 6. D_5 and D_6 are responsible for the shoulder at ~ 380 nm, while D_9 and D_{10} contribute to the strong absorbance at ~ 330 nm.

Table 4.2 Computed vertical and adiabatic energies for LFH^{\bullet} and $LF^{\bullet-}$ at the B3LYP/cc-pVTZ/PCM level of theory

LFH $^{\bullet}$				
State	Vertical Excitation, eV (nm)	Oscillator Strength ^a	Adiabatic Excitation, eV (nm) ^b	Character ^a
D1	2.132 (582)	0.127	1.808 (686)	$\pi\pi^*$ (67b \rightarrow 68b)
D2	2.792 (444)	0.008	2.402 (516)	$\pi\pi^*$ (68a \rightarrow 69a)
D3	2.875 (431)	0.057	2.489 (498)	$\pi\pi^*$ (66b \rightarrow 68b)
D4	3.045 (407)	0.000	2.501 (496)	$n_o\pi^*$ (65b \rightarrow 68b)
D5	3.441 (360)	0.093	3.170 (391)	$\pi\pi^*$ (68a \rightarrow 70a)
D6	3.495 (355)	0.022	3.199 (388)	$\pi\pi^*$ (64b \rightarrow 68b)
D9	3.860 (321)	0.094	3.715 (334)	$\pi\pi^*$ (61b \rightarrow 68b)
D10	4.204 (295)	0.090	3.992 (311)	$\pi\pi^*$ (68a \rightarrow 71a)
LF $^{\bullet-}$				
State	Vertical Excitation, eV (nm)	Oscillator Strength	Adiabatic Excitation, eV (nm)	Character
D1	2.204 (562)	0.003	1.835 (676)	$\pi\pi^*$ (68a \rightarrow 69a)
D2	2.712 (457)	0.003	2.404 (516)	$\pi\pi^*$ (68a \rightarrow 70a)
D3	2.834 (438)	0.142	2.555 (485)	$\pi\pi^*$ (67b \rightarrow 68b)
D4	3.109 (399)	0.000	2.632 (471)	$n_N\pi^*$ (65b \rightarrow 68b)
D5	3.304 (375)	0.081		$\pi\pi^*$ (66b \rightarrow 68b)
D6	3.467 (358)	0.297	3.155 (393)	$\pi\pi^*$ (68a \rightarrow 71a)

^a Oscillator strengths and electronic character are shown here for the vertical excitation.

^b Adiabatic excitation energies reported here also account for zero-point vibrational energies.

To obtain insights on the effect of the PCM environment, we also performed the same level of TD-DFT calculation in different PCM solvents ranging from ϵ values of 0, which is equivalent

to the gas phase, to 78.36, which corresponds to water (Table 4.3). While the energetics of the $D_1 \pi\pi^*$ excitation depends minimally on the ϵ value, with a ΔeV of 0.035 between gas phase and water, the excitation energy of the $n_O\pi^*$ state is highly influenced by the ϵ value, with a ΔeV of 0.44 between gas and water. Note that this is not the case for the $n_N\pi^*$ state in anionic semiquinone, which is less sensitive to the solvent polarity (Table 4.3). This suggests that while the absorption spectrum of FMNH $^\bullet$, which is dominated by $\pi\pi^*$ transitions, is minimally modulated by the protein environment surrounding the flavin, its photophysics and fluorescence properties are strongly influenced by a protein environment due to the sensitivity of the $n\pi^*$ energies to the environment. The gas-phase TD-DFT calculation yields a significantly more stable $n_O\pi^*$ excited state, which becomes the second vertical excited state instead of the fourth and has an adiabatic energy that is comparable with that of the fluorescent $\pi\pi^*$ D_1 excited state (Figure 4.4E).

Table 4.3 Solvent effect on the computed energies of $D_1 \pi\pi^*$ and $n_O\pi^*$ for LFH $^\bullet$ and $D_1 \pi\pi^*$ and $n_N\pi^*$ for LF $^{\bullet-}$.

Dielectric constant	$D_1 \pi\pi^*$ (eV)	$n_O\pi^*$ (eV)	Difference (eV)	$D_1 \pi\pi^*$ (eV)	$n_N\pi^*$ (eV)	Difference (eV)
0.000	2.121	2.714	0.593	2.109	2.950	0.841
1.430	2.110	2.801	0.691	2.135	2.979	0.844
2.017	2.102	2.877	0.774	2.163	3.022	0.859
6.078	2.132	3.045	0.913	2.204	3.109	0.905
32.613	2.150	3.130	0.980	2.222	3.159	0.937
78.355	2.156	3.151	0.995	2.227	3.173	0.946

The excitation spectrum of the neutral flavin semiquinone (Figure 4.3B) indicates that fluorescence only occurs when the flavin is excited to the D_1 state directly, whereas excitation to any electronic state above D_1 does not lead to fluorescence. Three possible processes not mutually exclusive could explain the fluorescence emission of the neutral semiquinone excited to the D_1 state, but not to higher electronic states: internal conversion through a dark $n_O\pi^*$ state, PET from nearby aromatic donors, or intersystem crossing (ISC) to a quartet $n_O\pi^*$ state. One could

reasonably conjecture that due to the dielectrics of the protein surrounding the flavin the dark $n_0\pi^*$ state is the lowest adiabatic excited state but is not accessible from the D_1 state, as qualitatively suggested by the trend seen in the TD-DFT calculation in different PCM solvents. Thus, excitation of FMNH^{*} to any energetic state higher than D_1 would populate the dark $n_0\pi^*$ state (Figure 4.4E) and produce no fluorescence. Direct excitation to the D_1 state would result in fluorescence emission because the dark $n_0\pi^*$ state would not be energetically accessible. Alternatively, if ultrafast PET to the excited state D_2 or higher states occurred on a time-scale faster than the nonradiative decay from high excited states to D_1 , fluorescence emission would be allowed only from the excited state D_1 . Ultrafast PET was reported for zinc porphyrins, for which the excited states S_1 and S_2 are well separated, i.e., by ca. 0.8 eV and internal conversion is therefore slow compared to PET.⁹² In the active site of NMO, there are several potential electron donors within 4 Å from the isoalloxazine ring of FMN, including Phe₇₁, Tyr₂₅₄, and Trp₃₂₅. Additionally, Tyr₁₀₉, Phe₁₃₄, Tyr₂₉₉, and Tyr₃₀₃ lie within 10 Å from the isoalloxazine ring of FMN (Figure 4.4C).⁵⁹ PET in the picosecond timescale to the lowest excited state of FADH^{*} was previously reported for *E. coli* DNA photolyase and a Type 1 cryptochrome mutant protein.^{24, 31} However, in all these reported cases PET involves the lowest excited state of FADH^{*} and occurs on a picosecond timescale; a timescale that may be too slow to compete with the internal conversion between the D_2 and D_1 of the neutral flavin semiquinone, which are separated by 0.66 eV (Table 4.3). ISC to the dark $n_0\pi^*$ state could also explain the lack of fluorescence from states energetically higher than D_1 in the neutral flavin semiquinone bound to NMO. ISC of a flavin semiquinone from the doublet to the quartet $n\pi^*$ state, consistent with El-Sayed rules,⁹³ was previously reported in DNA photolyase within ~100 ps of excitation.⁹⁴ Irrespective of whether internal conversion through a dark $n_0\pi^*$ state, PET, or ISC to a quartet $n_0\pi^*$ state, quenches the fluorescence emission of the

neutral flavin semiquinone, TD-DFT/PCM calculations provide support for the spectroscopic assignments of the UV-visible absorption bands and reveal the existence of a low-lying dark $n_{\text{O}}\pi^*$ state, whose properties can now be investigated further.

TD-DFT calculations on the anionic lumiflavin semiquinone ($\text{LF}^{\cdot-}$) show that the D_1 and D_2 states are weakly absorbing $\pi\pi^*$ state (Table 4.2). The lack of observed emission can be attributed to the low oscillator strength for D_1 , which is 0.003, compared to 0.082 for LFH^{\cdot} at the D_1 optimized geometry. A similar conclusion was recently drawn by Ai *et al.* in a gas phase CASPT2//CASSCF study of a reduced model of $\text{FMN}^{\cdot-}$.⁵⁸ The strong absorption features of $\text{FMN}^{\cdot-}$ are consistent with absorbance to the bright D_3 , D_5 , and D_6 $\pi\pi^*$ excited states in $\text{LF}^{\cdot-}$. We were unable to optimize D_5 since it is very close in adiabatic energy to the D_6 state, so it is not shown in Figure 4.4B. If it were to be included, it might add a little to the peak intensity at ~ 350 nm. However, the computed peak energies are in excellent agreement with the experiment. Note that in this case there is a low-lying D_4 $n_{\text{N}}\pi^*$ state as well, although it is an $n_{\text{N}}\pi^*$ state, while the $\text{LF}^{\cdot-}$ $n_{\text{O}}\pi^*$ state lies higher in energy.

4.4 Conclusion

In conclusion, NMO can stabilize FMN in several redox and protonation states and is a useful model system for studying the spectroscopy and photophysics of each of these states in a constant protein environment. In this work, we focus on FMNH^{\cdot} and $\text{FMN}^{\cdot-}$, which are both stabilized in NMO. FMNH^{\cdot} in NMO yields a strong fluorescence that violates the Kasha-Vavilov rule, while we do not observe any fluorescence in $\text{FMN}^{\cdot-}$. TD-DFT calculations are used to assign the absorption and fluorescence peaks and provide insight into the photophysics of these two radicals. Specifically, the calculations show that the first excited state in $\text{FMN}^{\cdot-}$ is a $\pi\pi^*$ state with low oscillator strength, while in FMNH^{\cdot} the lowest excited state is a bright emissive $\pi\pi^*$ state. A

dark $n_0\pi^*$ state exists in FMNH^{*} above the fluorescent $D_1 \pi\pi^*$ state that is likely responsible for its anti-Kasha behavior. The lack of fluorescence of FMN⁻ is likely due to the existence of D_1 and $D_2 \pi\pi^*$ states with low oscillator strength. A complete understanding of the photophysics of the FMNH^{*} will require further investigation, e.g., using accurate multi-configurational quantum chemical methods and hybrid quantum/molecular mechanical models to account for the effect of the protein environment and describe the $\pi\pi^*$, doublet $n\pi^*$, and quartet $n\pi^*$ states on an equal footing.

4.5 Acknowledgement

We acknowledge the NSF XSEDE for computational resources from Research Allocation CHE180027. We also acknowledge the use of Georgia State University's research computing resources that are supported by Georgia State's Research Solutions.

4.6 References

- [1] Warburg, O., and Christian, W. (1933) Über das gelbe Ferment und seine Wirkungen, *Biochem. Z.* 266, 377-411.
- [2] H, T. (1935) Preparation in pure state of the effect group of yellow enzymes., *Biochem. Z.*, 344-346.
- [3] Salomon, M., Christie, J. M., Knieb, E., Lempert, U., and Briggs, W. R. (2000) Photochemical and mutational analysis of the FMN-binding domains of the plant blue light receptor, phototropin, *Biochemistry* 39, 9401-9410.
- [4] Hearst, J. (1995) The structure of photolyase: using photon energy for DNA repair, *Science* 268, 1858-1859.
- [5] Ahmad, M., and Cashmore, A. R. (1993) HY4 gene of *A. thaliana* encodes a protein with characteristics of a blue-light photoreceptor, *Nature* 366, 162-166.
- [6] Masuda, S., and Bauer, C. E. (2002) AppA Is a Blue Light Photoreceptor that Antirepresses Photosynthesis Gene Expression in *Rhodobacter sphaeroides*, *Cell* 110, 613-623.
- [7] Christie J. M. , B. W. R., Briggs W. R. , Spudich J. L. (2005) *Handbook of Photosensory Receptors*, Wiley, Weinheim, Germany.
- [8] Sancar, A. (2003) Structure and Function of DNA Photolyase and Cryptochrome Blue-Light Photoreceptors, *Chemical reviews* 103, 2203-2238.
- [9] Sancar, A. (2004) Regulation of the Mammalian Circadian Clock by Cryptochrome, *Journal of Biological Chemistry* 279, 34079-34082.
- [10] Lin, C., and Shalitin, D. (2003) Cryptochrome structure and signal transduction, *Annual review of plant biology* 54, 469-496.

- [11] Weber, G. (1950) Fluorescence of riboflavin and flavin-adenine dinucleotide, *Biochemical Journal* 47, 114-121.
- [12] Li, G., and Glusac, K. D. (2008) Light-triggered proton and electron transfer in flavin cofactors, *J Phys Chem A* 112, 4573-4583.
- [13] Stanley, R. J., and MacFarlane. (2000) Ultrafast Excited State Dynamics of Oxidized Flavins: Direct Observations of Quenching by Purines, *The Journal of Physical Chemistry A* 104, 6899-6906.
- [14] Ghisla, S., Massey, V., Lhoste, J. M., and Mayhew, S. G. (1974) Fluorescence and optical characteristics of reduced flavines and flavoproteins, *Biochemistry* 13, 589-597.
- [15] Visser, A. J., Ghisla, S., Massey, V., Muller, F., and Veeger, C. (1979) Fluorescence properties of reduced flavins and flavoproteins, *European journal of biochemistry* 101, 13-21.
- [16] Kim, S. T., Heelis, P. F., Okamura, T., Hirata, Y., Mataga, N., and Sancar, A. (1991) Determination of rates and yields of interchromophore (folate---flavin) energy transfer and intermolecular (flavin---DNA) electron transfer in Escherichia coli photolyase by time-resolved fluorescence and absorption spectroscopy, *Biochemistry* 30, 11262-11270.
- [17] Song, S.-H., Öztürk, N., Denaro, T. R., Arat, N. Ö., Kao, Y.-T., Zhu, H., Zhong, D., Reppert, S. M., and Sancar, A. (2007) Formation and Function of Flavin Anion Radical in Cryptochrome 1 Blue-Light Photoreceptor of Monarch Butterfly, *Journal of Biological Chemistry* 282, 17608-17612.
- [18] McCormick, D. B. (1977) Interactions of flavins with amino acid residues: assessments from spectral and photochemical studies, *Photochemistry and photobiology* 26, 169-182.
- [19] van den Berg, P. A. W., van Hoek, A., Walentas, C. D., Perham, R. N., and Visser, A. J. W. G. Flavin Fluorescence Dynamics and Photoinduced Electron Transfer in Escherichia coli Glutathione Reductase, *Biophysical journal* 74, 2046-2058.
- [20] Mataga, N., Chosrowjan, H., Taniguchi, S., Tanaka, F., Kido, N., and Kitamura, M. (2002) Femtosecond Fluorescence Dynamics of Flavoproteins: Comparative Studies on Flavodoxin, Its Site-Directed Mutants, and Riboflavin Binding Protein Regarding Ultrafast Electron Transfer in Protein Nanospaces, *The Journal of Physical Chemistry B* 106, 8917-8920.
- [21] Zhong, D., and Zewail, A. H. (2001) Femtosecond dynamics of flavoproteins: Charge separation and recombination in riboflavine (vitamin B₂)-binding protein and in glucose oxidase enzyme, *Proceedings of the National Academy of Sciences* 98, 11867-11872.
- [22] Ghisla, S. (1980) [51] Fluorescence and optical characteristics of reduced flavins and flavoproteins, In *Methods in Enzymology*, pp 360-373, Academic Press.
- [23] Ehrenberg, A., Müller, F., and Hemmerich, P. (1967) Basicity, Visible Spectra, and Electron Spin Resonance of Flavosemiquinone Anions, *European journal of biochemistry* 2, 286-293.
- [24] Kim, S. T., Sancar, A., Essenmacher, C., and Babcock, G. T. (1993) Time-resolved EPR studies with DNA photolyase: excited-state FADH₀ abstracts an electron from Trp-306 to generate FADH⁻, the catalytically active form of the cofactor, *Proceedings of the National Academy of Sciences of the United States of America* 90, 8023-8027.
- [25] Kao, Y. T., Saxena, C., Wang, L., Sancar, A., and Zhong, D. (2005) Direct observation of thymine dimer repair in DNA by photolyase, *Proceedings of the National Academy of Sciences of the United States of America* 102, 16128-16132.
- [26] Lin, C., Robertson, D. E., Ahmad, M., Raibekas, A. A., Jorns, M. S., Dutton, P. L., and Cashmore, A. R. (1995) Association of flavin adenine dinucleotide with the Arabidopsis blue light receptor CRY1, *Science* 269, 968-970.

- [27] Bouly, J. P., Schleicher, E., Dionisio-Sese, M., Vandenbussche, F., Van Der Straeten, D., Bakrim, N., Meier, S., Batschauer, A., Galland, P., Bittl, R., and Ahmad, M. (2007) Cryptochrome blue light photoreceptors are activated through interconversion of flavin redox states, *The Journal of biological chemistry* 282, 9383-9391.
- [28] Berndt, A., Kottke, T., Breitzkreuz, H., Dvorsky, R., Hennig, S., Alexander, M., and Wolf, E. (2007) A novel photoreaction mechanism for the circadian blue light photoreceptor Drosophila cryptochrome, *The Journal of biological chemistry* 282, 13011-13021.
- [29] Schleicher, E., Kowalczyk, R. M., Kay, C. W., Hegemann, P., Bacher, A., Fischer, M., Bittl, R., Richter, G., and Weber, S. (2004) On the reaction mechanism of adduct formation in LOV domains of the plant blue-light receptor phototropin, *Journal of the American Chemical Society* 126, 11067-11076.
- [30] Gauden, M., van Stokkum, I. H. M., Key, J. M., Lührs, D. C., van Grondelle, R., Hegemann, P., and Kennis, J. T. M. (2006) Hydrogen-bond switching through a radical pair mechanism in a flavin-binding photoreceptor, *Proceedings of the National Academy of Sciences* 103, 10895-10900.
- [31] Kao, Y. T., Tan, C., Song, S. H., Ozturk, N., Li, J., Wang, L., Sancar, A., and Zhong, D. (2008) Ultrafast dynamics and anionic active states of the flavin cofactor in cryptochrome and photolyase, *Journal of the American Chemical Society* 130, 7695-7701.
- [32] Kao, Y. T., Saxena, C., He, T. F., Guo, L., Wang, L., Sancar, A., and Zhong, D. (2008) Ultrafast dynamics of flavins in five redox states, *Journal of the American Chemical Society* 130, 13132-13139.
- [33] Gozem, S., Mirzakulova, E., Schapiro, I., Melaccio, F., Glusac, K. D., and Olivucci, M. (2014) A conical intersection controls the deactivation of the bacterial luciferase fluorophore, *Angewandte Chemie (International ed. in English)* 53, 9870-9875.
- [34] Hemmerich, P., and Nagelschneider, G. (1970) Chemistry and molecular biology of flavins and flavoproteins, *FEBS Letters* 8, 69-83.
- [35] Massey, V., and Palmer, G. (1966) On the existence of spectrally distinct classes of flavoprotein semiquinones. A new method for the quantitative production of flavoprotein semiquinones, *Biochemistry* 5, 3181-3189.
- [36] Stankovich, M. T., Schopfer, L. M., and Massey, V. (1978) Determination of glucose oxidase oxidation-reduction potentials and the oxygen reactivity of fully reduced and semiquinoid forms, *The Journal of biological chemistry* 253, 4971-4979.
- [37] Pan, J., Byrdin, M., Aubert, C., Eker, A. P. M., Brettel, K., and Vos, M. H. (2004) Excited-State Properties of Flavin Radicals in Flavoproteins: Femtosecond Spectroscopy of DNA Photolyase, Glucose Oxidase, and Flavodoxin, *The Journal of Physical Chemistry B* 108, 10160-10167.
- [38] Alston, T. A., Mela, L., and Bright, H. J. (1977) 3-Nitropropionate, the toxic substance of Indigofera, is a suicide inactivator of succinate dehydrogenase, *Proceedings of the National Academy of Sciences of the United States of America* 74, 3767-3771.
- [39] Coles, C. J., Edmondson, D. E., and Singer, T. P. (1979) Inactivation of succinate dehydrogenase by 3-nitropropionate, *The Journal of biological chemistry* 254, 5161-5167.
- [40] Alexi, T., Hughes, P. E., Faull, R. L., and Williams, C. E. (1998) 3-Nitropropionic acid's lethal triplet: cooperative pathways of neurodegeneration, *Neuroreport* 9, R57-64.
- [41] Francis, K., Smitherman, C., Nishino, S. F., Spain, J. C., and Gadda, G. (2013) The biochemistry of the metabolic poison propionate 3-nitronate and its conjugate acid, 3-nitropropionate, *IUBMB life* 65, 759-768.

- [42] Zanetti-Polzi, L., Aschi, M., Daidone, I., and Amadei, A. (2017) Theoretical modeling of the absorption spectrum of aqueous riboflavin, *Chem Phys Lett* 669, 119-124.
- [43] Salzmann, S., Tatchen, J., and Marian, C. M. (2008) The photophysics of flavins: What makes the difference between gas phase and aqueous solution?, *Journal of Photochemistry and Photobiology A: Chemistry* 198, 221-231.
- [44] Neiss, C., Saalfrank, P., Parac, M., and Grimme, S. (2003) Quantum Chemical Calculation of Excited States of Flavin-Related Molecules, *The Journal of Physical Chemistry A* 107, 140-147.
- [45] Kar, R. K., Borin, V. A., Ding, Y., Matysik, J., and Schapiro, I. (2018) Spectroscopic Properties of Lumiflavin: A Quantum Chemical Study, *Photochemistry and photobiology*.
- [46] Choe, Y.-K., Nagase, S., and Nishimoto, K. (2007) Theoretical study of the electronic spectra of oxidized and reduced states of lumiflavin and its derivative, *Journal of Computational Chemistry* 28, 727-739.
- [47] Hasegawa, J.-y., Bureekaew, S., and Nakatsuji, H. (2007) SAC-CI theoretical study on the excited states of lumiflavin: Structure, excitation spectrum, and solvation effect, *Journal of Photochemistry and Photobiology A: Chemistry* 189, 205-210.
- [48] Sikorska, E., Khmelinskii, I. V., Koput, J., and Sikorski, M. (2004) Electronic structure of lumiflavin and its analogues in their ground and excited states, *Journal of Molecular Structure: THEOCHEM* 676, 155-160.
- [49] Salzmann, S., and Marian, C. M. (2008) Effects of protonation and deprotonation on the excitation energies of lumiflavin, *Chem Phys Lett* 463, 400-404.
- [50] Climent, T., González-Luque, R., Merchán, M., and Serrano-Andrés, L. (2006) Theoretical Insight into the Spectroscopy and Photochemistry of Isoalloxazine, the Flavin Core Ring, *The Journal of Physical Chemistry A* 110, 13584-13590.
- [51] Klaumunzer, B., Kroner, D., and Saalfrank, P. (2010) (TD-)DFT calculation of vibrational and vibronic spectra of riboflavin in solution, *The journal of physical chemistry. B* 114, 10826-10834.
- [52] Wu, M., and Eriksson, L. A. (2010) Absorption spectra of riboflavin--a difficult case for computational chemistry, *The journal of physical chemistry. A* 114, 10234-10242.
- [53] Karasulu, B., Götze, J. P., and Thiel, W. (2014) Assessment of Franck–Condon Methods for Computing Vibrationally Broadened UV–vis Absorption Spectra of Flavin Derivatives: Riboflavin, Roseoflavin, and 5-Thioflavin, *Journal of Chemical Theory and Computation* 10, 5549-5566.
- [54] Salzmann, S., Martinez-Junza, V., Zorn, B., Braslavsky, S. E., Mansurova, M., Marian, C. M., and Gärtner, W. (2009) Photophysical Properties of Structurally and Electronically Modified Flavin Derivatives Determined by Spectroscopy and Theoretical Calculations, *The Journal of Physical Chemistry A* 113, 9365-9375.
- [55] Zenichowski, K., Gothe, M., and Saalfrank, P. (2007) Exciting flavins: Absorption spectra and spin–orbit coupling in light–oxygen–voltage (LOV) domains, *Journal of Photochemistry and Photobiology A: Chemistry* 190, 290-300.
- [56] Davari, M. D., Kopka, B., Wingen, M., Bocola, M., Drepper, T., Jaeger, K.-E., Schwaneberg, U., and Krauss, U. (2016) Photophysics of the LOV-Based Fluorescent Protein Variant iLOV-Q489K Determined by Simulation and Experiment, *The Journal of Physical Chemistry B* 120, 3344-3352.

- [57] Khrenova, M. G., Nemukhin, A. V., and Domratcheva, T. (2015) Theoretical Characterization of the Flavin-Based Fluorescent Protein iLOV and its Q489K Mutant, *The journal of physical chemistry. B* 119, 5176-5183.
- [58] Romero, E., Gomez Castellanos, J. R., Gadda, G., Fraaije, M. W., and Mattevi, A. (2018) Same Substrate, Many Reactions: Oxygen Activation in Flavoenzymes, *Chemical reviews* 118, 1742-1769.
- [59] Salvi, F., Agniswamy, J., Yuan, H., Vercammen, K., Pelicaen, R., Cornelis, P., Spain, J. C., Weber, I. T., and Gadda, G. (2014) The combined structural and kinetic characterization of a bacterial nitronate monooxygenase from *Pseudomonas aeruginosa* PAO1 establishes NMO class I and II, *The Journal of biological chemistry* 289, 23764-23775.
- [60] Smitherman, C., and Gadda, G. (2013) Evidence for a Transient Peroxynitro Acid in the Reaction Catalyzed by Nitronate Monooxygenase with Propionate 3-Nitronate, *Biochemistry* 52, 2694-2704.
- [61] Müller, F. (1991) *Chemistry and Biochemistry of Flavoenzymes.*, CRC Press., Boca Raton, FL, USA.
- [62] Lee, C., Yang, W., and Parr, R. G. (1988) Development of the Colle-Salvetti correlation-energy formula into a functional of the electron density, *Physical review B* 37, 785.
- [63] Becke, A. D. (1993) Density-functional thermochemistry. III. The role of exact exchange, *The Journal of chemical physics* 98, 5648-5652.
- [64] Kendall, R. A., Dunning Jr, T. H., and Harrison, R. J. (1992) Electron affinities of the first-row atoms revisited. Systematic basis sets and wave functions, *The Journal of chemical physics* 96, 6796-6806.
- [65] Klaumünzer, B., Kröner, D., and Saalfrank, P. (2010) (TD-)DFT Calculation of Vibrational and Vibronic Spectra of Riboflavin in Solution, *The Journal of Physical Chemistry B* 114, 10826-10834.
- [66] Miertuš, S., Scrocco, E., and Tomasi, J. (1981) Electrostatic interaction of a solute with a continuum. A direct utilization of AB initio molecular potentials for the prevision of solvent effects, *Chemical Physics* 55, 117-129.
- [67] Tomasi, J., Mennucci, B., and Cammi, R. (2005) Quantum mechanical continuum solvation models, *Chemical reviews* 105, 2999-3094.
- [68] Li, L., Li, C., Zhang, Z., and Alexov, E. (2013) On the Dielectric “Constant” of Proteins: Smooth Dielectric Function for Macromolecular Modeling and Its Implementation in DelPhi, *Journal of Chemical Theory and Computation* 9, 2126-2136.
- [69] Mozhayskiy, V., and Krylov, A. ezSpectrum, 2009, see <http://iopenshell.usc.edu/downloads>, *Google Scholar*.
- [70] Frisch, M., Trucks, G., Schlegel, H., Scuseria, G., Robb, M., Cheeseman, J., Scalmani, G., Barone, V., Petersson, G., and Nakatsuji, H. (2016) Gaussian 16, revision A.03, *Gaussian Inc., Wallingford CT*.
- [71] Moore, R. L., Baru, C., Baxter, D., Fox, G. C., Majumdar, A., Papadopoulos, P., Pfeiffer, W., Sinkovits, R. S., Strande, S., and Tatineni, M. Gateways to discovery: Cyberinfrastructure for the long tail of science, p 39, ACM.
- [72] Sarajlic, S., Edirisinghe, N., Wu, Y., Jiang, Y., and Faroux, G. Training-based Workforce Development in Advanced Computing for Research and Education (ACoRE), p 71, ACM.
- [73] Beinert, H. (1956) Spectral Characteristics of Flavin at the Semiquinoid Oxidation Level, *Journal of American Chemistry Society* 78, 5323-5328.

- [74] Müller, F., Brustlein, M., Hemmerich, P., Massey, V., and Walker, W. H. (1972) Light-absorption studies on neutral flavin radicals, *European journal of biochemistry* 25, 573-580.
- [75] Müller, F., Massey, V., Heizmann, C., Hemmerich, P., Lhoste, J. M., and Gould, D. C. (1969) The Reduction of Flavins by Borohydride: 3,4-Dihydroflavin, *European journal of biochemistry* 9, 392-401.
- [76] Massey, V., Curti, B., Muller, F., and Mayhew, S. G. (1968) On the reaction of borohydride with D- and L-amino acid oxidases, *The Journal of biological chemistry* 243, 1329-1330.
- [77] Draper, R. D., and Ingraham, L. L. (1968) A potentiometric study of the flavin semiquinone equilibrium, *Archives of biochemistry and biophysics* 125, 802-808.
- [78] Mayhew, S. G. (1999) The effects of pH and semiquinone formation on the oxidation-reduction potentials of flavin mononucleotide. A reappraisal, *European journal of biochemistry* 265, 698-702.
- [79] Drössler, P., Holzer, W., Penzkofer, A., and Hegemann, P. (2002) pH dependence of the absorption and emission behaviour of riboflavin in aqueous solution, *Chemical Physics* 282, 429-439.
- [80] Beldjoudi, Y., Osorio-Román, I., Nascimento, M. A., and Rawson, J. M. (2017) A fluorescent dithiadiazolyl radical: structure and optical properties of phenanthrenyl dithiadiazolyl in solution and polymer composites, *Journal of Materials Chemistry C* 5, 2794-2799.
- [81] Eckstein, J. W., Cho, K. W., Colepicolo, P., Ghisla, S., Hastings, J. W., and Wilson, T. (1990) A time-dependent bacterial bioluminescence emission spectrum in an in vitro single turnover system: energy transfer alone cannot account for the yellow emission of *Vibrio fischeri* Y-1, *Proceedings of the National Academy of Sciences* 87, 1466-1470.
- [82] Kurfürst, M., Ghisla, S., and Hastings, J. W. (1984) Characterization and postulated structure of the primary emitter in the bacterial luciferase reaction, *Proceedings of the National Academy of Sciences* 81, 2990-2994.
- [83] Zhou, D., Mirzakulova, E., Khatmullin, R., Schapiro, I., Olivucci, M., and Glusac, K. D. (2011) Fast Excited-State Deactivation in N(5)-Ethyl-4a-hydroxyflavin Pseudobase, *The Journal of Physical Chemistry B* 115, 7136-7143.
- [84] KOTAKI, A., and YAGI, K. (1970) Fluorescence Properties of Flavins in Various Solvents, *The Journal of Biochemistry* 68, 509-516.
- [85] Heelis, P. F. (1982) The photophysical and photochemical properties of flavins (isoalloxazines), *Chemical Society Reviews* 11, 15-39.
- [86] Chapman, S., Faulkner, C., Kaiserli, E., Garcia-Mata, C., Savenkov, E. I., Roberts, A. G., Oparka, K. J., and Christie, J. M. (2008) The photoreversible fluorescent protein iLOV outperforms GFP as a reporter of plant virus infection, *Proceedings of the National Academy of Sciences* 105, 20038-20043.
- [87] Mukherjee, A., Walker, J., Weyant, K. B., and Schroeder, C. M. (2013) Characterization of Flavin-Based Fluorescent Proteins: An Emerging Class of Fluorescent Reporters, *PLOS ONE* 8, e64753.
- [88] Kasha, M. (1950) Characterization of electronic transitions in complex molecules, *Discussions of the Faraday Society* 9, 14-19.
- [89] Berlman, I. (1971) *Handbook of fluorescence spectra of aromatic molecules*, Academic Press, New York.
- [90] IUPAC (1997) *Compendium of Chemical Terminology* 2nd ed., Blackwell Scientific Publications, Oxford.

- [91] Demchenko, A. P., Tomin, V. I., and Chou, P.-T. (2017) Breaking the Kasha Rule for More Efficient Photochemistry, *Chemical reviews* 117, 13353-13381.
- [92] Hayes, R. T., Walsh, C. J., and Wasielewski, M. R. (2004) Competitive Electron Transfer from the S₂ and S₁ Excited States of Zinc meso-Tetraphenylporphyrin to a Covalently Bound Pyromellitimide: Dependence on Donor–Acceptor Structure and Solvent, *The Journal of Physical Chemistry A* 108, 2375-2381.
- [93] El-Sayed, M. A. (1963) Spin—Orbit Coupling and the Radiationless Processes in Nitrogen Heterocyclics, *The Journal of Chemical Physics* 38, 2834-2838.
- [94] Okamura, T., Sancar, A., Heelis, P. F., Hirata, Y., and Mataga, N. (1989) Doublet-quartet intersystem crossing of flavin radical in DNA photolyase, *Journal of the American Chemical Society* 111, 5967-5969.

5 CHAPTER 5: A REVERSIBLE, CHARGE-INDUCED INTRAMOLECULAR C4A-S-CYSTEINYL-FLAVIN IN CHOLINE OXIDASE VARIANT S101C

(This chapter has been published verbatim in Su, D., Yuan, H.L., and Gadda, G. (2017), *Biochemistry* 56: 6677-6690. The author's contribution involves data analysis and interpretation.)

5.1 Abstract

Choline oxidase serves as a paradigm for alcohol oxidation catalyzed by flavin-dependent enzymes. In its active site, S101 is 4 Å from the flavin C4a atom on an extended loop. Enzyme variants substituted at S101 were generated in a previous study and investigated mechanistically [Yuan, H., Gadda, G. (2011) *Biochemistry* 50, 770-779]. In this study, the typical UV-visible absorption spectrum of oxidized flavin was observed for the S101C enzyme in HEPES, TES or sodium phosphate, whereas an absorption spectrum suggesting the presence of a Ca4 flavin adduct with cysteine was obtained in Tris-Cl at pH 8.0. pH titrations of the UV-visible absorption spectrum of the wild-type, S101A, S101C, and H99N enzymes in the presence and absence of Tris allowed for the determination of two pK_a values that define a pH range in which the C4a-S-cysteinyll flavin is stabilized. Inhibition studies and stopped-flow kinetics demonstrated that binding of protonated Tris in the active site of the S101C enzyme is required to form the C4a-S-cysteinyll flavin. Deuterium kinetic isotope effects and proton inventories on the S101C enzyme mixed in a stopped-flow spectrophotometer with Tris established a mechanism for the reversible formation of the C4a-S-cysteinyll flavin. The study provides a detailed mechanistic analysis for the reversible formation of a bicovalent C4a-S-cysteinyll-8 α -N³-histidyl flavin in choline oxidase, identifying an optimal pH range and a mechanistic rationale for the stabilization of *de novo* C4a-S-cysteinyll-flavins. Moreover, it presents an example of an intramolecular reaction of an enzyme-bound flavin without a substrate.

5.2 Introduction

An increasing number of flavoproteins have the flavin cofactor covalently linked to the protein moiety, despite 85-90% are estimated to have the flavin tightly bound but not covalently associated with the protein.^{1, 2} The first reported enzyme with a flavin covalently attached to the protein moiety was mammalian succinate dehydrogenase in 1970.³ Most of the covalent attachments of the flavins to the proteins occur at either the 8 α -CH₃ group or C6 atom of the isoalloxazine, irrespective of whether the flavin is FMN or FAD.^{1, 2} The residues that have been found covalently linked to the 8 α -CH₃ of the isoalloxazine are histidine, cysteine, tyrosine, and aspartate, yielding 8 α -N¹-histidyl-, 8 α -N³-histidyl-, 8 α -S-cysteinyl-, 8 α -O-tyrosyl-, and 8 α -O-aspartidyl-flavins, respectively.^{1, 2, 4} Instead, only 6-S-cysteinyl-flavin linkages have been found thus far for the linkage at the C6 atom of the flavin.^{1, 2} Recently, bicovalent 8 α -N¹-histidyl- and 6-S-cysteinyl-FAD linkages were found in glucooligosaccharide oxidase,^{5, 6} hexose oxidase,⁷ aclacinomycin oxidoreductase⁸ and the berberine bridge enzyme.^{9, 10} The first example of an engineered bicovalently-linked flavoprotein is 6-hydroxy-D-nicotine oxidase, where mutation of H130 to cysteine yielded a new 6-S-cysteinyl-flavin linkage besides the naturally occurring 8 α -N¹-histidyl linkage.¹¹ The engineered 6-S-cysteinyl-flavin bond could be cleaved by treatment with performic acid of the denatured 6-hydroxy-D-nicotine oxidase, but no attempts were reported to cleave the bond in the folded and active enzyme.¹¹ In general, covalent linkages of the flavin to the protein serve to stabilize protein structure,¹²⁻¹⁴ prevent loss of the flavin cofactor,¹⁵ modulate the redox potential of the flavin cofactor,¹⁴⁻¹⁹ facilitate electron transfer reactions²⁰ and quantum mechanical transfers of hydride ions from the substrate to the flavin,²¹ or contribute to substrate binding.¹⁴ In all cases, the covalent linkages between the 6 or 8 α positions of the isoalloxazine and the protein are irreversible and preserved during the functional cycles of the enzymes.

Transient, covalent flavinylation to active site cysteine residues is also known to occur at the C4a atom of the isoalloxazine. A well-known example is the C4a-S-cysteinyl-flavin with C140 in a mercuric ion reductase variant in which C135, C558, and C559, were replaced with alanine residues.²² Based on mechanistic and biochemical studies, similar C4a-S-cysteinyl-flavin species have been proposed for other members of the flavoprotein disulfide reductase enzymes of which mercuric ion reductase is a member, such as pig heart lipoamide dehydrogenase,^{23, 24} glutathione reductase,²⁵ and thioredoxin reductase.²⁶ UV-Visible absorbance, Fourier Transform Infrared Spectroscopy, and X-ray crystallography, provided unequivocal evidence for a C4a-S-cysteinyl-flavin adduct in the LOV domain of bacterial and fungal and plant photoreceptors.²⁷⁻³⁰ Typically, the C4a-S-cysteinyl-flavins are kinetically competent intermediates in the flavoprotein disulfide reductases and participate in signal transduction through the light-dark cycle of photoreceptors.^{22, 27-31} To the best of our knowledge, reversible C4a-S-cysteinyl-flavins have not been engineered in flavoproteins, irrespective of whether the flavin is already noncovalently or covalently bound to the protein moiety.

In the X-ray, crystallographic structure of choline oxidase, the FAD cofactor is covalently attached to the protein via H99 through an 8α -N³-histidyl linkage (Figure 5.1). The enzyme, which catalyzes the oxidation of choline to glycine betaine through two FAD-associated oxidation reactions, has been characterized in its biochemical, mechanistic, and structural properties,^{21, 32-48} becoming a paradigm for the oxidation of alcohols catalyzed by flavoproteins.⁴⁹⁻⁵¹ A recent study in which S101 was substituted with alanine, cysteine, threonine or valine, demonstrated the importance of the hydrophilic character of the serine residue for the hydride transfer reaction catalyzed by choline oxidase.^{37, 38} A crystallographic structure of the S101A variant of choline oxidase to 2.2 Å resolution showed that the active site residues are in the same positions and

orientations in the mutant and wild-type enzymes, with no significant differences observed between the backbone atoms of the two enzymes with an rmsd value of 0.41 Å for 527 equivalent C α atoms.³⁸ In the active site of the wild-type enzyme, the hydroxyl O atom of S101, which is part of an extended flexible loop, points toward the flavin C4a atom at <4 Å distance (Figure 5.1).^{35, 44}

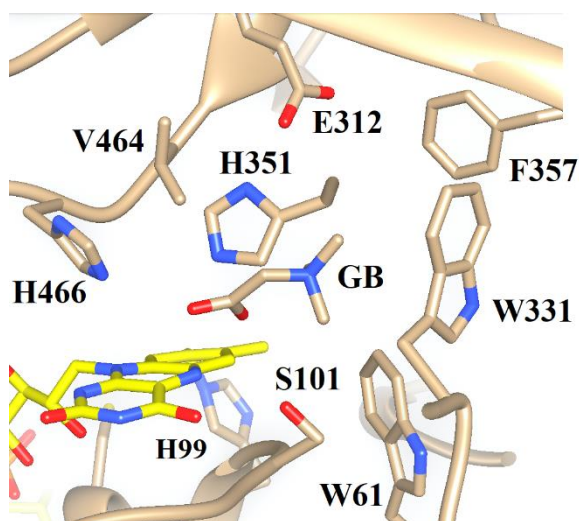


Figure 5.1 The active site of choline oxidase wild-type with the reaction product glycine betaine bound (PDB entry 4MJW). The C atoms of the FAD cofactor are displayed as yellow sticks, whereas those of select protein portions and of glycine betaine are shown as tan sticks; N and O atoms are colored in blue and red, respectively. GB, glycine betaine; except for W61 and W331, amino acid residues shown have been previously characterized with mutagenesis.

Following upon an initial serendipitous observation of an unusual UV-visible absorption spectrum of the S101C variant of choline oxidase in Tris buffer (Hongling Yuan and Giovanni Gadda; unpublished data), in this study the S101C enzyme variant was characterized using UV-visible absorption spectroscopy in various buffers and pH values, inhibition studies using steady-state kinetics, solvent kinetic isotope effects and proton inventory using rapid kinetics. The assignment of the pK_a values for the ionizations of the various species involved in the reversible formation of the engineered C4a-S-cysteinyl-flavin in the S101C enzyme was aided by determining the pH effects on the UV-visible absorption spectra of the wild-type, H99N, and

S101A enzymes. A mechanism for the reversible formation of the extra C4a-S-cysteinyl-flavin linkage in the S101C enzyme is presented along with the evidence in its support.

5.3 Material and Methods

Materials and Instruments. The H99N, S101C, and S101A variants and the wild-type form of choline oxidase were purified according to the procedures described in.^{21, 37, 38} Choline chloride was from ICN Pharmaceutical Inc.; Tris was from Fisher Scientific. All other reagents were of the highest purity commercially available.

UV-visible absorption spectra of the enzyme-bound flavin were recorded using an Agilent Technologies model HP 8453 diode array spectrophotometer equipped with a thermostated water bath. The enzymatic activity of choline oxidase was measured polarographically using a computer-interfaced Oxy-32 oxygen monitoring system (Hansatech Instrument, U. K.). Stopped-flow experiments were carried out using a Hi-Tech SF-61 Double Mixing Stopped Flow system.

UV-visible Absorption Spectroscopy. For the pH dependence of the UV-visible absorption spectra, the enzymes were gel filtered just prior to use through a desalting PD-10 column equilibrated with 20 mM sodium phosphate and 20 mM sodium pyrophosphate in the presence or absence of 20 mM Tris at a pH adjusted to ~6.0. The enzyme solution (2 mL) was placed in a cuvette with a concentration of enzyme-bound flavin ~10 μ M and the absorption spectrum was recorded. The UV-visible absorption spectra of the enzyme solution were recorded after serial additions of 1M NaOH (1-10 μ L) under stirring until the pH was incrementally changed to ~12.0. After each careful and slow addition of the base the enzyme solution could equilibrate until no changes in the pH value and absorbance were observed, which typically required 2-3 min.

Enzyme Kinetic Assays. Reversible inhibition studies were carried out by varying the concentrations of both choline and Tris in air-saturated 50 mM potassium phosphate, pH 6.0, by monitoring the rate of oxygen consumption with a computer-interfaced Oxy-32 oxygen-monitoring system (Hansatech Instrument, U. K.) thermostated at 25 °C. The reversible formation of the C4a-S-cysteinyl-flavin adduct was monitored directly in an SF-61DX2 Hi-Tech KinetAsyst high performance stopped-flow spectrophotometer thermostated at 25 °C by monitoring the decrease in absorbance at 456 nm upon mixing the enzyme solution with an equal volume of Tris solution. The solutions of both the enzyme and Tris were prepared in 50 mM potassium phosphate, pH 8.0, or 50 mM sodium pyrophosphate, pH 8.5 or 9.0. The pH of the Tris solution was adjusted after dissolving the compound in the buffer to avoid pH effects. The apparent rate constants were determined under pseudo-first order conditions by mixing equal volumes of an enzyme solution (~10 μM after mixing) and varying concentrations of Tris (2.5-100 mM after mixing). When D₂O was used instead of water, the pD value of the buffered solutions containing the enzyme and Tris were adjusted using NaOD or DCl based on the empirical relationship of eq 1, which describes the correction of the pH-meter reading and the pD value at varying mole fractions of D₂O (n) and accounts for the isotope effect on the ionization of the buffer.⁵² Solvent viscosity effects were measured in the presence of 9% glycerol as viscosigen in both the solutions containing the enzyme and Tris, which yielded a relative viscosity of 1.25 that was equivalent to that of D₂O.⁵³

$$(\Delta\text{pH})_n = 0.076n^2 + 0.3314n \quad (1)$$

Data Analysis. Data were fit with KaleidaGraph software (Synergy Software, Reading, PA) and the Hi-Kinetic Studio Software Suite (Hi-Tech Scientific, Bradford on Avon, U.K.). The kinetic data with inhibitor were fit to eq 2, which describes a competitive inhibition pattern of the

inhibitor versus choline; I is the concentration of inhibitor and K_{is} is the inhibition constant for the slope term.

Stopped-flow traces were fit to eq 3, which describes a double-exponential processes for the decrease in absorbance of the enzyme-bound oxidized flavin; k_{obs1} and k_{obs2} represent the observed first-order rate constants associated with the decrease in absorbance at 456 nm, t is time, A_t is the absorbance at 456 nm at any given time, A_1 , and A_2 are the amplitudes of the absorption changes, and A_∞ is the absorbance at infinite time.

The rapid kinetics parameters were extracted from the dependence of the observed rate constant on the concentration of Tris by using eq 4; k_{obs1} is the observed first-order rate constant for the fast phase of absorbance decrease at 456 nm (see Results for a rationale for the use of the fast phase), k_3 is the limiting first-order rate constant for the formation of the C4a-S-cysteinyflavin adduct at saturating concentrations of Tris, k_4 is the first-order rate constant for the reverse of the formation of the C4a-S-cysteinyflavin adduct, and K_d^{app} is the concentration of Tris at which half-maximal formation of the C4a-S-cysteinyflavin adduct is observed.

The effect of pH on the UV-visible absorption spectra of the various variants of choline oxidase was determined with eqs 5-7 to establish the pK_a values for the ionizations relevant to the 8α -N³-histidyl-FAD of choline oxidase; because all the enzyme variants yielded a high pK_a value >11.3 that was separated ≥ 2 pH units from other lower pK_a values, the data at low and high pH values were fit independently; isosbestic points were chosen when available for the determination of the pK_a values involving the ionizations of other flavin associated group. Eq 5 describes a curve with one pK_a value and plateau regions at both low and high pH values; eq 6 describes a curve with two pK_a values and three plateau regions at low, middle, and high pH values, and eq 7 describes a curve with slopes of 1 and -1 and three plateau regions at low, middle, high pH values.

$$\frac{v}{e} = \frac{k_{cat}A}{K_a\left(1 + \frac{I}{K_{is}}\right) + A} \quad (2)$$

$$A_t = A_1 \exp(-k_{obs1}t) + A_2 \exp(-k_{obs2}t) + A_\infty \quad (3)$$

$$k_{obs1} = \frac{k_3 A}{K_d^{app} + A} + k_4 \quad (4)$$

$$Y = \frac{A}{1 + 10^{(pH - pK_a)}} + \frac{B}{1 + 10^{(pK_a - pH)}} \quad (5)$$

$$Y = \frac{A}{1 + 10^{(pH - pK_{a1})}} + \frac{B}{1 + 10^{(pH - pK_{a2})}} + \frac{C}{1 + 10^{(pK_{a2} - pH)}} \quad (6)$$

$$Y = \frac{A \times 10^{-pK_{a1}} + B \times 10^{-pH}}{10^{-pK_{a1}} + 10^{-pH}} + \frac{C \times 10^{-pK_{a2}} + A \times 10^{-pH}}{10^{-pK_{a2}} + 10^{-pH}} \quad (7)$$

5.4 Results

Effect of Tris on the UV-Visible Absorption Spectrum of the S101C Enzyme. The UV-visible absorption spectrum of the S101C enzyme was acquired at pH 8.0 and 25 °C in various buffers. In 20 mM Tris-Cl, a broad absorption band with a peak at 376 nm was observed (Figure 5.2A), consistent with the enzyme being in a mixture of a C4a flavin adduct and the oxidized state. The same enzyme variant in 20 mM sodium phosphate, TES, or HEPES, showed the typical maxima of the oxidized flavin at 371 nm and 456 nm (Figure 5.2A). In contrast, the wild-type, S101T, and S101A enzymes in 20 mM Tris-Cl displayed flavin maxima in the near-UV and visible regions typical of oxidized flavins (Figure 5.2B). Thus, a C4a-S-cysteinyl-flavin is stabilized in the choline oxidase variant with C101 in the presence of Tris at pH 8.0.

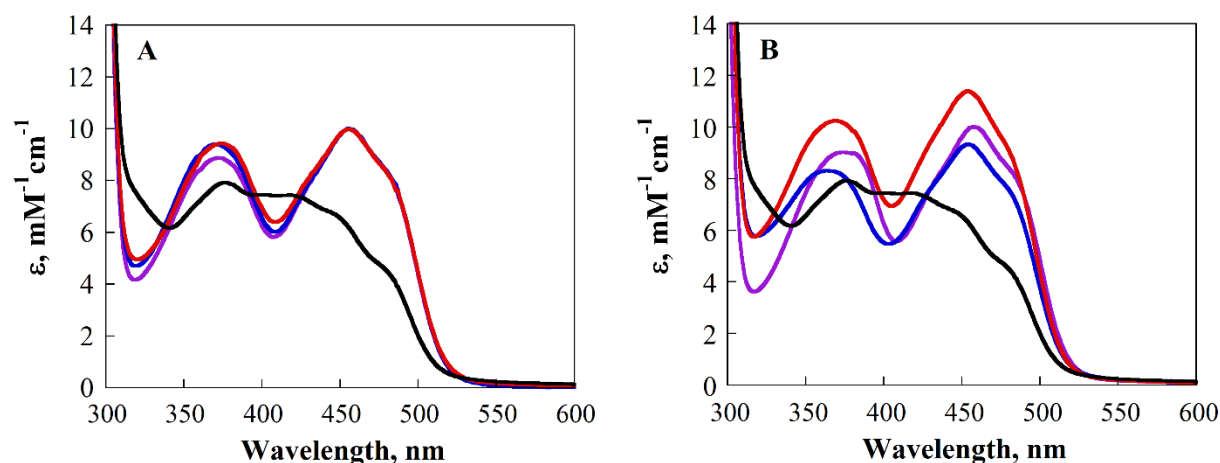


Figure 5.2. Effect of Tris on the UV-visible absorption spectrum of the S101C enzyme. (A) S101C enzyme in 20 mM Tris-Cl (black), TES (red), HEPES (blue), and sodium phosphate (purple), pH 8.0 and 25 °C. (B) UV-visible absorption spectra of the S101C (black), S101T (blue), S101A (purple), and wild-type (red) enzymes in 20 mM Tris-Cl, pH 8.0 and 25 °C.

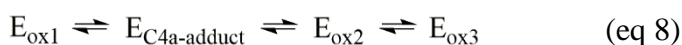
Effect of pH on the UV-Visible Absorption Spectrum of the S101C Enzyme with Tris.

The effect of pH on the UV-visible absorption spectrum of the S101C in the presence of 20 mM Tris was determined to establish the pK_a values for ionizations relevant to the stabilization of the C4a-S-cysteinyl-flavin. In the presence of Tris at pH 6.2, the S101C enzyme exhibited absorption maxima at 371 nm and 455 nm indicative of the flavin being in the oxidized state (blue species in Figure 5.3A); both maxima decreased with increasing pH from 6.2 to 8.7 with a concomitant increase of absorbance at 410 nm, yielding a C4a-S-cysteinyl-flavin (black species in Figure 5.3A). Further increasing pH to 10.2 resulted in an oxidized flavin with the two maxima at 354 nm and 448 nm (red species in Figure 5.3A).

The determination of the pK_a values for the equilibria involving the C4a-S-cysteinyl-flavin required establishing the isosbestic points between the oxidized flavin species at low and high pH values, which were determined by plotting the difference spectra between the species at pH 10.2

minus the species seen at the other pH values (intersecting points between the blue and red species in Figure 5.3B). A plot of the $\Delta\epsilon_{(438\text{ nm} - 402\text{ nm})}$ as a function of the pH value yielded two pK_a values of 6.8 ± 0.1 and 9.5 ± 0.1 for an unprotonated group and a protonated group that are required for the stabilization of the C4a-S-cysteinyl-flavin, respectively (Figure 5.3B inset).

Further increasing pH to more alkaline values yielded a hypsochromic shift of the flavin high-energy band to 344 nm, and a concomitant bathochromic shift of the low-energy band to 455 nm, with a set of isosbestic points at 367 nm and 428 nm (Figure 5.3C). A pK_{a3} value of ≥ 11.3 was established by plotting the differences between the positive peak at 380 nm and the negative peak at 340 nm of the difference spectra as a function of pH (Figure 5.3D). Thus, the individual analysis of the absorption spectra of the S101C enzyme in the presence of Tris identified three equilibria of the enzyme versus pH, involving three forms of oxidized enzyme and a form of the enzyme with a C4a-S-cysteinyl-flavin (eq 8).



A global fitting of the data from pH 6.2 to pH 12.0 using the Specfit32 software to an equilibrium model of four species (eq 8) in the S101C enzyme in the presence of Tris returned three pK_a values of 6.9, 9.3, and ≥ 11.1 (Figure 5.3E), in good agreement with the results obtained from the individual analysis of the difference spectra. The UV-visible absorption spectra of the four enzyme-species extracted from the global fitting analysis were in good agreement with the species seen experimentally (Figure 5.3F).

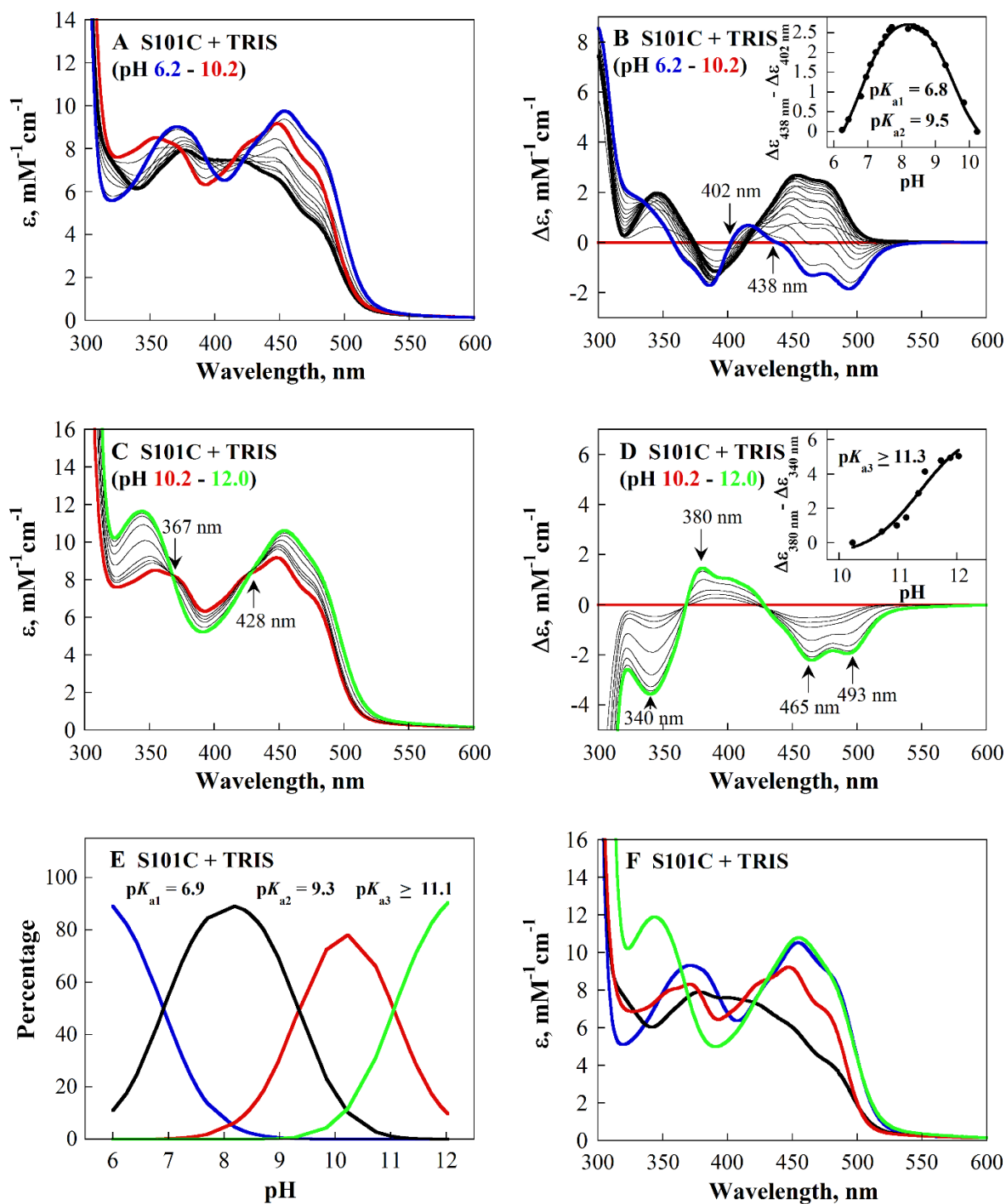


Figure 5.3 Effect of pH on the UV-visible absorption spectrum of the S101C enzyme with 20 mM Tris in 20 mM sodium phosphate, 20 mM sodium pyrophosphate, 15 °C. (A) S101C enzyme in the range of pH 6.2 (blue) to pH 10.2 (red). (B) Difference UV-visible absorption spectra between the species at pH 10.2 minus the species seen at lower pH values in panel A. Inset: plot of the $\Delta\epsilon_{(438\text{ nm} - 402\text{ nm})}$ as a function of the pH, the curve is the fit of the data to eq 7. (C) S101C enzyme in the range of pH 10.2 (red) to pH 12.0 (green). (D) Difference UV-visible absorption spectra between the species at pH 10.2 minus the species seen at higher pH values in panel C. Inset: plot of the $\Delta\epsilon_{(380\text{ nm} - 340\text{ nm})}$ as a function of the pH, the curve is the fit of the data to eq 5. (E) Global fitting of the data from pH 6.2 to pH 12.0 using the Specfit32 software to an equilibrium model of four species shown in eq 8. (F) Simulated UV-visible absorption spectra extracted from the global fitting analysis.

Effect of pH on the UV-Visible Absorption Spectra of the S101C, S101A, and Wild-type

Enzymes. In the absence of Tris, the UV-visible absorption spectrum of the S101C enzyme at pH 6.3 displayed two maxima at 370 nm and 457 nm (Figure 5.4A). Increasing pH yielded two sets of spectral changes, which identified two well-separated pK_a values of 8.0 ± 0.1 , which was associated with hypsochromic shifts of both bands of the oxidized flavin (Figure 5.4A-B), and of ≥ 12.0 , which was associated with spectral changes like those seen at high pH in the S101C enzyme with Tris (Figure 5.4C-D). No flavin species resembling a C4a-S-cysteinyl-flavin was observed in the pH titration of the S101C enzyme without Tris.

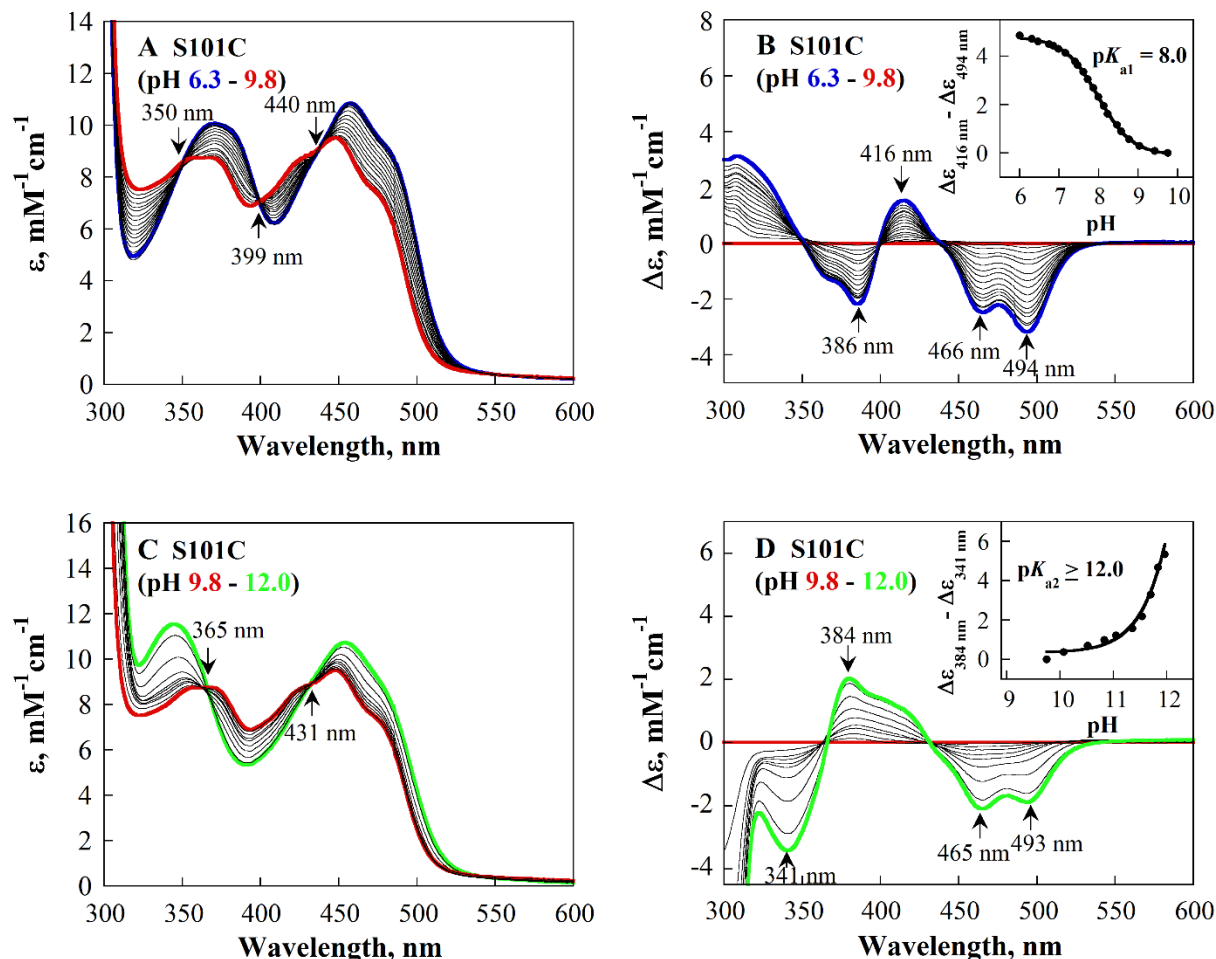


Figure 5.4 Effect of pH on the UV-visible absorption spectrum of the S101C enzyme in 20 mM sodium phosphate, 20 mM sodium pyrophosphate, 15 °C. (A) S101C enzyme in the range of pH 6.3 (blue) to pH 9.8 (red). (B) Difference UV-visible absorption spectra between the species at pH 9.8 minus the species seen at lower pH values in panel A. Inset: plot of the $\Delta\epsilon_{(416\text{ nm} - 494\text{ nm})}$ as a function of the pH, the curve is the fit of the data to eq 5. (C) S101C enzyme in the range of pH 9.8 (red) to pH 12.0 (green). (D) Difference UV-visible absorption spectra between the species at pH 9.8 minus the species seen at higher pH values in panel C. Inset: plot of the $\Delta\epsilon_{(384\text{ nm} - 341\text{ nm})}$ as a function of the pH, the curve is the fit of the data to eq 5.

The pH titrations of the wild-type and S101A enzymes were also carried out as controls. Both the wild-type and S101A enzymes in the absence of Tris yielded results like those of the S101C enzyme without Tris (Figure 5.5 and 5.6), with spectral changes associated with

hypsochromic shifts of the bands of the oxidized flavin at low pH values and a large hypsochromic shift of the flavin high-energy band at more alkaline pH values. The pK_a values associated with the spectral changes in the wild-type enzyme were 8.2 ± 0.1 and ≥ 11.6 (Figure 5.5), and 8.6 ± 0.1 and ≥ 12.0 for the S101A enzyme (Figure 5.6).

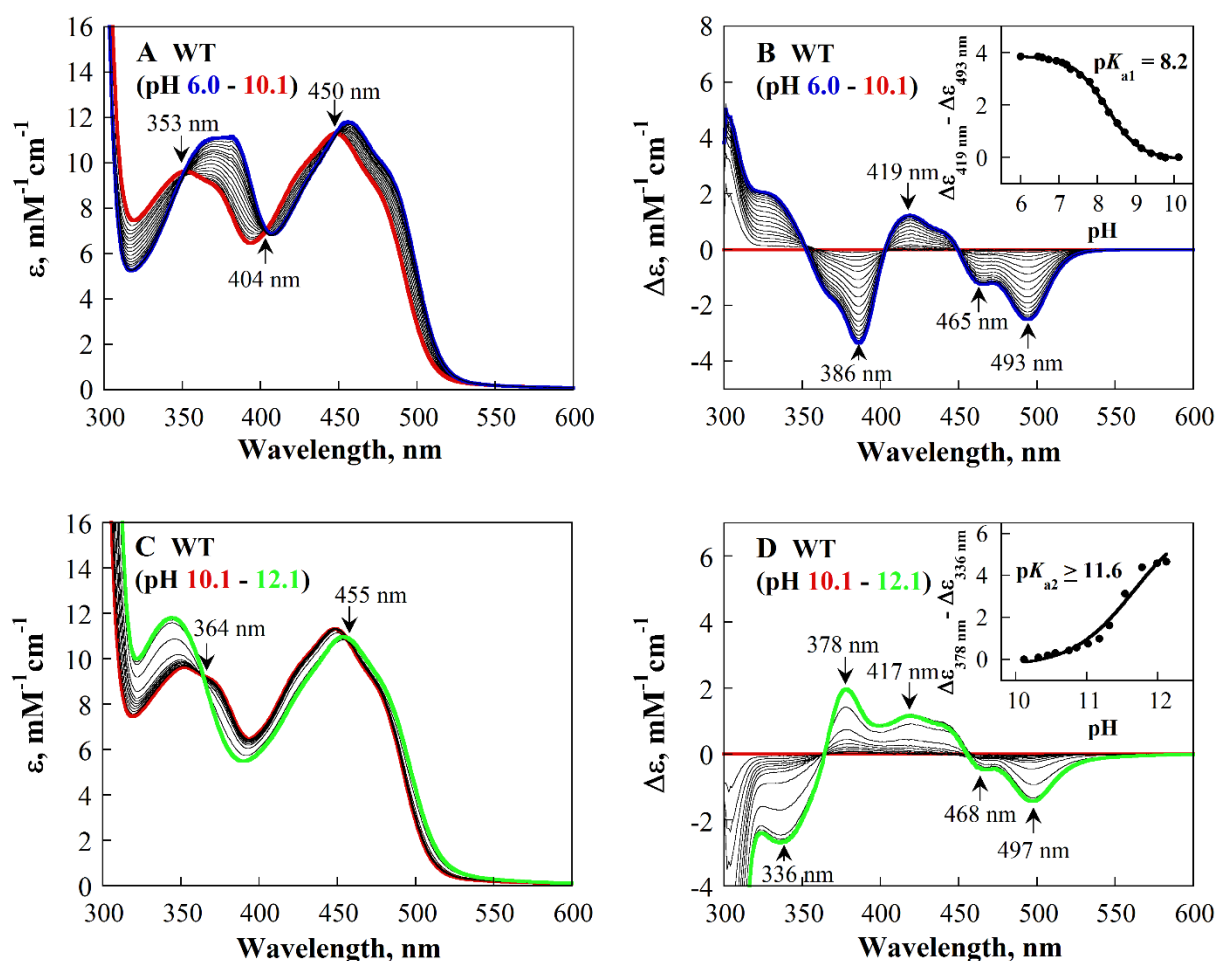


Figure 5.5 Effect of pH on the UV-visible absorption spectrum of the wild-type enzyme in 20 mM sodium phosphate, 20 mM sodium pyrophosphate, 15 °C. (A) Wild-type enzyme in the range of pH 6.0 (blue) to pH 10.1 (red). (B) Difference UV-visible absorption spectra between the species at pH 10.1 minus the species seen at lower pH values in panel A. Inset: plot of the $\Delta\epsilon_{(419\text{ nm} - 493\text{ nm})}$ as a function of the pH, the curve is the fit of the data to eq 5. (C) Wild-type enzyme in the range of pH 10.1 (red) to pH 12.1 (green). (D) Difference UV-visible absorption spectra

between the species at pH 10.1 minus the species seen at higher pH values in panel C. Inset: plot of the $\Delta\epsilon_{(378 \text{ nm} - 336 \text{ nm})}$ as a function of the pH, the curve is the fit of the data to eq 5.

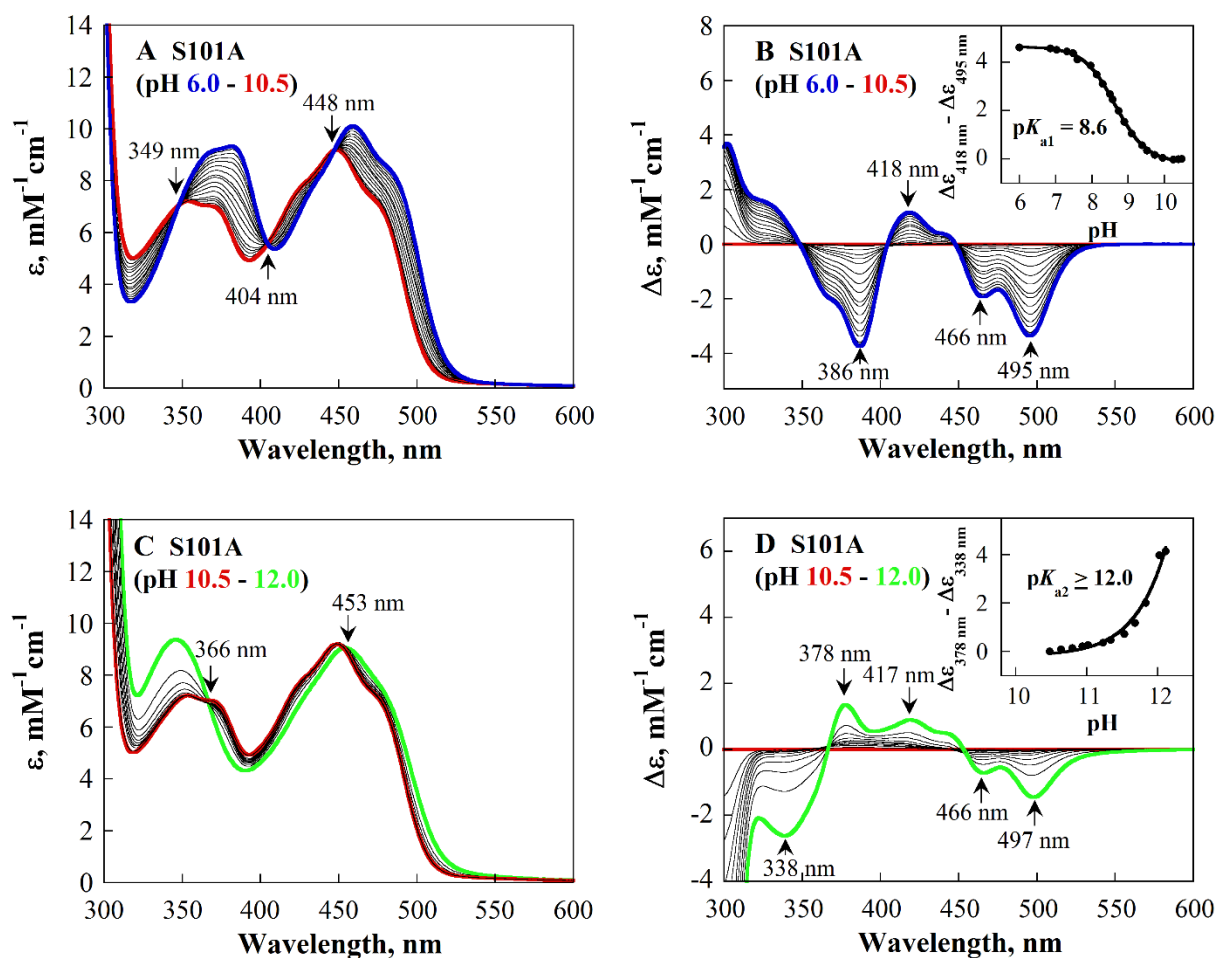


Figure 5.6 Effect of pH on the UV-visible absorption spectrum of the S101A enzyme in 20 mM sodium phosphate, 20 mM sodium pyrophosphate, 15 °C. (A) S101A enzyme in the range of pH 6.0 (blue) to pH 10.5 (red). (B) Difference UV-visible absorption spectra between the species at pH 10.5 minus the species seen at lower pH values in panel A. Inset: plot of the $\Delta\epsilon_{(418 \text{ nm} - 495 \text{ nm})}$ as a function of the pH, the curve is the fit of the data to eq 5. (C) S101A enzyme in the range of pH 10.5 (red) to pH 12.0 (green). (D) Difference UV-visible absorption spectra between the species at pH 10.5 minus the species seen at higher pH values in panel C. Inset: plot of the $\Delta\epsilon_{(378 \text{ nm} - 338 \text{ nm})}$ as a function of the pH, the curve is the fit of the data to eq 5.

Effect of pH on the UV-Visible Absorption Spectrum of the Wild-type Enzyme with Tris.

In the presence of Tris, the pH dependence of the UV-visible absorption spectrum of the wild-type enzyme was like that without Tris (Figure 5.7), but in the pH range from 6.0 to 10.5 two ionizations were present instead of the single one seen when Tris was absent (Figure 5.7B). A pK_a of 7.3 ± 0.1 , which accounted for $\sim 80\%$ of the change in the $\Delta\varepsilon_{(417 \text{ nm} - 493 \text{ nm})}$ as a function of pH, and a pK_a of 8.9 ± 0.1 , which accounted for $\sim 20\%$ of the change in the $\Delta\varepsilon_{(417 \text{ nm} - 493 \text{ nm})}$ as a function of pH, were established.

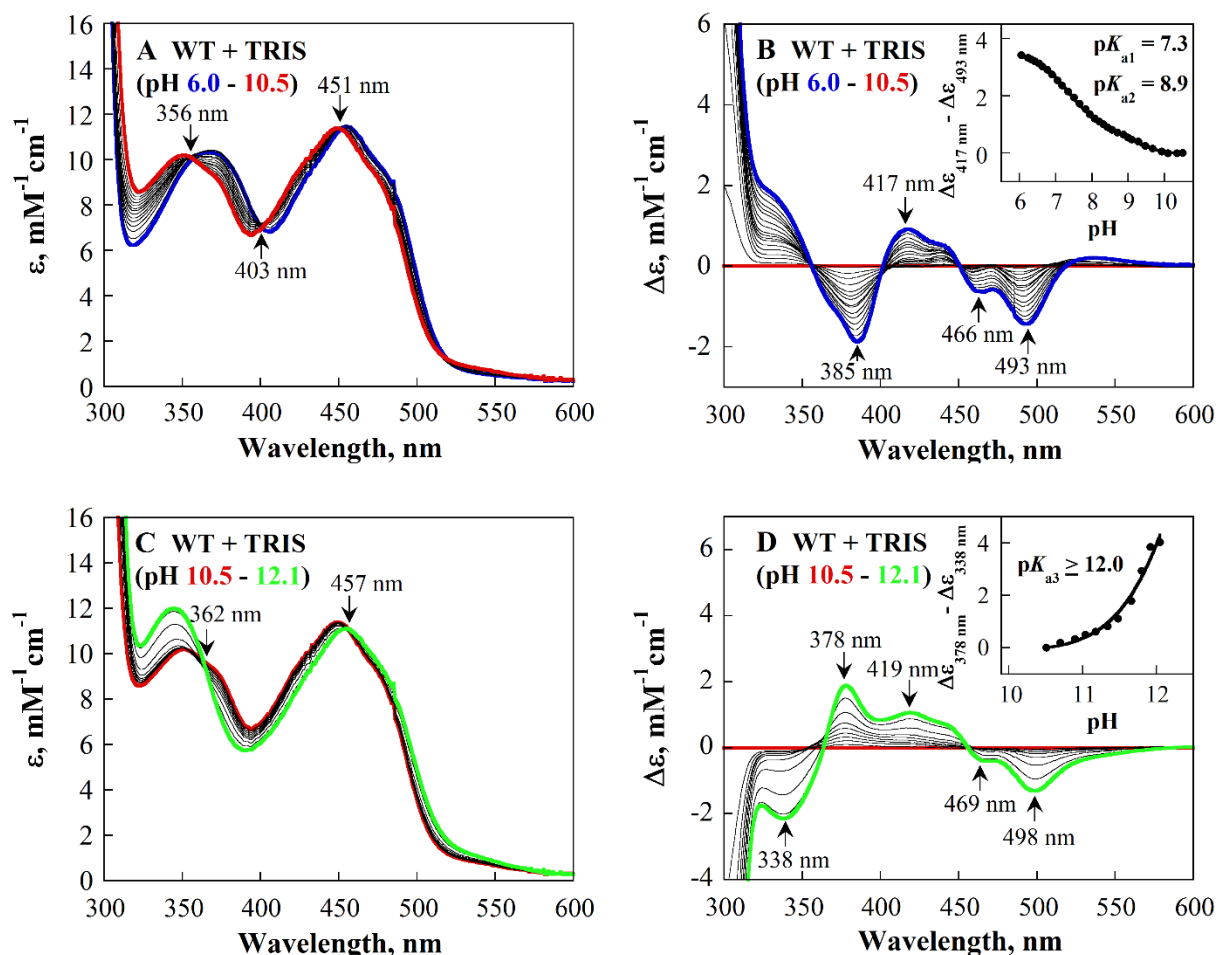


Figure 5.7 Effect of pH on the UV-visible absorption spectrum of the wild-type enzyme with 20 mM Tris, in 20 mM sodium phosphate, 20 mM sodium pyrophosphate, 15 °C. (A) Wild-type enzyme in the range of pH 6.0 (blue) to pH 10.5 (red). (B) Difference UV-visible absorption spectra between the species at pH 10.5 minus the species seen at lower pH values in panel A. Inset: plot of the $\Delta\epsilon_{(417\text{ nm} - 493\text{ nm})}$ as a function of the pH, the curve is the fit of the data to eq 6. (C) Wild-type in the range of pH 10.5 (red) to pH 12.1 (green). (D) Difference UV-visible absorption spectra between the species at pH 10.5 minus the species seen at higher pH values in panel C. Inset: plot of the $\Delta\epsilon_{(378\text{ nm} - 338\text{ nm})}$ as a function of the pH, the curve is the fit of the data to eq 5.

Effect of pH on the UV-Visible Absorption Spectrum of the H99N Enzyme. The effect of pH on the UV-visible absorption spectrum of the H99N enzyme, in which the flavin is tightly but not covalently bound to the protein²¹, was determined to establish which spectral changes and pK_a

value were associated with the ionization of the N3 atom of the flavin. As expected, only a single ionization was observed with the H99N enzyme, with a hypsochromic shift of the high-energy band from 395 nm at pH 7.5 to 358 nm at pH 11.9 (Figure 5.8A). As shown in Figure 5.8B, a single pK_a value of 10.0 ± 0.1 was determined. A small perturbation of the UV-visible absorption spectrum of the H99N enzyme that could not be fit due to its negligible magnitude was also observed between pH 7.5 and pH 9.1 (Figure 5.8A), probably due to a pH-dependent change in the microenvironment around the flavin.

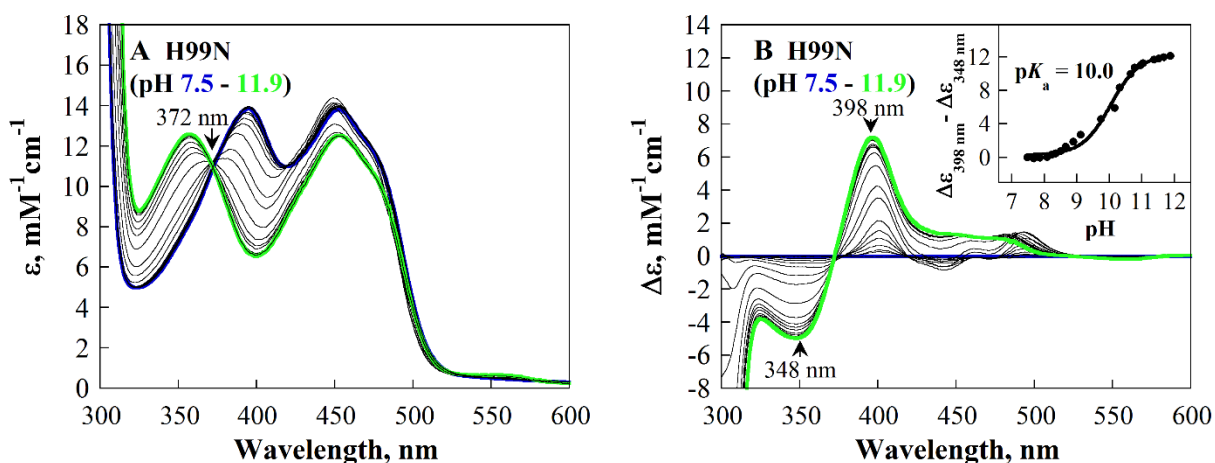


Figure 5.8 Effect of pH on the UV-visible absorption spectrum of the H99N enzyme in 20 mM sodium phosphate, 20 mM sodium pyrophosphate, 15 °C. (A) H99N enzyme in the range of pH 7.5 (blue) to pH 11.9 (green). (B) Difference UV-visible absorption spectra between the species at pH 11.9 minus the species seen at lower pH values in panel A. Inset: plot of the $\Delta\epsilon(398 \text{ nm} - 348 \text{ nm})$ as a function of the pH, the curve is the fit of the data to eq 5.

Competitive Inhibition of Choline Oxidase by Tris. A previous study established that many ternary amines are competitive inhibitors of choline oxidase with choline as a substrate.⁵⁴ The effect of Tris as an inhibitor of choline oxidase was studied here by determining the initial rates of reaction in a Clark-type electrode equilibrated at atmospheric oxygen with choline as a substrate for wild-type choline oxidase in 50 mM sodium phosphate, pH 6.0 and 25 °C. As shown

in Figure 5.9, a double reciprocal plot of the initial rates of reaction *versus* the concentration of choline acquired at fixed concentrations of Tris yielded lines intersecting on the y-axis. These data are consistent with Tris being a competitive inhibitor of choline in wild-type choline oxidase.

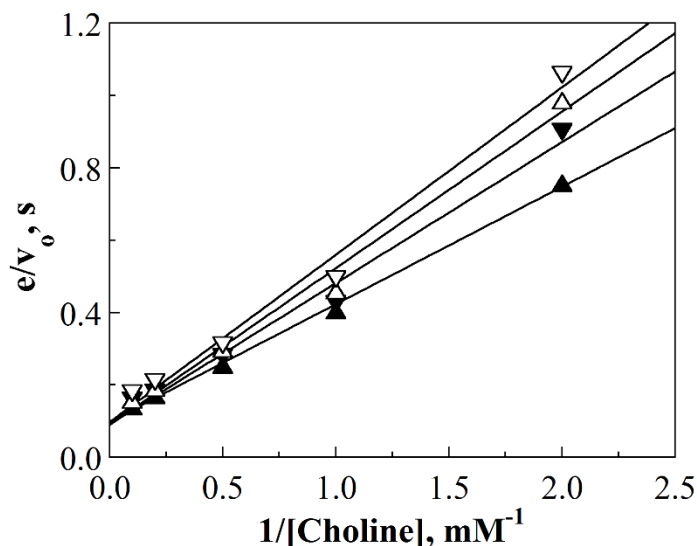


Figure 5.9. Double reciprocal plot of the inhibition of the wild-type enzyme by Tris with choline as a substrate. Initial rates were measured in air-saturated 50 mM sodium phosphate, pH 6.0 and 25 °C. Tris concentrations were 0 (▲), 2 (▼), 5 (△) and 10 mM (▽). Data were fit with eq 2.

Glycine Betaine Titration of the S101C Enzyme-Tris Complex. The active site of choline oxidase is sufficient to accommodate a single glycine betaine molecule, as shown in the crystal structure of the enzyme-glycine betaine complex recently reported (Figure 5.1).³⁵ Thus, if Tris binds at the active site of the enzyme it should be displaced by increasing concentrations of glycine betaine. As shown in Figure 5.10A, with increasing concentration of glycine betaine the S101C enzyme in 20 mM Tris-Cl, pH 8.0 and 25 °C, showed a progressive decay of the C4a-S-cysteinyl-flavin and formation of oxidized flavin, as indicated by the decrease in absorbance in the 400 nm-region and concomitant increases in absorbance in the 370 nm and 450 nm regions of the

electromagnetic spectrum. Figure 5.10B shows the computed UV-visible absorption spectrum of the C4a-S-cysteinyl-flavin, which was obtained by subtracting the spectrum corresponding to 40%¹ oxidized S101C enzyme from the mixture spectrum of the S101C enzyme at 0 M glycine betaine. The resulting computed UV-visible absorption spectrum of the C4a-S-cysteinyl-flavin exhibited an absorbance maximum at 399 nm ($\epsilon_{399} = 8.6 \text{ mM}^{-1}\text{cm}^{-1}$).

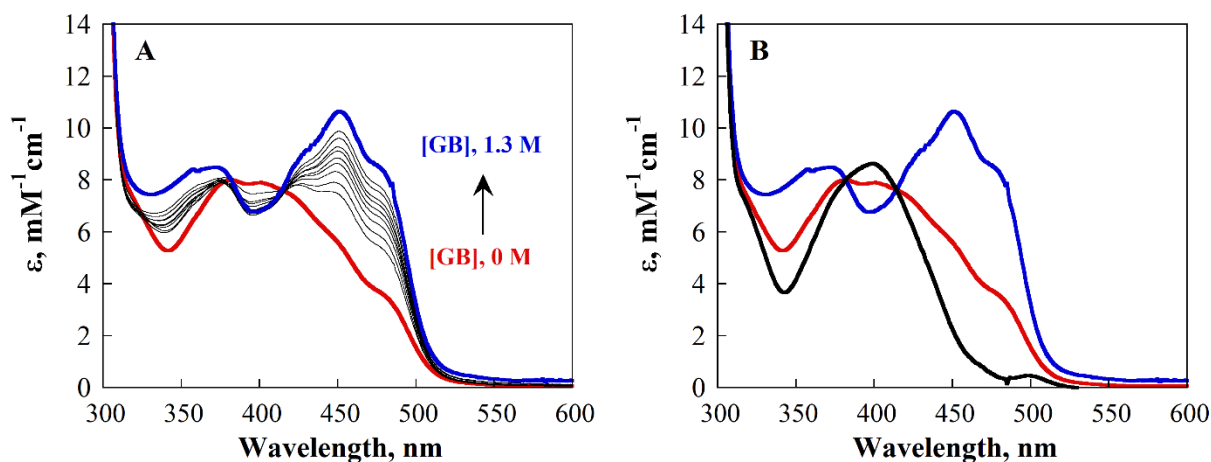


Figure 5.10 Glycine betaine titration of the S101C enzyme-Tris complex in 20 mM Tris-Cl, pH 8.0 and 25 °C. (A) The UV-visible absorption spectrum of the S101C enzyme in the presence of glycine betaine ranging from 0 M (red) to 1.3 M (blue). (B) Calculated UV-visible absorption spectrum of the C4a-S-cysteinyl-flavin (black) obtained from the difference spectrum of the enzyme in the absence of glycine betaine (red) minus 40% spectrum¹ of the enzyme in the presence of 1.3 M glycine betaine (blue) and normalized back to 100%.

Stopped-flow Kinetics for Formation of the C4a-S-cysteinyl-flavin. The S101C enzyme was mixed with varying concentrations of Tris in 50 mM sodium phosphate, at varying pH values around the pK_a value of Tris (i.e., $pK_a = 8.1$) in a stopped-flow spectrophotometer to establish

¹ The macroscopic dissociation constant for the enzyme-Tris complex that results in the formation of the C4a-S-cysteinyl-flavin (K_d^{app}) determined in this study is $\sim 14 \text{ mM}$ at pH 8.0 (Table 1). The glycine betaine titration of the S101C enzyme-Tris complex shown in Figure 10 was conducted in 20 mM Tris-Cl, corresponding to $\sim 60\%$ of the S101C enzyme being in complex with Tris and $\sim 40\%$ being in the oxidized, free form.

whether the protonated, unprotonated or both species of Tris were responsible for the formation of the C4a-S-cysteinyl-flavin and its kinetics. As shown in Figure 5.11A for the case of pH 8.5, the oxidized flavin in the S101C enzyme was converted to the C4a-S-cysteinyl-flavin within 2 s after mixing the enzyme with Tris. The absorbance of the enzyme-bound flavin at 456 nm decreased in a biphasic fashion, with a fast phase accounting for $\geq 95\%$ of the absorbance change, followed by a slow phase that accounted for $\leq 5\%$ of the total absorbance change. The observed rate constant for the fast phase of the absorbance decrease of the flavin at 456 nm increased hyperbolically with increasing concentration of Tris yielding a y-axis intercept (Figure 5.11B), allowing for the determination of the first-order rate constant for the formation of the C4a-S-cysteinyl-flavin at saturating Tris (k_3), the first-order rate constant for the reverse reaction of formation of the C4a-S-cysteinyl-flavin (k_4), and the macroscopic dissociation constant for the enzyme-Tris complex that results in the formation of the C4a-S-cysteinyl-flavin (K_d^{app}). The observed rate constant for the slow phase for the decrease at 456 nm was independent of the concentration of Tris with an average value of 0.7 s^{-1} and a relative amplitude $\leq 5\%$ of the total absorption change, possibly due to a small fraction of enzyme not being fully functional.

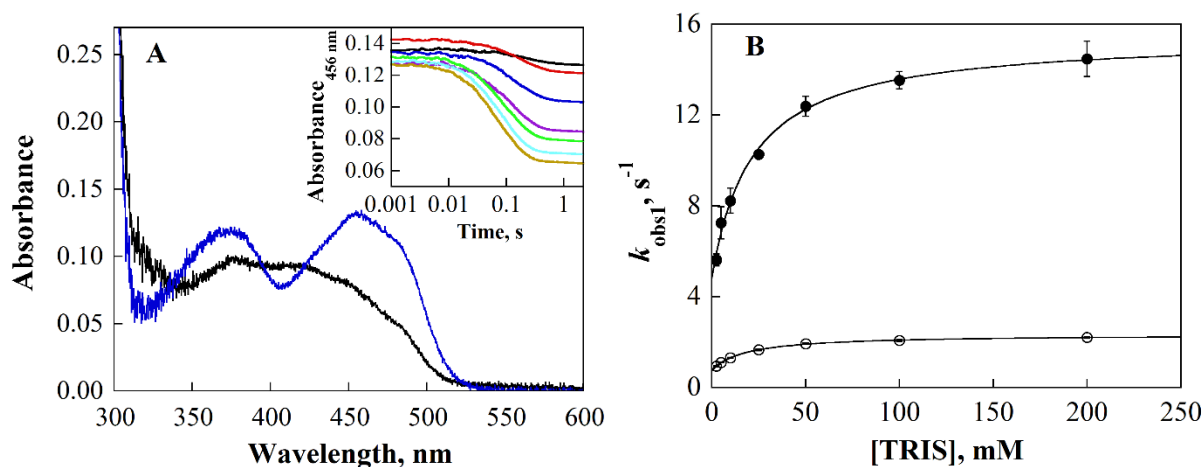


Figure 5.11 Stopped-flow kinetics for formation of the C4a-S-cysteinyl-flavin in the S101C enzyme with Tris in 50 mM sodium phosphate pH 8.5 and 25 °C. (A) UV-Visible absorption spectrum of the S101C enzyme prior to (blue) and after reacting for 2 s with 100 mM Tris. Inset: absorbance decreasing traces of the flavin at 456 nm with 2.5 mM (black), 5 mM (red), 10 mM (blue), 25 mM (purple), 50 mM (green), 100 mM (cyan) and 200 mM (brown) Tris. All traces shown were obtained from averages of five shots and fit to eq 3. Time indicated is after the end of the flow, i.e. 2.2 ms. (B) Observed rate constants of the absorbance decrease at 456 nm as a function of Tris concentration in H₂O (solid) and D₂O (empty). Averages of five replicates of each data points were shown and fit to eq 4.

Similar results were obtained when the S101C enzyme was mixed in the stopped-flow spectrophotometer with Tris at pH 8.0 or 9.0. As reported in Table 1, the k_3 and k_4 values did not change between pH 8.0 and 9.0, with values of $\sim 11 \text{ s}^{-1}$ and $\sim 5 \text{ s}^{-1}$, respectively, establishing this range as being pH independent. The K_d^{app} had similar values between pH 8.0 and 9.0 when the concentration of protonated Tris was used in the calculation, but not when the concentration of the unprotonated Tris or the total concentration of Tris were used (Table 5.1), consistent with protonated Tris being responsible for the observed effects.

Table 5.1 Kinetic rate constants for the reversible formation of the C4a-S-cysteinyl-flavin in the S101C enzyme with Tris ^a.

pH	K_d^{app} , mM			k_3 , s ⁻¹	k_4 , s ⁻¹
	Total ^b	protonated ^b	deprotonated ^b		
8.0	14 ± 4	9 ± 3	5 ± 1	10.2 ± 0.5	4.7 ± 0.7
8.5	21 ± 5	7 ± 2	14 ± 3	10.6 ± 0.4	4.8 ± 0.4
9.0	42 ± 10	6 ± 1	36 ± 9	12.3 ± 0.8	5.5 ± 0.3
Average	NA ^c	7 ± 3	NA ^c	11.0 ± 0.6	5.1 ± 0.5

^a Conditions: 50 mM sodium pyrophosphate and 25 °C; ^b Concentrations of protonated and unprotonated Tris were calculated from the total concentration of Tris based on the pK_a value of 8.1 for Tris in bulk solvent; ^c NA, not applicable.

Deuterium Kinetic Isotope Effects and Proton Inventories on the Reversible Formation of the C4a-S-cysteinyl-flavin. The effects of deuterated solvent on the stopped-flow kinetics were determined to establish whether solvent exchangeable protons were in flight in the transition states for the reaction of reversible formation of the C4a-S-cysteinyl-flavin. The S101C enzyme was mixed with Tris in a stopped-flow spectrophotometer in protiated or deuterated aqueous 50 mM sodium phosphate, pL 8.5 and 25 °C. Qualitatively the stopped-flow data in D₂O were identical to those in H₂O, but large solvent kinetic isotope effects >6.0 were determined for both the ^{D2O}k₃ and ^{D2O}k₄ values (Table 5.2). A control experiment assessing the effect of 9% glycerol, which has a microviscosity equivalent to that of D₂O at 25 °C, yielded glycerol effects on all the measurable kinetic rate constants that were not significantly different than one (Table 5.2), ruling out potential solvent viscosity effects. When the solvent kinetic isotope effect and glycerol effect were repeated at pL 8.8, the results were like those obtained at pL 8.5 (Table 5.2), as expected because both pL 8.5 and pL 8.8 are in the pL-independent region (Table 5.1).

Table 5.2 Solvent kinetic isotope effects on the reversible formation of the C4a-S-cysteinyl-flavin in the S101C enzyme with Tris ^a.

pL	^{D2O} k ₃	^{D2O} k ₄	glycerol k ₃	glycerol k ₄
8.5	6.3 ± 0.2	7.3 ± 0.4	1.0 ± 0.1	1.1 ± 0.1
8.8	6.1 ± 0.3	7.8 ± 0.6	1.0 ± 0.1	1.1 ± 0.1

^a Conditions: 50 mM sodium pyrophosphate and 25 °C.

The number of solvent exchangeable protons responsible for the large deuterium kinetic isotope effects associated with the reversible formation of the C4a-S-cysteiny-flavin was determined by mixing the S101C enzyme with Tris in buffered solutions at pL 8.8 with varying mole fractions of D₂O. As shown in Figure 5.12, both proton inventories of k_3 and k_4 were linear, consistent with a single proton in flight in the transition state for the reversible formation of the C4a-S-cysteiny-flavin in choline oxidase.

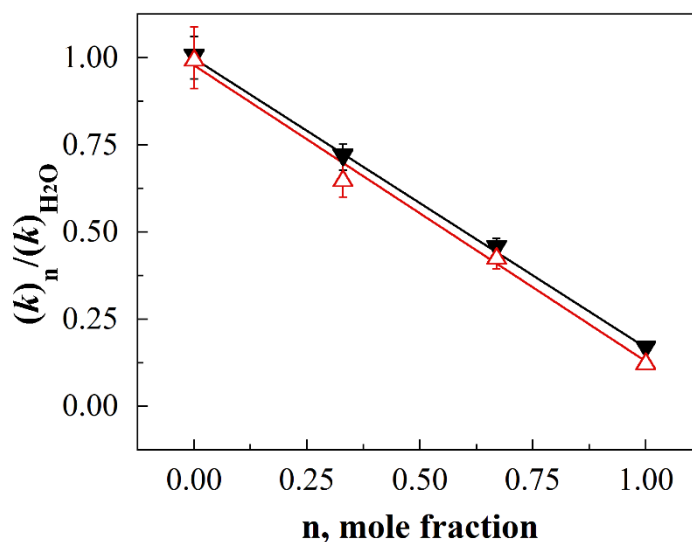


Figure 5.12 Proton inventories of k_{for} (\blacktriangledown) and k_{rev} (\triangle) of the reversible formation of the C4a-S-cysteiny-flavin in the S101C enzyme in 50 mM sodium phosphate, pL 8.8 and 25 °C. Five replicates of each data point were performed.

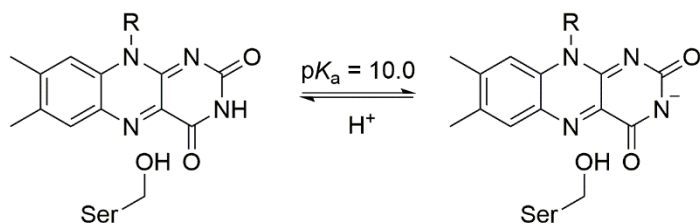
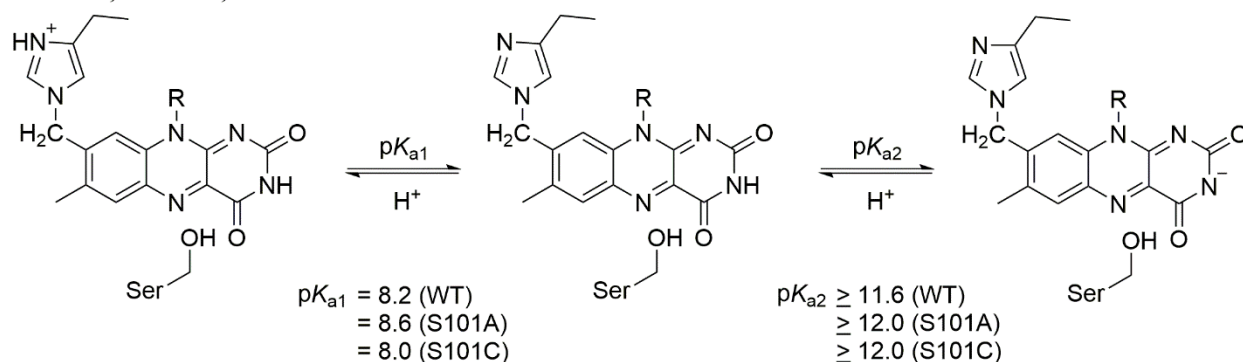
5.4 Discussion

In this study, a reversible, bicovalently-linked flavin was formed in choline oxidase with the introduction of a novel C4a-S-cysteiny-flavin linkage in addition to the naturally occurring 8 α -N³-histidyl linkage between the FAD and the side chain of H99. This was achieved through the replacement of the S101 residue proximal to the C4a atom of the enzyme-bound FAD with cysteine

and the incubation of the resulting S101C enzyme with protonated Tris. The effects of pH on the UV-visible absorption spectrum of the enzyme-bound flavin were used to extract information on the pK_a values for the ionizations of groups required for the stabilization of the C4a-S-cysteinyl-flavin. This information, along with the results of mechanistic probes, such as rapid kinetics, deuterium kinetic isotope effects and proton inventories, was employed to elucidate the mechanism of formation of the C4a-S-cysteinyl-flavin at the optimal pH range.

pK_a Values of the Flavin N3 Atom and the Histidyl N1 Atom in Wild-type Choline Oxidase. In choline oxidase, the ionization of the N3 atom of the flavin in the oxidized state has a pK_a value of ≥ 11.6 , and the ionization of the N1 atom of H99, which is the site of covalent attachment of FAD to the protein through an 8α -N³-histidyl linkage, has a pK_a value of 8.2. Evidence for this conclusion comes from the comparison of the pH profiles of the UV-visible absorption spectra of the wild-type and H99N enzymes. Because the H99N enzyme lacks the histidyl linkage with the flavin and consequently does not have an ionization at the N1 atom of H99, the pK_a value of 10.0 observed in the pH titration of the H99N enzyme could be unequivocally assigned to the ionization of the N3 atom of the flavin (Scheme 5.1A). Upon deprotonation of the flavin N3 atom there is an increase in absorbance and a hypsochromic shift of the high-energy band from 395 nm to 358 nm at high pH (Figure 5.8), as typically observed for the ionization of the N3 atom in other flavoproteins and model systems.⁵⁵⁻⁵⁷ The spectral changes in the H99N enzyme were like those seen at alkaline pH values with the wild-type enzyme, allowing for the assignment of the pK_a values ≥ 11.6 seen in Fig. 5 to the ionization of the N3 atom of the flavin in the wild-type form of choline oxidase. The ionization of the flavin N3 atom is maintained in the enzyme with S101 replaced with alanine or cysteine (Scheme 5.1B).

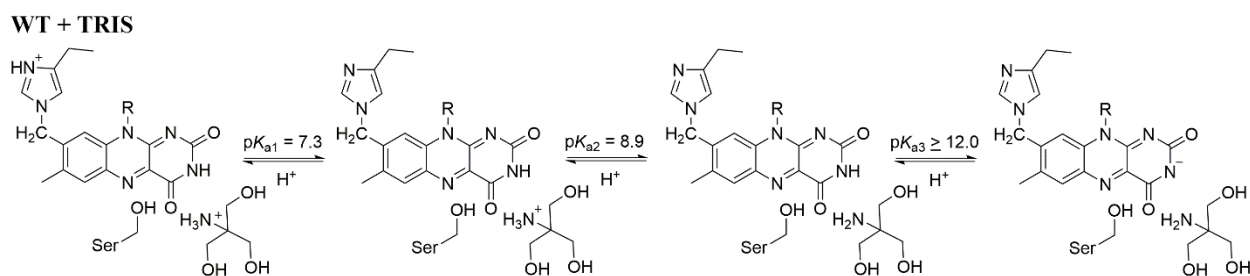
The second pK_a value of 8.2 seen in the pH titration of the wild-type enzyme in the absence of Tris (Figure 5.5) could be assigned to the ionization of the N1 atom of H99 of choline oxidase (Scheme 5.1B), since this is the only other pH-sensitive site expected to alter the absorbance of the flavin. The deprotonation of the N1 atom of H99 is associated with a large hypsochromic shift of the high-energy band of the flavin from 370 nm to 353 nm concomitant with a decrease in absorbance, and a small hypsochromic shift of the low-energy band of the flavin (Figure 5.5). As expected, the ionizations of the N3 atom of the flavin and the N1 atom of H99 were present also in the enzymes in which S101 was replaced with alanine or cysteine (Scheme 5.1B), and the wild-type enzyme in the presence of Tris, although with pK_a values slightly different due to the replacement of an amino acid residue close to the flavin or the presence of Tris bound at the active site of the enzyme (*see below*). For comparison, in 8α -N-imidazolyl-riboflavin free in solution the N3 atom of the flavin has a pK_a value of ~ 9.7 and the N atom of the 8α -imidazole has a pK_a value ~ 6.0 ,^{58, 59} further underscoring the modulation of the hystidyl-flavin by the protein microenvironment surrounding the flavin in choline oxidase. Consistent with the notion of the protein microenvironment surrounding the flavin modulating the equilibrium for the ionization of the hystidyl-flavin, pK_a values of 5.4 and 6.2 were previously reported for cholesterol oxidase from *Schizophyllum commune* and *Gleocystidium chrysocreas*, respectively.⁶⁰

A. H99N**B. WT, S101A, S101C**

Scheme 5.1 Ionization of the N3 atom of the flavin in the H99N enzyme (A), and in the wild-type, S101A, and S101C enzymes (B), and of the histidyl N1 atom of the $8\alpha\text{-N}^3\text{-histidyl-FAD}$ in the wild-type, S101A, and S101C enzymes (B).

Effect of Tris Binding on the $\text{p}K_a$ Value of the Histidyl N1 Atom in Wild-type Choline Oxidase. Binding of Tris in the active site of wild-type choline oxidase lowers the $\text{p}K_a$ value for the ionization of the N1 atom of H99 by ~ 1 pH unit. Evidence for this conclusion comes from the effect of Tris on the pH titration of the UV-visible absorption spectrum of the wild-type enzyme and the inhibition of its catalytic activity with choline as a substrate exerted by Tris. In the presence of 20 mM Tris, the wild-type enzyme showed two $\text{p}K_a$ values in the pH range from 6.0 to 10.5 (Figure 5.7), as compared to a single $\text{p}K_a$ value observed without Tris (Figure 5.5). The $\text{p}K_a$ value of 7.3 seen in the wild-type enzyme with Tris is assigned to the N1 atom of H99 (Scheme 5.2), based on the hypsochromic shifts of the flavin bands and the large magnitude of the spectral changes accounting for $\sim 80\%$ of the total change observed (Figure 5.7). On the other hand, the

small spectral changes associated with the pK_a value seen at 8.9, which account for ~20% of the total absorption changes in the wild-type enzyme with Tris, are consistent with a perturbation of the flavin absorbance due to a nearby molecule but not of the histidyl-flavin itself, for which much bigger changes would be expected. Thus, the pK_a value of 8.9 is assigned to Tris when the molecule is bound at the active site of the enzyme (Scheme 5.2). Alternatively, one would have to envision an altered absorbance of the flavin in the active site of the enzyme due to a change in the ionization of Tris when free in solution and at a low concentration of 20 mM, which is unprecedented and highly unlikely. The competitive inhibition pattern seen with Tris *versus* choline as a substrate for the wild-type enzyme is consistent, although by itself it does not prove, with Tris competing with choline for binding at the active site of the enzyme. In this regard, a previous study established that trimethylamine, dimethylethylamine, and diethylmethylamine, which have structures resembling that of Tris, act as competitive inhibitors versus choline as a substrate for choline oxidase.⁵⁴ The protonated state of Tris is favored when the compound is bound to choline oxidase as compared to bulk solvent, as suggested by the increase of the pK_a value for Tris from 8. in solution to 8.9 in the active site of the enzyme.



Scheme 5.2 Ionization of the histidyl N1 atom of H99, the flavin N3 atom of the 8α -N³-histidyl-FAD, and Tris, in wild-type choline oxidase when Tris is present.

Stabilization of the C4a-S-cysteinyl-flavin in the S101C Enzyme. A C4a-S-cysteinyl-flavin is stabilized in the choline oxidase variant S101C when protonated Tris is bound at the active

site of the enzyme in the pH range ~ 7.0 and ~ 9.5 ². The involvement of C101 in the C4a-S-cysteinyl-flavin is established by the detection of an absorbance spectrum consistent with a flavin C4a-adduct only with the S101C enzyme, but not with the wild-type or other S101 variants of the enzyme that contain an alanine or a threonine (Figure 5.2). The requirement for Tris to stabilize the C4a-S-cysteinyl-flavin is supported by the comparison of the UV-visible absorption spectrum of the S101C enzyme in Tris buffer and in other buffers such as TES, HEPES or sodium phosphate, showing that a flavin species with broad maximal absorbance at 376 nm is seen only when Tris is present (Figure 5.2). Both the wavelength of maximal absorbance and the intensity of the peak of the C4a-S-cysteinyl-flavin in choline oxidase ($\epsilon_{399} = 8.6 \text{ mM}^{-1}\text{cm}^{-1}$, Figure 5.10B) agree with the features of C4a-S-cysteinyl-flavins previously observed in a triple mutant of mercuric ion reductase ($\epsilon_{382} = 7.5 \text{ mM}^{-1}\text{cm}^{-1}$),²² lipoamide dehydrogenase ($\epsilon_{384} = 8.7 \text{ mM}^{-1}\text{cm}^{-1}$),²³ and the LOV domain of phototropin ($\epsilon_{378} = 8.7 \text{ mM}^{-1}\text{cm}^{-1}$).²⁷

Evidence for protonated Tris, rather than its unprotonated species, being the effector for the formation of the C4a-S-cysteinyl-flavin comes from the rapid kinetics data with the S101C enzyme and Tris determined in the stopped-flow spectrophotometer. The observation that the K_d^{app} had the same value at pH 8.0, 8.5, and 9.0, only when the concentrations of protonated Tris was used in the calculations, but not the concentrations of unprotonated or total Tris (Table 5.1), unequivocally establishes the former as the active species required for the formation of the C4a-S-cysteinyl-flavin in the S101C enzyme. Further support for placing Tris at the active site of choline oxidase is provided by the glycine betaine titration of the S101C enzyme-Tris complex at pH 8.0, resulting in the decay of the C4a-S-cysteinyl-flavin (Figure 5.10) due to the displacement

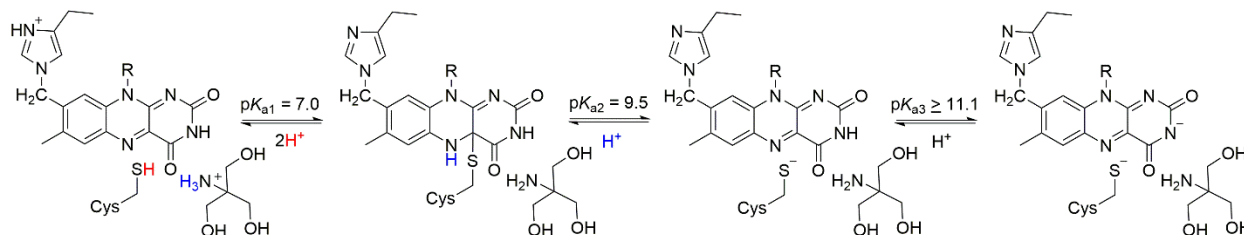
² Because the $\text{p}K_a$ values obtained in the pH titration of the S101C enzyme in the presence of Tris through a global fitting of the data (Fig. 3E) and those obtained with eq 7 were slightly different but in agreement with each other, i.e., 6.8-6.9 and 9.3-9.5, the approximate values of ~ 7.0 and ~ 9.5 are considered.

of the Tris upon binding of glycine betaine in the active site of the enzyme. The competitive inhibition pattern of Tris *versus* choline as a substrate for the wild-type enzyme, and the perturbation of the electromagnetic spectrum of the enzyme-bound flavin yielding an extra pK_a value of 8.9 when the wild-type enzyme is in the presence of Tris (*see above*), corroborate the ability of choline oxidase to bind Tris in its active site. The requirement for a positively charged ligand for the formation of a C4a-S-cysteinyl-flavin has been reported in previous studies on other enzymes. Binding of NAD^+ promotes the formation of the C4a-S-cysteinyl-flavin in a monoalkylated derivative of pig heart lipoamide dehydrogenase²³ and the formation of the C4a-S-cysteinyl-flavin in the mercuric ion reductase triple mutant only occurs in the presence of $NADP^+$.²²

In the pH titration of the UV-visible absorption spectrum of the S101C enzyme with Tris, a coupled system involving the deprotonation of H99, C101, and the bound protonated Tris, as well as the protonation of the N5 atom of the flavin, contributes to the observed macroscopic pK_{a1} of ~7.0 associated with the formation of the C4a-S-cysteinyl linkage. The assignment of the pK_a of ~9.5 to the N5 atom of the C4a-S-cysteinyl-flavin is instead because its deprotonation will allow a redistribution of the valence electrons between the N5 and C4a atoms of the flavin with consequent cleavage of the C4a-S bond. An apparent pK_a of ~6.8 was previously assigned to the side chain of C140 involved in the formation of the C4a-S-cysteinyl-flavin in the mercuric ion reductase triple mutant by pH titration on the UV-visible absorption spectrum of the enzyme.²² A recent study on the C2 component of the two-component monooxygenase using rapid kinetics established a similar value of ~9.5 for the ionization of the N5 atom of the flavin in the C4a-hydroperoxo-flavin bound to the enzyme.⁶¹ Scheme 5.3 illustrates the three pH-dependent equilibria that are established between the C4a-S-cysteinyl-flavin and the three oxidized forms of

the S101C enzyme when Tris is present (Figure 5.3), where the two equilibria at pH ~ 7.0 and ~ 9.5 define the optimum range of pH for stabilization of the C4a-S-cysteinyl-flavin, and that at pH ≥ 11.1 is for the ionization of the N3 atom of the flavin.

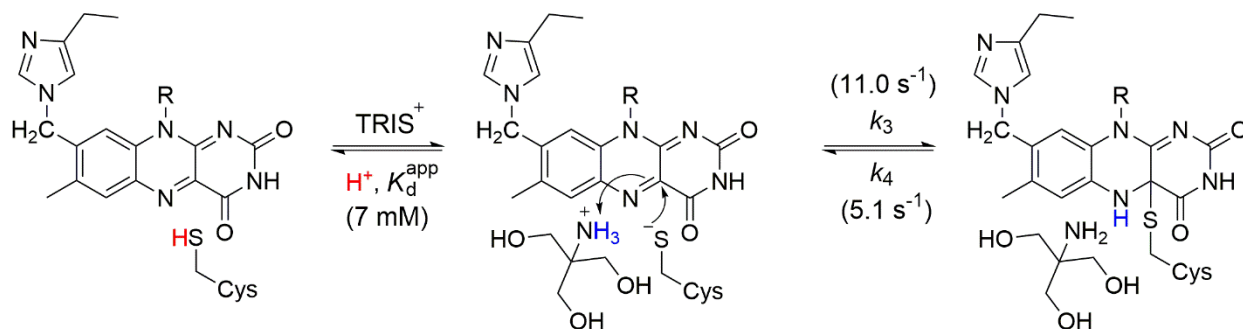
S101C + TRIS



Scheme 5.3 Stabilization of the C4a-S-cysteinyl-flavin in the S101C enzyme with Tris. The ionization of H99 of the C4a-S-cysteinyl-flavin is based on the behavior of the wild-type enzyme in the presence of Tris, showing a pK_a value of 7.3. The ionization of Tris is based on the pK_a value of 8.9 as determined in the complex with the wild-type enzyme. In the S101C enzyme with Tris, these pK_a values were not directly established. The ionization of C101 above pH 9.5 is arbitrarily assigned here based on chemical reasoning but without experimental evidence.

Mechanism of Formation of the C4a-S-cysteinyl-flavin in the S101C Enzyme with Tris.

The minimal mechanism of Scheme 5.4 illustrates the biochemical details for the reversible formation of the C4a-S-cysteinyl-flavin elicited by protonated Tris in the S101C enzyme under optimal pH, i.e., between pH ~ 7.0 and ~ 9.5 . Upon formation of a complex of the oxidized enzyme and protonated Tris, the side chain of C101 deprotonates; the resulting thiolate forms the C4a-S-cysteinyl-flavin through a nucleophilic reaction with the C4a atom of the flavin; the protonated Tris donates a proton to the N5 atom of the flavin. Evidence for the mechanism of Scheme 5.4 comes from the rapid kinetics data of the S101C enzyme with Tris, the associated deuterium kinetic isotope effects and proton inventories, and the thermodynamic titrations of the UV-visible absorption spectrum of the S101C, wild-type, and other variants of choline oxidase as a function of pH discussed above.



Scheme 5.4 Minimal mechanism for the reversible formation of the C4a-S-cysteinyl-flavin in the S101C enzyme with protonated Tris in the pH range 8.0-9.0. The kinetic parameters shown in parenthesis are from the average values in Table 1.

Formation of a complex of the oxidized enzyme with Tris is established by the hyperbolic pattern of the observed rate constant for the absorbance decrease at 456 nm ($k_{\text{obs}1}$) as a function of the concentration of Tris upon mixing the S101C enzyme and Tris in a stopped-flow spectrophotometer (Figure 5.11). As discussed above, the observation that the K_d^{app} value for the formation of the complex has the same value irrespective of the pH when the concentration of protonated Tris is used for the calculation demonstrates that Tris must be protonated to elicit its effect. Several lines of evidence for binding of Tris at the active site of the enzyme, either the S101C or the wild-type form, have been presented above. The K_d^{app} value of ~ 7.0 mM determined here for binding of protonated Tris to the S101C enzyme is comparable to the inhibition constants previously determined for other tertiary amines that act as competitive inhibitors versus choline in wild-type choline oxidase, with K_{is} values between 2.4 mM and 9.0 mM determined at pH 8.0 with trimethylamine, dimethylethylamine, and diethylmethylamine.⁵⁴

Formation of a complex between the enzyme and protonated Tris in the active site of the S101C enzyme results in the rapid deprotonation of the thiol side chain of C101 that triggers the nucleophilic reaction of C101 with the C4a atom and the protonation of the N5 atom of the flavin by Tris, with the latter being rate-limiting for the process with a rate constant of ~ 11 s⁻¹ at the pH

optimum of 7.0-9.5 (step k_3 in Scheme 5.4). The proton inventory establishes that a single proton is in flight in the transition state for the formation of the C4a-S-cysteinyl-flavin (Figure 5.12). The large solvent deuterium kinetic isotope effect of ~ 6.2 (Table 5.2) determined on k_3 is consistent with a symmetrical transition state for a proton transfer between the two N atoms of Tris and the flavin (Scheme 5.4).⁶² Further evidence for a rate-limiting proton transfer from Tris to the flavin comes from the equilibrium isotope effect of ~ 1.2 computed for $^{D_2O}k_4/^{D_2O}k_3$ at pL 8.5-8.8, which also rules out the alternative possibility of a proton transfer involving C101 for which an inverse equilibrium isotope effect of ~ 0.55 is expected. Deprotonation of the cysteine thiol must be induced by binding of protonated Tris in the active site of the enzyme because in the absence of Tris the S101C enzyme does not stabilize the C4a-S-cysteinyl-flavin. This is perhaps due to C101 being protonated at least up to pH 9.5³ in the active site of the enzyme in the absence of protonated Tris possibly due to an electrostatic effect of E312, which is not neutralized by binding a positively charged ligand in the free enzyme as it occurs with Tris. The possibility that a conformational change of the loop harboring C101 arising from the binding of the positively charged Tris in the active site of the enzyme is (partially) responsible for the deprotonation of C101 that results in the formation of the C4a-S-cysteinyl-flavin cannot be ruled out. E312 was previously shown to be important for binding the trimethylammonium group of ligands with mutagenesis, substrate analogs and competitive inhibitors.^{39, 45} The interaction of the side chain of E312 with the positive charge of the ligand in the active site of choline oxidase was directly observed in the crystallographic structure of the wild-type enzyme in complex with glycine betaine (Figure 5.1).³⁵ The lowering of the pK_a value of the histidyl-flavin H99 from 8.2 to 7.3 in the wild-type choline

³Above pH 9.5, the deprotonation of the N5 atom of the C4a-S-cysteinyl-flavin triggers the cleavage of the C4a-S bond yielding oxidized flavin, as discussed below.

oxidase in the presence of Tris is consistent with stabilization of unprotonated species for groups that ionize in the active site of the enzyme, thus indirectly supporting the notion that a similar modulation of the pK_a value may occur for the thiol side chain of C101. It is worth noting that an alternate mechanism for the formation of a C4a-S-cysteinyl-flavin from a protonated thiol was proposed for mercuric ion reductase based on the observation that the C4a-S-cysteinyl-flavin is formed below a pK_a of ~ 6.8 , which the authors assigned to the thiol participating in the formation of the flavin adduct.²²

Formation of the C4a-S-cysteinyl-flavin is reversible, with a rate constant for the reverse reaction of $\sim 5 \text{ s}^{-1}$, as indicated by the y-intercept being significantly different from zero in a plot of the $k_{\text{obs}1}$ value as a function of the concentration of protonated Tris (Figure 5.11). The reverse reaction is triggered by the deprotonation of the N5 atom of the C4a-S-cysteinyl-flavin by Tris base, which is associated with a large solvent deuterium kinetic isotope effect of ~ 7.5 determined on the rate constant for the reverse formation (k_4) of the C4a-S-cysteinyl-flavin (Table 5.2). A single proton is in flight in the transition state for the reverse formation of the C4a-S-cysteinyl-flavin, as suggested by the proton inventory on the k_4 value (Figure 5.12). A pK_a of ~ 8.9 is assigned to Tris when bound at the active site of the wild-type enzyme (Scheme 5.2), which is close to the pK_a of ~ 9.5 of the N5 atom of the C4a-S-cysteinyl-flavin. Thus, the forward and reverse steps of the formation of the C4a-S-cysteinyl-flavin are controlled by proton transfers between acid/conjugate base of nearly-matched acidities, consistent with the similar value of k_3 and k_4 (Table 5.1), and a symmetrical transition state for proton transfer that results in isotope effects for the forward and reverse reactions close to 7.⁶²

5.5 Conclusion

In summary, we have used mutagenesis, rapid kinetics, and mechanistic probes such as pH, kinetic isotope effects and proton inventories, to engineer a reversible, C4a-S-cysteinyl-flavin linkage in choline oxidase. Formation of the C4a-S-cysteinyl-flavin linkage between the side chain of C101 and the 8 α -N³-histidyl flavin in the active site of the S101C enzyme is triggered by the binding of protonated Tris in the active site of the enzyme, and it occurs on a timescale that is amenable to investigation by using a stopped-flow spectrophotometer. The pH titration data of the UV-visible absorption spectrum of the enzyme-bound flavin have established that the C4a-S-cysteinyl-flavin is stabilized between pH ~7.0 and ~9.5, in which the side chain of C101 is unprotonated and the N5 atom of the C4a-S-cysteinyl-flavin is protonated. The presence of Tris bound at the active site of the enzyme is required to deprotonate the cysteine and to trigger the formation of the C4a-S-cysteinyl-flavin, and for the stabilization of the C4a-S-cysteinyl-flavin, as indicated by the decay of the C4a-S-cysteinyl-flavin when the bound Tris is replaced by glycine betaine. This study establishes that the *de novo* engineering of a reversible bivalent C4a-S-cysteinyl-8 α -N³-histidyl flavin is feasible in a flavoprotein; it provides a detailed mechanistic analysis for the reversible formation of the engineered linkage between the flavin and the protein, identifying an optimal pH range and a mechanistic rationale for the stabilization of the C4a-S-cysteinyl-flavin. Finally, this study presents an example of an intramolecular reaction of an enzyme-bound flavin with the side chain of an active site residue that does not involve a substrate but rather it is triggered by the binding of an exogenous ligand in the active site of the enzyme.

5.7 Acknowledgement

We would like to thank Bruce Palfey, Dale Edmondson, Andreas Bommarius, Stefan Lutz, and their research groups, for insightful discussions.

5.8 References

- [1] Heuts, D. P., Scrutton, N. S., McIntire, W. S., and Fraaije, M. W. (2009) What's in a covalent bond? On the role and formation of covalently bound flavin cofactors, *FEBS J.* 276, 3405-3427.
- [2] Mewies, M., McIntire, W. S., and Scrutton, N. S. (1998) Covalent attachment of flavin adenine dinucleotide (FAD) and flavin mononucleotide (FMN) to enzymes: the current state of affairs, *Protein Sci.* 7, 7-20.
- [3] Walker, W. H., and Singer, T. P. (1970) Identification of the covalently bound flavin of succinate dehydrogenase as 8- α -(histidyl) flavin adenine dinucleotide, *J. Biol. Chem.* 245, 4224-4225.
- [4] Podzelinska, K., Latimer, R., Bhattacharya, A., Vining, L. C., Zechel, D. L., and Jia, Z. (2010) Chloramphenicol biosynthesis: the structure of CmlS, a flavin-dependent halogenase showing a covalent flavin-aspartate bond, *J. Mol. Biol.* 397, 316-331.
- [5] Huang, C. H., Lai, W. L., Lee, M. H., Chen, C. J., Vasella, A., Tsai, Y. C., and Liaw, S. H. (2005) Crystal structure of glucooligosaccharide oxidase from *Acremonium strictum*: a novel flavinylation of 6-S-cysteinyl, 8 α -N1-histidyl FAD, *J. Biol. Chem.* 280, 38831-38838.
- [6] Lee, M. H., Lai, W. L., Lin, S. F., Hsu, C. S., Liaw, S. H., and Tsai, Y. C. (2005) Structural characterization of glucooligosaccharide oxidase from *Acremonium strictum*, *Appl. Environ. Microbiol.* 71, 8881-8887.
- [7] Rand, T., Qvist, K. B., Walter, C. P., and Poulsen, C. H. (2006) Characterization of the flavin association in hexose oxidase from *Chondrus crispus*, *FEBS J.* 273, 2693-2703.
- [8] Alexeev, I., Sultana, A., Mantsala, P., Niemi, J., and Schneider, G. (2007) Aclacinomycin oxidoreductase (AknOx) from the biosynthetic pathway of the antibiotic aclacinomycin is an unusual flavoenzyme with a dual active site, *Proc. Natl. Acad. Sci. USA* 104, 6170-6175.
- [9] Winkler, A., Hartner, F., Kutchan, T. M., Glieder, A., and Macheroux, P. (2006) Biochemical evidence that berberine bridge enzyme belongs to a novel family of flavoproteins containing a bi-covalently attached FAD cofactor, *J. Biol. Chem.* 281, 21276-21285.
- [10] Winkler, A., Lyskowski, A., Riedl, S., Puhl, M., Kutchan, T. M., Macheroux, P., and Gruber, K. (2008) A concerted mechanism for berberine bridge enzyme, *Nat. Chem. Biol.* 4, 739-741.
- [11] Kopacz, M. M., and Fraaije, M. W. (2014) Turning a monocovalent flavoprotein into a bicovalent flavoprotein by structure-inspired mutagenesis, *Bioorg. Med. Chem.* 22, 5621-5627.
- [12] Caldinelli, L., Iametti, S., Barbiroli, A., Bonomi, F., Fessas, D., Molla, G., Pilone, M. S., and Pollegioni, L. (2005) Dissecting the structural determinants of the stability of cholesterol oxidase containing covalently bound flavin, *J. Biol. Chem.* 280, 22572-22581.
- [13] Caldinelli, L., Iametti, S., Barbiroli, A., Fessas, D., Bonomi, F., Piubelli, L., Molla, G., and Pollegioni, L. (2008) Relevance of the flavin binding to the stability and folding of engineered cholesterol oxidase containing noncovalently bound FAD, *Protein Sci.* 17, 409-419.
- [14] Huang, C.-H., Winkler, A., Chen, C.-L., Lai, W.-L., Tsai, Y.-C., Macheroux, P., and Liaw, S.-H. (2008) Functional roles of the 6-S-cysteinyl, 8 α -N1-histidyl FAD in glucooligosaccharide oxidase from *Acremonium strictum*, *J. Biol. Chem.* 283, 30990-30996.
- [15] Hassan-Abdallah, A., Zhao, G., and Jorns, M. S. (2006) Role of the covalent flavin linkage in monomeric sarcosine oxidase, *Biochemistry* 45, 9454-9462.
- [16] Heuts, D. P., Winter, R. T., Damsma, G. E., Janssen, D. B., and Fraaije, M. W. (2008) The role of double covalent flavin binding in chito-oligosaccharide oxidase from *Fusarium graminearum*, *Biochem. J.* 413, 175-183.

- [17] Winkler, A., Kutchan, T. M., and Macheroux, P. (2007) 6-S-cysteinylation of bi-covalently attached FAD in berberine bridge enzyme tunes the redox potential for optimal activity, *J. Biol. Chem.* 282, 24437-24443.
- [18] Motteran, L., Pilone, M. S., Molla, G., Ghisla, S., and Pollegioni, L. (2001) Cholesterol oxidase from *brevibacterium sterolicum*: the relationship between covalent flavinylation and redox properties, *Biol. Chem.* 276, 18024-18030.
- [19] Fraaije, M. W., van den Heuvel, R. H. H., van Berkel, W. J. H., and Mattevi, A. (1999) Covalent flavinylation is essential for efficient redox catalysis in vanillyl-alcohol oxidase, *J. Biol. Chem.* 274, 35514-35520.
- [20] Kim, J., Fuller, J. H., Kuusk, V., Cunane, L., Chen, Z.-w., Mathews, F. S., and McIntire, W. S. (1995) The cytochrome subunit is necessary for covalent FAD attachment to the flavoprotein subunit of p-cresol methylhydroxylase, *J. Biol. Chem.* 270, 31202-31209.
- [21] Quaye, O., Cowins, S., and Gadda, G. (2009) Contribution of flavin covalent linkage with histidine 99 to the reaction catalyzed by choline oxidase, *J. Biol. Chem.* 284, 16990-16997.
- [22] Miller, S. M., Massey, V., Ballou, D., Williams, C. H., Jr., Distefano, M. D., Moore, M. J., and Walsh, C. T. (1990) Use of a site-directed triple mutant to trap intermediates: demonstration that the flavin C(4a)-thiol adduct and reduced flavin are kinetically competent intermediates in mercuric ion reductase, *Biochemistry* 29, 2831-2841.
- [23] Thorpe, C., and Williams, C. H. (1976) Spectral evidence for a flavin adduct in a monoalkylated derivative of pig heart lipoamide dehydrogenase, *J. Biol. Chem.* 251, 7726-7728.
- [24] Thorpe, C., and Williams, C. H., Jr. (1981) Lipoamide dehydrogenase from pig heart. Pyridine nucleotide induced changes in monoalkylated two-electron reduced enzyme, *Biochemistry* 20, 1507-1513.
- [25] Huber, P. W., and Brandt, K. G. (1980) Kinetic studies of the mechanism of pyridine nucleotide dependent reduction of yeast glutathione reductase, *Biochemistry* 19, 4569-4575.
- [26] O'Donnell, M. E., and Williams, C. H. (1984) Reconstitution of *Escherichia coli* thioredoxin reductase with 1-deazaFAD. Evidence for 1-deazaFAD C-4a adduct formation linked to the ionization of an active site base, *J. Biol. Chem.* 259, 2243-2251.
- [27] Salomon, M., Christie, J. M., Knieb, E., Lempert, U., and Briggs, W. R. (2000) Photochemical and Mutational Analysis of the FMN-Binding Domains of the Plant Blue Light Receptor, Phototropin, *Biochemistry* 39, 9401-9410.
- [28] Iwata, T., Tokutomi, S., and Kandori, H. (2002) Photoreaction of the cysteine S-H group in the LOV2 domain of *Adiantum* phytochrome3, *J. Am. Chem. Soc.* 124, 11840-11841.
- [29] Swartz, T. E., Wenzel, P. J., Corchnoy, S. B., Briggs, W. R., and Bogomolni, R. A. (2002) Vibration spectroscopy reveals light-induced chromophore and protein structural changes in the lov2 domain of the plant blue-light receptor phototropin 1, *Biochemistry* 41, 7183-7189.
- [30] Crosson, S., and Moffat, K. (2002) Photoexcited structure of a plant photoreceptor domain reveals a light-driven molecular switch, *Plant Cell* 14, 1067-1075.
- [31] Sahlman, L., Lambeir, A. M., and Lindskog, S. (1986) Rapid-scan stopped-flow studies of the pH dependence of the reaction between mercuric reductase and NADPH, *Eur. J. Biochem.* 156, 479-488.
- [32] Ghanem, M., and Gadda, G. (2006) Effects of reversing the protein positive charge in the proximity of the flavin N(1) locus of choline oxidase, *Biochemistry* 45, 3437-3447.
- [33] Salvi, F., Rodriguez, I., Hamelberg, D., and Gadda, G. (2016) Role of f357 as an oxygen gate in the oxidative half-reaction of choline oxidase, *Biochemistry* 55, 1473-1484.

- [34] Smitherman, C., Rungsruriyachai, K., Germann, M. W., and Gadda, G. (2015) Identification of the catalytic base for alcohol activation in choline oxidase, *Biochemistry* 54, 413-421.
- [35] Salvi, F., Wang, Y. F., Weber, I. T., and Gadda, G. (2014) Structure of choline oxidase in complex with the reaction product glycine betaine, *Acta Crystallogr. D Biol. Crystallogr.* 70, 405-413.
- [36] Gannavaram, S., and Gadda, G. (2013) Relative timing of hydrogen and proton transfers in the reaction of flavin oxidation catalyzed by choline oxidase, *Biochemistry* 52, 1221-1226.
- [37] Yuan, H., and Gadda, G. (2011) Importance of a serine proximal to the C(4a) and N(5) flavin atoms for hydride transfer in choline oxidase, *Biochemistry* 50, 770-779.
- [38] Finnegan, S., Yuan, H., Wang, Y. F., Orville, A. M., Weber, I. T., and Gadda, G. (2010) Structural and kinetic studies on the Ser101Ala variant of choline oxidase: catalysis by compromise, *Arch. Biochem. Biophys.* 501, 207-213.
- [39] Quaye, O., Nguyen, T., Gannavaram, S., Pennati, A., and Gadda, G. (2010) Rescuing of the hydride transfer reaction in the Glu312Asp variant of choline oxidase by a substrate analogue, *Arch. Biochem. Biophys.* 499, 1-5.
- [40] Finnegan, S., Agniswamy, J., Weber, I. T., and Gadda, G. (2010) Role of valine 464 in the flavin oxidation reaction catalyzed by choline oxidase, *Biochemistry* 49, 2952-2961.
- [41] Rungsruriyachai, K., and Gadda, G. (2010) Role of asparagine 510 in the relative timing of substrate bond cleavages in the reaction catalyzed by choline oxidase, *Biochemistry* 49, 2483-2490.
- [42] Xin, Y., Gadda, G., and Hamelberg, D. (2009) The cluster of hydrophobic residues controls the entrance to the active site of choline oxidase, *Biochemistry* 48, 9599-9605.
- [43] Quaye, O., and Gadda, G. (2009) Effect of a conservative mutation of an active site residue involved in substrate binding on the hydride tunneling reaction catalyzed by choline oxidase, *Arch. Biochem. Biophys.* 489, 10-14.
- [44] Orville, A. M., Lountos, G. T., Finnegan, S., Gadda, G., and Prabhakar, R. (2009) Crystallographic, spectroscopic, and computational analysis of a flavin C4a-oxygen adduct in choline oxidase, *Biochemistry* 48, 720-728.
- [45] Quaye, O., Lountos, G. T., Fan, F., Orville, A. M., and Gadda, G. (2008) Role of Glu312 in binding and positioning of the substrate for the hydride transfer reaction in choline oxidase, *Biochemistry* 47, 243-256.
- [46] Fan, F., and Gadda, G. (2007) An internal equilibrium preorganizes the enzyme-substrate complex for hydride tunneling in choline oxidase, *Biochemistry* 46, 6402-6408.
- [47] Fan, F., and Gadda, G. (2005) Oxygen- and temperature-dependent kinetic isotope effects in choline oxidase: correlating reversible hydride transfer with environmentally enhanced tunneling, *J. Am. Chem. Soc.* 127, 17954-17961.
- [48] Fan, F., and Gadda, G. (2005) On the catalytic mechanism of choline oxidase, *J. Am. Chem. Soc.* 127, 2067-2074.
- [49] Gadda, G. (2008) Hydride transfer made easy in the reaction of alcohol oxidation catalyzed by flavin-dependent oxidases, *Biochemistry* 47, 13745-13753.
- [50] Gadda, G. (2012) Oxygen activation in flavoprotein oxidases: the importance of being positive, *Biochemistry* 51, 2662-2669.
- [51] Romero, E., and Gadda, G. (2014) Alcohol oxidation by flavoenzymes, *Biomol. Conc.* 5, 299-318.
- [52] Schowen, K. B., and Schowen, R. L. (1982) Solvent isotope effects of enzyme systems, *Methods Enzymol.* 87, 551-606.

- [53] Lide, D. R. (2000) *Handbook of Chemistry and Physics*, CRC Press, Boca Raton, FL.
- [54] Gadda, G., Powell, N. L., and Menon, P. (2004) The trimethylammonium headgroup of choline is a major determinant for substrate binding and specificity in choline oxidase, *Arch. Biochem. Biophys.* 430, 264-273.
- [55] Gadda, G., and Fitzpatrick, P. F. (1998) Biochemical and physical characterization of the active FAD-containing form of nitroalkane oxidase from *Fusarium oxysporum*, *Biochemistry* 37, 6154-6164.
- [56] Li, G., and Glusac, K. D. (2008) Light-triggered proton and electron transfer in flavin cofactors, *J. Phys. Chem. A* 112, 4573-4583.
- [57] Macheroux, P., Massey, V., Thiele, D. J., and Volokita, M. (1991) Expression of spinach glycolate oxidase in *Saccharomyces cerevisiae*: purification and characterization, *Biochemistry* 30, 4612-4619.
- [58] Williamson, G., and Edmondson, D. E. (1985) Effect of pH on oxidation-reduction potentials of 8 α -N-imidazole-substituted flavins, *Biochemistry* 24, 7790-7797.
- [59] Williamson, G., and Edmondson, D. E. (1985) Proton nuclear magnetic resonance studies of 8 α -N-imidazolylriboflavin in its oxidized and reduced forms, *Biochemistry* 24, 7918-7926.
- [60] De Francesco, R., and Edmondson, D. E. (1988) pKa values of the 8 α -imidazole substituents in selected flavoenzymes containing 8 α -histidylflavins, *Arch. Biochem. Biophys.* 264, 281-287.
- [61] Thotsaporn, K., Chenprakhon, P., Sucharitakul, J., Mattevi, A., and Chaiyen, P. (2011) Stabilization of C4a-hydroperoxyflavin in a two-component flavin-dependent monooxygenase is achieved through interactions at flavin N5 and C4a atoms, *J. Biol. Chem.* 286, 28170-28180.
- [62] Westheimer, F. H. (1961) The Magnitude of the Primary Kinetic Isotope Effect for Compounds of Hydrogen and Deuterium, *Chem. Rev.* 61, 265-273

6 CHAPTER 6: A TRANSIENT, PHOTOINDUCED INTRAMOLECULAR C4A-N-HISTIDYL-FLAVIN IN CHOLINE OXIDASE

(The author's contribution involves spectroscopic characterization of wild-type and S101A enzyme, data analysis and interpretation.)

6.1 Abstract

Fluorescence excitation spectrum is a powerful tool to investigate transient photoinduced intermediates and energy transfer of fluorophores over the course of excited states. Flavin fluorescence emission is widely used to study numerous biochemical and biophysical processes in flavoproteins due to its high sensitivity to environments. In comparison, flavin fluorescence excitation spectroscopy does not receive much attention in the study of flavoproteins including four classes of flavin-dependent photoreceptors. In this study, we report a photoinduced transient C4a-N-histidyl-FAD in choline oxidase with the aid of fluorescence excitation spectroscopy. Site-directed mutagenesis, solvent equilibrium isotope effects and pH effects on the Stokes shifts of flavin in choline oxidase wild-type demonstrated H466 as the adduct on the C4a atom of flavin upon excitation, and provided a mechanistic rationale involving photoinduced electron transfer (PET) for the formation of the novel photoinduced transient flavin C4a adduct. Moreover, it presents an example of the application of flavin fluorescence excitation spectroscopy in the understanding of excited-state processes in a flavin-dependent light-sensitive protein.

6.2 Introduction

Flavins are highly reactive molecules utilized by a wide-array of enzymes to carry out a variety of biological processes such as detoxification, oxidation, biosynthesis, and DNA damage repair.¹ Flavin mononucleotide (FMN) and flavin adenine dinucleotide (FAD) are capable of carrying out a wide array of chemical reactions due to the versatility of the isoalloxazine ring by

catalyzing single and double electron transfers and nucleophilic and electrophilic attacks.^{1, 2} The reactivity of the flavin is readily detectable due to the spectral characteristics of the conjugated isoalloxazine ring. The redox state of the flavin is easily followed based on distinct spectral signature in each oxidation and reduced state.³ A distinct biophysical characteristic of flavin cofactors are the ability to fluoresce when excited. Flavin emission is sensitive to the environment with changes in wavelength, intensity and life time being observed due to changes in confinement, pH, temperature and solvent.⁴⁻⁹ The high sensitivity of emission allows it being a powerful tool to investigate the biochemical and biophysical processes in flavoproteins. The life time, wavelength, intensity and quantum yield of the flavin fluorescence emission are often exploited to follow ligand binding, catalysis, conformational changes and excited-state processes in flavoproteins.⁹⁻¹³ Fluorescence excitation spectroscopy, on the other hand, is also a useful tool especially for the investigation of transient intermediates and energy transfer over the course of excited-state process but not commonly utilized in study of flavoproteins.

Flavin, upon light excitation, can serve as either an electron donor or acceptor through photoinduced electron transfer (PET), which quenches the flavin fluorescence.^{9, 11} The polarity and ionization states of the isoalloxazine ring are altered affecting the proton affinity at both the N1 and N5 atoms in excited state.¹⁴⁻¹⁶ The excited-state proton transfer (ESPT) could thus occurs between nitrogen atom in flavin, resulting in a red shift of the emission spectrum.^{14, 17} Due to its reactivity in excited states, flavin is utilized by four classes of photoreceptors, e.g. cryptochrome blue-light photoreceptors, blue-light BLUF domains, DNA photolyase, and LOV domains. The photocycles of cryptochromes and BLUF domains are triggered by photoinduced electron transfer from adjacent tryptophans or tyrosines to the excited oxidized FAD.¹⁸⁻²⁰ The catalytic repair of pyrimidine dimer or (6-4) photoproducts by DNA photolyases is initiated by photoinduced

electron transfer from the excited reduced FAD hydroquinone to the damaged DNA.^{21, 22} The signal transduction cascading from LOV domains involves the formation of a C4a-S-Cysteinyl-FMN with a proximal cysteine. The well accepted mechanism for the flavin adduct formation in LOV domains also involves photoinduced electron transfer from the proximal cysteine to FMN, followed by a radical recombination of the yielded FMN semiquinone and cysteine radical.^{23, 24} To our knowledge, C4a-S-Cysteinyl-FMN in LOV domain is the only photoinduced flavin C4a adduct being reported and well characterized.

In the crystallographic structure of choline oxidase, the FAD cofactor is covalently bound to protein via H99 through an 8α -N³-histidyl linkage (Figure 6.1).²⁵ The enzyme catalyzes the oxidation of choline to glycine betaine following two FAD-dependent oxidation reactions.²⁶ Previous study carried out on a glutamine variant have shown that H466 was the catalytic base that activated the substrate for catalysis through the abstraction of a hydroxyl proton.²⁷ In a recent study, a reversible, charge-induced C4a-S-cysteinyl-flavin was engineered in choline oxidase by replacing Serine 101 with a cysteine (Figure 6.1).²⁸ The formation of the C4a-S-cysteinyl-flavin is initiated by binding protonated Tris, which is required to deprotonate the cysteine and to trigger the nucleophilic addition of cysteine thiolate to the C4a atom of the flavin.

In this study, a transient photoinduced flavin C4a adduct was observed in choline oxidase wild-type by fluorescence excitation spectroscopy. The choline oxidase wild-type was characterized using UV-visible absorption spectroscopy and fluorescence spectroscopy in various pH values, and solvent equilibrium isotope effects. The investigation of the residue involved in the formation of the C4a-N-histidyl-FAD was aided by determining the pH effects on the stoke shifts of the wild-type, H466N and S101A enzymes. A mechanism for the formation of the transient photoinduced C4a-N-histidyl-FAD is discussed with the evidence in its support.

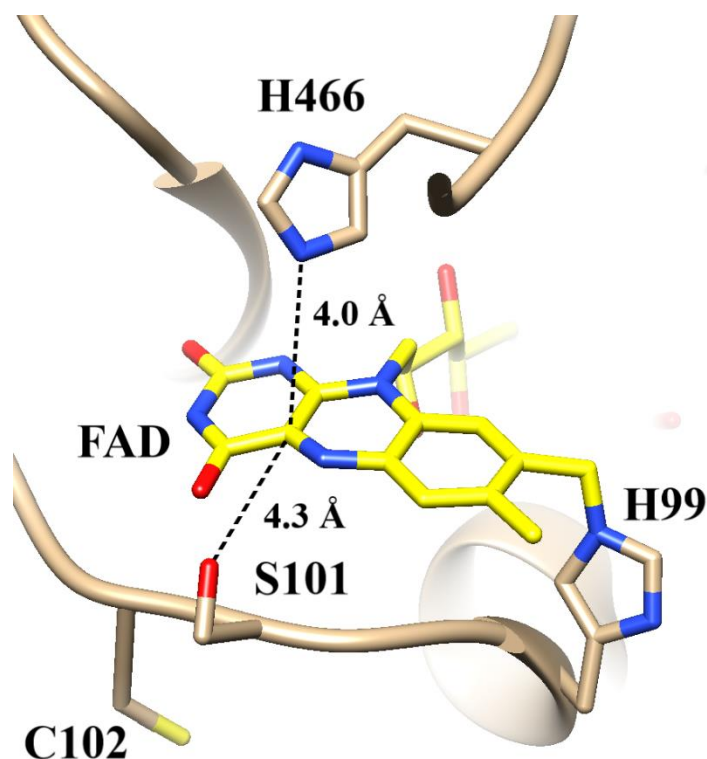


Figure 6.1 The active site of choline oxidase wild-type (PDB 4MJW). The C atoms of the FAD cofactor are shown in yellow, whereas those of H99, S101, C102 and H466 are displayed in tan; N, O, and S are colored in blue, red and yellow respectively

6.3 Material and Methods

Materials. Recombinant choline oxidase wild-type and variant enzymes were obtained through methods previously described.²⁹⁻³¹ Flavin adenine dinucleotide, glucose oxidase, and glucose were purchased from Sigma Aldrich (St. Louis, MO). Glycerol was purchased from Fisher (Pittsburgh, PA). Deuterium oxide was obtained from Cambridge Isotope Co. (Andover, MA). All other reagents were of the highest purity commercially available.

Spectroscopic Studies. All enzymes were prepared fresh just prior to measurements by gel-filtration through PD-10 desalting columns (General Electric, Fairfield, CT) into buffers ranging from pH 6.0 to 10.0. UV-visible absorption spectra were recorded in buffers at 15 °C, using an Agilent Technologies diode-array model HP 8453 spectrophotometer (Agilent Technologies,

Santa Clara, CA). Fluorescence excitation and emission spectra were recorded in corresponding buffers at 15 °C, with a Shimadzu Spectrofluorometer Model RF-5301 PC. Wavelength accuracy of the spectrofluorometer was ± 1.5 nm with a response time of 20 ms and a sampling interval of 1 nm. Flavin excitation wavelengths were initially determined through excitation scanning at 3 nm/min upon setting the emission wavelength to 520 nm. The sample was diluted to a final FAD concentration of 2.0 μ M using the extinction coefficients experimentally determined previously.²⁹⁻
³¹ Samples were excited at λ_{max} value as determined from the excitation scan measured from 300 to 500 nm and the emission scan was measured from 475 to 650 nm. Enzyme samples that were prepared in deuterated buffers underwent the same gel-filtration procedure used for protiated buffers with an adjusted pD value for the isotope effect observed from the pH electrode.³²

Anaerobic fluorescence spectra were measured in 20 mM sodium pyrophosphate, pH 6.0 and 10.0, at 15 °C using an anaerobic fluorescent cuvette (FireflySci, Brooklyn, NY). The anaerobic cuvette contained 7 mM glucose in buffer whereas S101A variant (2 μ M in flavin content) and glucose oxidase (1 μ M final concentration) enzymes were contained in the side arm. The cuvette apparatus was made anaerobic by a 15-minute treatment of flushing with oxygen-free argon flush. Once the flushing had completed, the enzymes were mixed with glucose to ensure complete scavenging of oxygen traces prior to measuring the fluorescence excitation and emission spectra.

Data Analysis. Data were fit with KaleidaGraph software (Synergy Software, Reading, PA). The pL effects on $\Delta\lambda$ ($\lambda_{\text{em}} - \lambda_{\text{ex}}$) of choline oxidase wild-type enzyme was determined with eq.1 to establish the pK_a value for the ionizations relevant to the formation of the photoinduced flavin species. Eq.1 describes a curve with one pK_a value and plateau regions at both low and high pH values.

$$\Delta\lambda = \frac{\Delta\lambda_{\text{lim}1} + \Delta\lambda_{\text{lim}2} \left(\frac{10^{-\text{pK}_a}}{10^{-\text{pH}}} \right)}{1 + \frac{10^{-\text{pK}_a}}{10^{-\text{pH}}}} \quad (1)$$

6.4 Results

Effect of pH on the Fluorescence Spectra of FAD in Free Solution. The fluorescence excitation and emission spectra of FAD in free solution and choline oxidase wild-type were measured in the pH range from 6.0 and 10.0 to investigate photoinduced species present in choline oxidase and ionizations relevant to the stabilization of photoinduced species. At pH 6.0, the UV-visible absorption spectrum of FAD in free solution demonstrated two peaks (λ_{abs}) at 375 nm and 450 nm. The excitation spectrum of FAD in free solution mimicked the general shape of its absorption spectrum with two maxima (λ_{ex}) at 374 nm and 454 nm, consistent with the Kasha-Vavilov's rule (Figure 6.2 A). The emission spectrum demonstrated a single band with the peak (λ_{em}) at 526 nm. At pH 10.0, the spectral behavior of FAD in free solution did not differ by more than 2 nm from those at pH 6.0, with λ_{abs} at 373 nm and 451 nm, λ_{ex} at 373 nm and 453 nm, and λ_{em} at 527 nm respectively (Figure 6.2B).

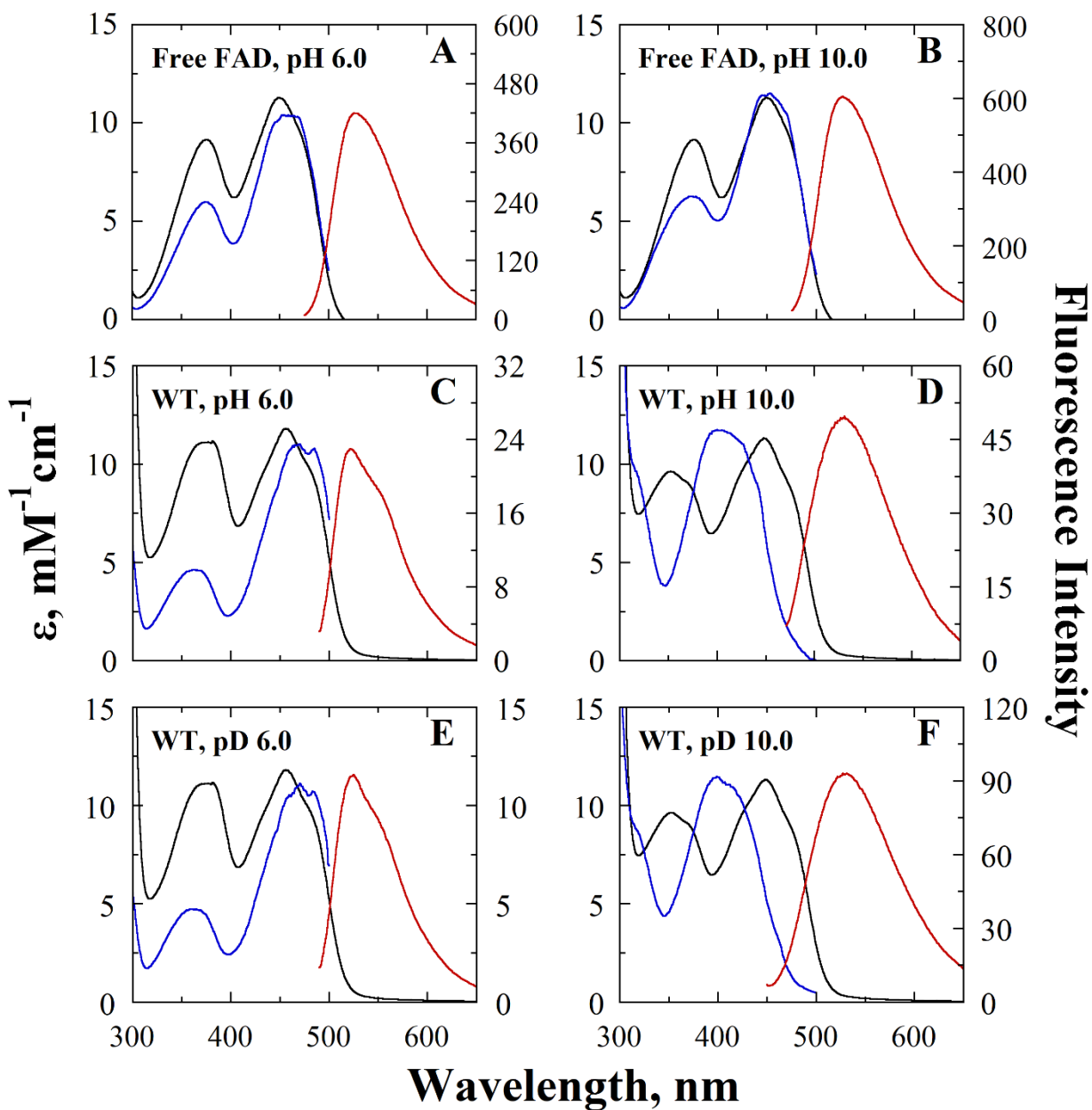


Figure 6.2 Fluorescence and absorption spectroscopy of FAD in free solution and choline oxidase. Spectra are for absorbance (black), fluorescence excitation (blue), and fluorescence emission (red) in 20 mM sodium pyrophosphate at the pH or pD indicated, 15 °C. FAD in free solution at pH 6.0 (A); free solution at 10.0 (B); wild-type enzyme at pH 6.0 (C); wild-type enzyme at pH 10.0 (D); wild-type enzyme at pD 6.0 (E); wild-type enzyme at pD 10.0 (F).

Effect of pL on the Fluorescence Spectra of FAD in Choline Oxidase Wild-type Enzyme.

The spectral behavior of FAD in choline oxidase wild-type at pH 6.0 resembled those of FAD in free solution. The fluorescence excitation spectrum with peaks at 364 nm and 468 nm followed the general shape of its UV-visible absorption spectrum with maxima at 375 nm and 456 nm. The emission spectrum showed a band with peak at 526 nm (Figure 6.2C). At pH 10.0, the increase in pH yielded hypsochromic shifts of both bands in the UV-visible absorption spectrum to 352 nm and 448 nm, associated with the ionization of N1 atom of covalently linked H99.²⁸ The fluorescence excitation spectrum showed only one broad band centered at 399 nm, instead of two bands observed for FAD in free solution and in choline oxidase at pH 6.0. The distinct excitation spectrum of FAD in choline oxidase with respect to its UV-visible absorption spectrum alluded to the formation of a transient photoinduced flavin species. A single band with peak at 528 nm was determined for the emission spectrum (Figure 6.2D). A similar spectral behavior was observed for FAD in choline oxidase wild-type prepared in D₂O at pD 6.0 and 10.0 with respect to those prepared in H₂O. (Figure 6.2E and F).

The determination of the pK_a value for the equilibria involving the photoinduced flavin species was achieved by plotting the difference ($\Delta\lambda$) between the band maxima of the lowest energy/longest wavelength of the excitation spectra (λ_{ex}) and the band maxima of the emission spectra (λ_{em}), which essentially represent the same electron transition, as a function of the pH value from 6.0 to 10.0. In choline oxidase wild-type prepared in H₂O, $\Delta\lambda$ of FAD increased from a limiting value of 58 ± 2 nm at acidic pH to 127 ± 2 nm at basic pH, with a pK_a value of 7.3 ± 0.1 (Figure 6.3). The pD-dependence of $\Delta\lambda$ in choline oxidase demonstrated no significance difference with respect to pH-dependence of $\Delta\lambda$, measuring a pK_a value of 7.3 ± 0.1 with limiting values of 60 ± 2 nm and 132 ± 2 nm, respectively (Figure 6.3). The pH-dependence of $\Delta\lambda$ of FAD in free

solution was also determined. As no photoinduced species was detected for FAD in free solution, there was no pK_a being observed (Figure 6.3), with an average $\Delta\lambda$ of 73 nm.

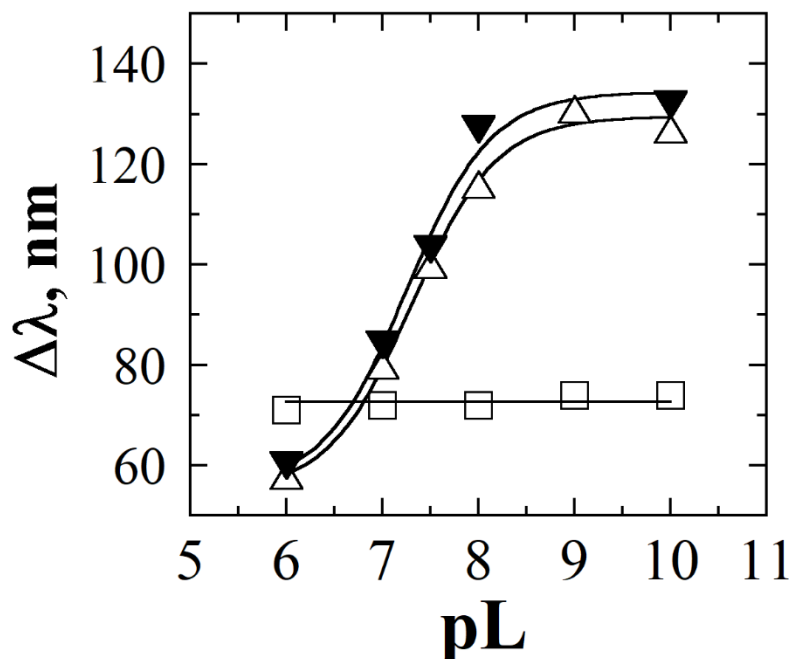


Figure 6.3 Effect of pL on $\Delta\lambda$ ($\lambda_{em} - \lambda_{ex}$) of FAD in free solution and wild-type enzyme in 20 mM sodium pyrophosphate and 20 mM sodium phosphate at 15 °C. FAD in free solution prepared in H₂O (□); wild-type enzyme prepared in H₂O (Δ); wild-type enzyme prepared in D₂O (▼). pL represents the negative logarithm of the concentration of protium or deuterium ions. Data for wild-type enzyme were fit with Eq 1.

Effect of pH on the Fluorescence Spectra of FAD in Choline Oxidase H466N Enzyme.

The histidine residue at the 466 position is located on an extended flexible loop composed of thirty amino acids on the *si* face of the flavin cofactor, approximately 4.0 Å from the C4a atom (Figure 6.1). The same experimental method as described with choline oxidase wild-type was carried out with the H466Q variant enzyme to probe the role of histidine in the formation of the photoinduced flavin species. UV-visible absorption, excitation and emission spectra were measured from pH 6.0 to 10.0 at 15 °C with the spectra at pH 10.0 shown in Figure 6.4A. Fluorescence excitation spectra exhibited red shifts across the entire pH range reflecting minimal peak shifts as compared to the

UV-visible absorption spectra. Due to all spectral peaks (i.e. λ_{abs} , λ_{ex} , λ_{em}) being similar in value at each pH value tested, only the average values are reported. The average values for λ_{abs} , λ_{ex} , λ_{em} are 453, 469, and 520 nm, respectively. In D₂O as a buffered solvent, values of λ_{abs} , λ_{ex} , λ_{em} were 453, 464, and 521 nm, respectively. Lack of a pL effect on $\Delta\lambda$ were consistent with the absence or lack of the photoinduced flavin species in the H466Q variant.

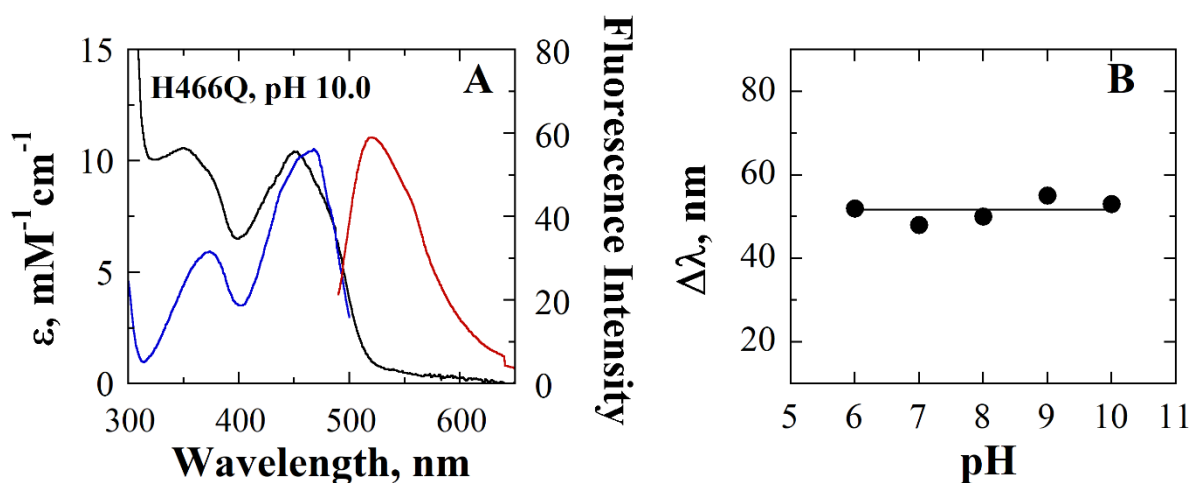


Figure 6.4 Fluorescence and absorption spectroscopy of H466Q variant enzyme. (A) Spectra are for absorbance (black), fluorescence excitation (blue), and fluorescence emission (red) in 20 mM sodium pyrophosphate at pH 10.0, 15 °C. (B) Effect of pH on $\Delta\lambda$ ($\lambda_{\text{em}} - \lambda_{\text{ex}}$) of FAD in H466Q variant enzyme in 20 mM sodium pyrophosphate and 20 mM sodium phosphate prepared in H₂O (●) in at 15 °C.

Effect of pH on the Fluorescence Spectra of FAD in Choline Oxidase S101A Enzyme.

The serine residue at the 101 position is located on a loop comprising eight amino acids with the hydroxyl oxygen atom pointing toward the flavin C4a atom at a ~ 4.3 Å distance (Figure 6.1). The involvement of the serine residue in the formation of the C4a flavin adduct was probed using choline oxidase variant in which the serine was mutated to an alanine residue. The excitation and emission spectra are shown in Figure 6.5. The fluorescence excitation spectrum was very similar

to the observed spectrum of choline oxidase wild-type at pH 10.0 in which a single peak was observed at 396 nm and a pronounced shoulder at 417 nm. The flavin was excited at 396 nm and emitted maximum fluorescence at 526 nm and, again, excited at 417 nm with emission maximum at 528 nm. The similarity in fluorescence between choline oxidase S101A and wild-type indicated the absence of serine 101 in the formation of the photoinduced FAD species.

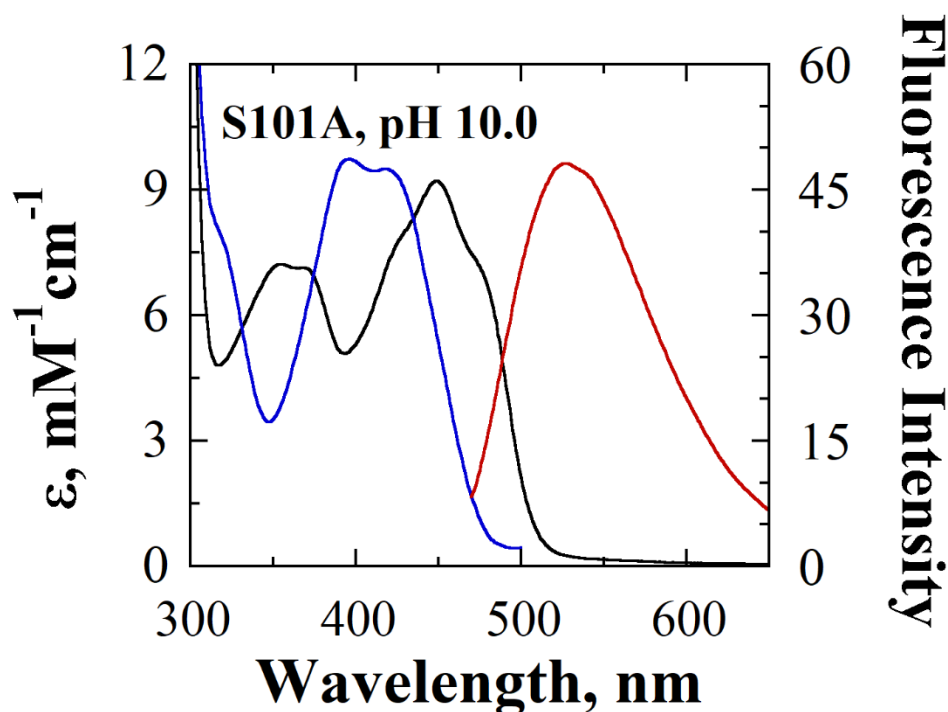


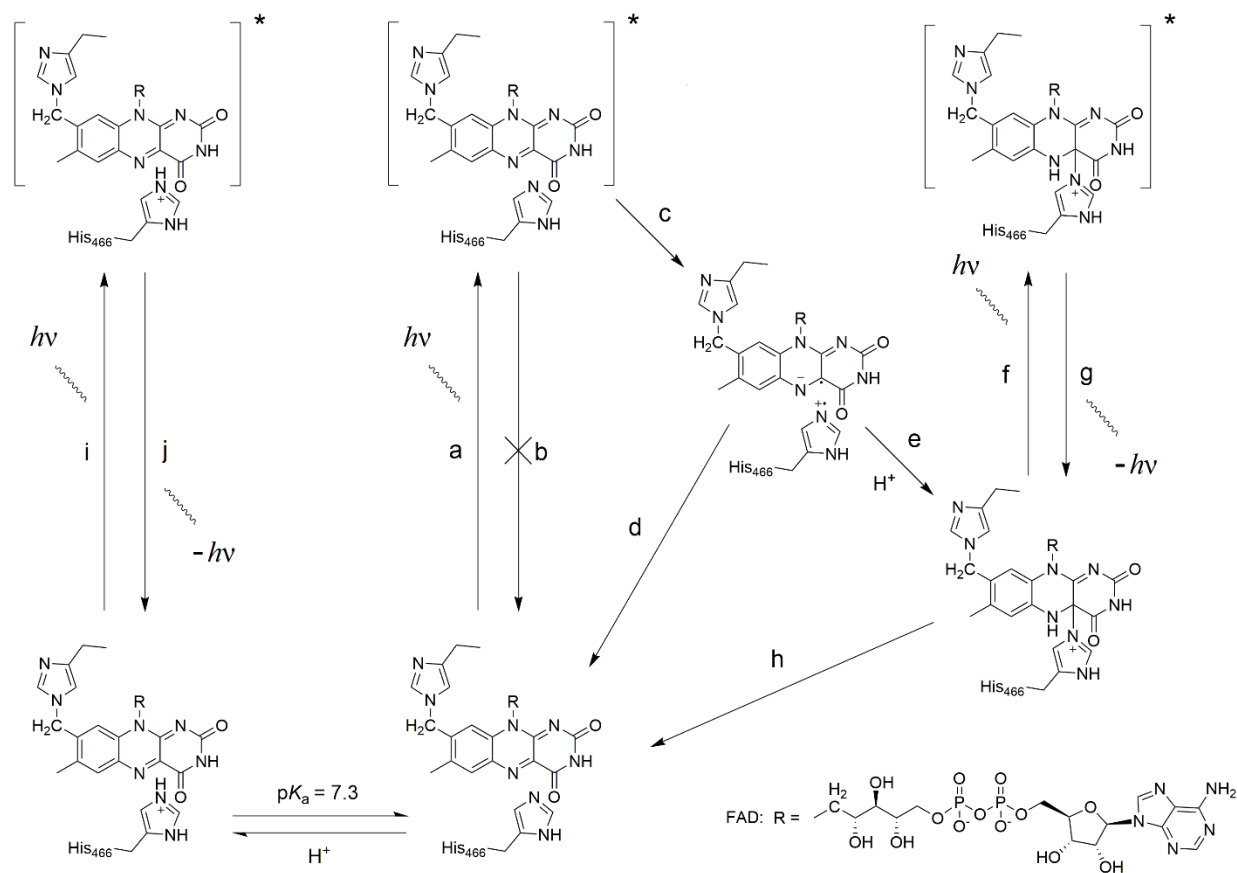
Figure 6.5 Fluorescence and absorption spectroscopy of S101A variant enzyme. Spectra are for absorbance (black), fluorescence excitation (blue), and fluorescence emission (red) in 20 mM sodium pyrophosphate at pH 10.0, 15 °C.

Anaerobic Fluorescence Spectroscopy of S101A Variant. Fluorescence spectra of S101A were measured with oxygen removed from the enzyme system to investigate the participation of oxygen in the formation of the photoinduced flavin species. The excitation spectrum of S101A variant at pH 10.0 showed a single broad spectrum with a major and minor peak too close in

wavelength to be resolved into two separate peaks at 395 and 420 nm. The fluorescence emission yielded a λ_{max} at 529 nm with excitation set to 395 nm. The spectral peaks in an anaerobic environment were not different from the peaks measured in the presence of oxygen, which ruled out the involvement of oxygen in the formation of the photoinduced flavin species.

6.5 Discussion

The spectroscopic investigation on choline oxidase presented in this study provides evidence that a photoinduced C4a-N-histidyl-FAD is formed in choline oxidase wild-type. At basic pH, excitation with light from ~ 300 nm to ~ 550 nm promotes the FAD cofactor to the excited singlet state (Step a in Scheme 6.1). A subsequent electron transfer rapidly occurs from the proximal deprotonated H466 to the excited FAD (Step c), quenching its deactivation to the ground state through fluorescence (Step b). The two highly reactive radical species, FAD semiquinone and histidine radical, then either follow charge recombination to oxidized ground-state FAD and histidine (Step d) or react with each other to yield C4a-N-histidyl-FAD (Step e). The C4a-N-histidyl-FAD instantaneously ($\leq 10^{-15}$ s) absorbs photon to its excited singlet state (Step f),³³ followed by the excited state deactivation through fluorescence which is observed in the fluorescence excitation spectrum (Step g). The oxidized ground-state FAD and histidine are recovered upon the breakage of the C4a-N-histidyl bond (Step h). The evidence is presented and discussed below.



Scheme 6.1 Schematic representation of excited state reaction in choline oxidase wild-type. The oxidized FAD in choline oxidase was excited to singlet excited state by photons (a). At basic pH, the excited-state decay of FAD through fluorescence (b) was quenched by the photoinduced electron transfer from the active site H466 to excited-state FAD (c). The yielded FAD semiquinone and histidine radical could either follow charge recombination back to ground-state oxidized FAD and histidine (d), or form C4a-N³-histidyl FAD through radical combination (e). The C4a-N³-histidyl FAD was excited to singlet excited state (f) and decayed through fluorescence (g), which was observed as the fluorescence excitation spectrum of the flavin C4a adduct. The break of C4a-N³-histidyl bond yielded the oxidized FAD and histidine (h). At acidic pH, the protonated H466 impeded the photoinduced electron transfer. Upon photon excitation (i), the excited-state FAD decayed to ground state through fluorescence (j), which was observed as the fluorescence excitation spectrum of oxidized FAD.

A transient photoinduced flavin species was detected at basic pH and consistent with a C4a flavin adduct as evidence by the formation of a single spectral peak at ~400 nm in fluorescence excitation spectrum. According to the Kasha-Vavilov rule, which assumes the internal conversion

from higher excited states to the lowest excited state are much faster than any other competing excited-state processes, the fluorescence excitation spectrum of a fluorophore should mimic its absorption spectrum.³³⁻³⁶ Some exceptions to the Kasha-Vavilov rule for flavin are known, such as blue shifts or quenching of emission when flavin is excited to higher excited states.^{3, 9, 11} But in both cases, the excitation spectra of flavin still resemble the overall, or low-energy portion of its UV-visible absorption spectra. In this study, the distinct excitation spectra of FAD in choline oxidase wild-type with respect to its UV-visible absorption spectra at basic pH (Figure 6.2 D and F) were indicative of the formation of a photoinduced flavin C4a adduct, instead of reflecting the electron transitions of the oxidized FAD. An alternative flavin species that exhibits a single absorption peak at ~ 400 nm is the protonated cationic oxidized flavin.^{14, 37} However, the pK_a value of the equilibrium of cationic and neutral oxidized flavin is low, with a value of ~ 0.1 in the ground state and ~ 1.8 in the excited state, which is not consistent with the formation of the transient photoinduced species at basic pH.^{1, 14} Besides, the broad emission centered at ~ 660 nm of cationic oxidized flavin was not observed.¹⁴

The transient photoinduced flavin C4a adduct in choline oxidase wild-type at basic pH is a C4a-N-histidyl-FAD with H466. The involvement of H466 in the photoinduced C4a-N-histidyl-FAD is established by the absence of fluorescence excitation spectrum consistent with a flavin C4a adduct in the H466N variant enzyme and the pH effect on the formation of the C4a-N-histidyl-FAD in the wild-type enzyme. The pK_a value of ~7.3 for the observation of the photoinduced flavin C4a adduct accorded with the pK_a value of ~ 7.5 of the previously determined catalytic base H466.²⁷ The lone electron pair on the N atom of the deprotonated histidine at basic pH facilitates the photoinduced electron transfer from the histidine to the excited oxidized FAD, thus quenches the fluorescence of the oxidized FAD (Figure 6.2 D and F) and leads to the formation of the

photoinduced C4a-N-histidyl-FAD. Consistently, the quenching rates of excited 3,3',4,4'-benzophenonetetracarboxylic acid (TCBP) through electron transfer were determined to be a magnitude faster by deprotonated histidine and *N*-acetylhistidine with respect to their protonated counterparts.³⁸ The involvement of the adjacent S101 and molecular oxygen in the photoinduced flavin C4a adduct can be ruled out because the characteristic spectrum of the photoinduced flavin C4a adduct was observed anaerobically in the S101A variant enzyme. In LOV domain, the photoinduced C4a-S-cysteinyl-flavin is generated in the signal state with a proximal cysteine.^{23, 24} It is worth noting that a cysteine located at 102 position is close to the FAD in choline oxidase (Figure 6.1). However, the side chain of C102 points away from the C4a atom of the FAD and its mobility is limited by the rigidity of the peptide bond, preventing C102 forming a covalent linkage with C4a atom of the FAD. Further evidence for H466 being involved in the photoinduced flavin C4a adduct comes from the solvent equilibrium isotope effect of ~ 1.0 calculated for the division of pK_a determined in H₂O over that in D₂O, which also rules out the possibility of participation of C102 for which an inverse isotope of ~ 0.55 is expected.³⁹

A mechanism involving photoinduced electron transfer for the formation of the C4a-N-histidyl-FAD is supported by the efficient quenching of the fluorescence of the oxidized FAD in choline oxidase at pH 10.0. The quenching of flavin fluorescence via photoinduced electron transfer from proximal electron donors have been well studied in free solution and proteins. In free solution, the intrinsic lifetime of the excited isoalloxazine ring of oxidized FAD in the open conformation is ~ 2.5 ns. The electron transfer from the adenine moiety to the excited isoalloxazine ring in the stacked conformation occurs in ~ 9.2 ps, a much faster process that accounts for the fluorescence quenching of FAD with respect to that of oxidized FMN without the adenine moiety.⁹ An ultrafast photoinduced electron transfer within ~ 1 ps from a proximal tryptophan triad to

excited oxidized FAD was determined in Type 1 cryptochromes and DNA photolyase.¹¹ Photoinduced electron transfer also underlies the fluorescence quenching mechanism of nonfluorescent and weakly fluorescent flavoproteins including flavodoxin, riboflavin binding protein, glucose oxidase, medium-chain Acyl-CoA dehydrogenase and D-amino acid oxidase-benzoate complex.⁴⁰⁻⁴² H466 is located 4 Å from the FAD in choline oxidase, allowing for electron transfer dynamics in 1-10 ps estimated at such a distance.⁴³ Alternative mechanism explaining the fluorescence quenching of the oxidized FAD and the formation of the C4a-N-histidyl-FAD in choline oxidase involves a nucleophilic addition on the excited flavin C4a atom. However, density function theory calculation on lumiflavin does not support this mechanism by revealing a negative charge increase on C4a atom in excited state compared to ground state.¹⁶ In addition, an efficient fluorescence quenching of the oxidized FAD requires an excited-state process much faster than the radiative deactivation through fluorescence. Although bond breaking and making could occur in femtosecond to sub-nanosecond time scale,⁴⁴ the nucleophilic addition of H466 on the C4a atom requires a geometric optimization of H466 and FAD to accommodate the change in hybridization of the C4a atom from sp^2 to sp^3 (Figure 6.1), which is not kinetically comparable to the radiative deactivation of the oxidized FAD through fluorescence.

6.6 Conclusion

In conclusion, a transient C4a-N-histidyl-FAD was observed using fluorescence spectroscopy in choline oxidase and investigated by mutagenesis, pH effects and equilibrium isotope effect. Formation of the C4a-N-histidyl-FAD linkage between the side chain of H466 and the 8α -N³-histidyl flavin in the active site of choline oxidase is triggered by the excitation of the oxidized FAD by light within its absorption spectrum, and it is followed by an electron transfer that quenches the excitation deactivation of the oxidized FAD through fluorescence. The yielded

FAD semiquinone and histidine radical react through radical recombination to give the C4a-N-histidyl-FAD, which is instantaneously excited by light and deactivates through fluorescence. This study established a new example of flavin-dependent light-sensitive protein that forms a transient covalent linkage with an active-site histidine; it also illustrates the strong application of fluorescence excitation spectra in understanding transient excited-state reactions in light sensitive flavoproteins besides the well-recognized tool of fluorescence emission.

6.7 Acknowledgement

We would like to thank Dr. Samer Gozem and Dr. Donald Hamelberg for inspirational discussions.

6.8 References

- [1] Miura, R. (2001) Versatility and specificity in flavoenzymes: control mechanisms of flavin reactivity, *Chemical record 1*, 183-194.
- [2] Romero, E., Gomez Castellanos, J. R., Gadda, G., Fraaije, M. W., and Mattevi, A. (2018) Same Substrate, Many Reactions: Oxygen Activation in Flavoenzymes, *Chemical reviews 118*, 1742-1769.
- [3] Su, D., Kabir, M. P., Orozco-Gonzalez, Y., Gozem, S., and Gadda, G. (2019) Cover Feature: Fluorescence Properties of Flavin Semiquinone Radicals in Nitronate Monooxygenase (ChemBioChem 13/2019), *ChemBioChem 20*, 1614-1614.
- [4] KOTAKI, A., and YAGI, K. (1970) Fluorescence Properties of Flavins in Various Solvents, *The Journal of Biochemistry 68*, 509-516.
- [5] Ghisla, S., Massey, V., Lhoste, J.-M., and Mayhew, S. G. (1974) Fluorescence and optical characteristics of reduced flavines and flavoproteins, *Biochemistry 13*, 589-597.
- [6] Visser, A. J., Ghisla, S., Massey, V., Muller, F., and Veeger, C. (1979) Fluorescence properties of reduced flavins and flavoproteins, *European journal of biochemistry 101*, 13-21.
- [7] Gozem, S., Mirzakulova, E., Schapiro, I., Melaccio, F., Glusac, K. D., and Olivucci, M. (2014) A conical intersection controls the deactivation of the bacterial luciferase fluorophore, *Angewandte Chemie (International ed. in English) 53*, 9870-9875.
- [8] Stanley, R. J., and MacFarlane. (2000) Ultrafast Excited State Dynamics of Oxidized Flavins: Direct Observations of Quenching by Purines, *The Journal of Physical Chemistry A 104*, 6899-6906.
- [9] Kao, Y.-T., Saxena, C., He, T.-F., Guo, L., Wang, L., Sancar, A., and Zhong, D. (2008) Ultrafast Dynamics of Flavins in Five Redox States, *Journal of the American Chemical Society 130*, 13132-13139.
- [10] Kim, S. T., Heelis, P. F., Okamura, T., Hirata, Y., Mataga, N., and Sancar, A. (1991) Determination of rates and yields of interchromophore (folate .fwdarw. flavin) energy transfer

- and intermolecular (flavin .fwdarw. DNA) electron transfer in *Escherichia coli* photolyase by time-resolved fluorescence and absorption spectroscopy, *Biochemistry* 30, 11262-11270.
- [11] Kao, Y. T., Tan, C., Song, S. H., Ozturk, N., Li, J., Wang, L., Sancar, A., and Zhong, D. (2008) Ultrafast dynamics and anionic active states of the flavin cofactor in cryptochrome and photolyase, *Journal of the American Chemical Society* 130, 7695-7701.
- [12] Laptенок, S. P., Bouzhir-Sima, L., Lambry, J. C., Myllykallio, H., Liebl, U., and Vos, M. H. (2013) Ultrafast real-time visualization of active site flexibility of flavoenzyme thymidylate synthase ThyX, *Proceedings of the National Academy of Sciences of the United States of America* 110, 8924-8929.
- [13] Yang, H., Luo, G., Karnchanaphanurach, P., Louie, T.-M., Rech, I., Cova, S., Xun, L., and Xie, X. S. (2003) Protein Conformational Dynamics Probed by Single-Molecule Electron Transfer, *Science* 302, 262-266.
- [14] Quick, M., Weigel, A., and Ernsting, N. P. (2013) Fluorescence following Excited-State Protonation of Riboflavin at N(5), *The Journal of Physical Chemistry B* 117, 5441-5447.
- [15] Salzmann, S., and Marian, C. M. (2008) Effects of protonation and deprotonation on the excitation energies of lumiflavin, *Chem Phys Lett* 463, 400-404.
- [16] Martin, C. B., Tsao, M.-L., Hadad, C. M., and Platz, M. S. (2002) The Reaction of Triplet Flavin with Indole. A Study of the Cascade of Reactive Intermediates Using Density Functional Theory and Time Resolved Infrared Spectroscopy, *Journal of the American Chemical Society* 124, 7226-7234.
- [17] Song, P.-S., Sun, M., Koziolowa, A., and Koziol, J. (1974) *Phototautomerism of lumichrome and alloxazines*, Vol. 96.
- [18] Zeugner, A., Byrdin, M., Bouly, J.-P., Bakrim, N., Giovani, B., Brettel, K., and Ahmad, M. (2005) Light-induced Electron Transfer in Arabidopsis Cryptochrome-1 Correlates with in Vivo Function, *Journal of Biological Chemistry* 280, 19437-19440.
- [19] Giovani, B., Byrdin, M., Ahmad, M., and Brettel, K. (2003) Light-induced electron transfer in a cryptochrome blue-light photoreceptor, *Nature structural biology* 10, 489-490.
- [20] Gauden, M., van Stokkum, I. H. M., Key, J. M., Lührs, D. C., van Grondelle, R., Hegemann, P., and Kennis, J. T. M. (2006) Hydrogen-bond switching through a radical pair mechanism in a flavin-binding photoreceptor, *Proceedings of the National Academy of Sciences* 103, 10895-10900.
- [21] Kim, S. T., Sancar, A., Essenmacher, C., and Babcock, G. T. (1993) Time-resolved EPR studies with DNA photolyase: excited-state FADH⁰ abstracts an electron from Trp-306 to generate FADH⁻, the catalytically active form of the cofactor, *Proceedings of the National Academy of Sciences of the United States of America* 90, 8023-8027.
- [22] Kao, Y.-T., Saxena, C., Wang, L., Sancar, A., and Zhong, D. (2005) Direct observation of thymine dimer repair in DNA by photolyase, *Proceedings of the National Academy of Sciences of the United States of America* 102, 16128-16132.
- [23] Schleicher, E., Kowalczyk, R. M., Kay, C. W. M., Hegemann, P., Bacher, A., Fischer, M., Bittl, R., Richter, G., and Weber, S. (2004) On the Reaction Mechanism of Adduct Formation in LOV Domains of the Plant Blue-Light Receptor Phototropin, *Journal of the American Chemical Society* 126, 11067-11076.
- [24] Zhu, J., Mathes, T., Hontani, Y., Alexandre, M. T. A., Toh, K. C., Hegemann, P., and Kennis, J. T. M. (2016) Photoadduct Formation from the FMN Singlet Excited State in the LOV2 Domain of *Chlamydomonas reinhardtii* Phototropin, *The Journal of Physical Chemistry Letters* 7, 4380-4384.

- [25] Salvi, F., Wang, Y. F., Weber, I. T., and Gadda, G. (2014) Structure of choline oxidase in complex with the reaction product glycine betaine, *Acta crystallographica. Section D, Biological crystallography* 70, 405-413.
- [26] Fan, F., and Gadda, G. (2005) On the catalytic mechanism of choline oxidase, *Journal of the American Chemical Society* 127, 2067-2074.
- [27] Smitherman, C., Rungsrisuriyachai, K., Germann, M. W., and Gadda, G. (2015) Identification of the Catalytic Base for Alcohol Activation in Choline Oxidase, *Biochemistry* 54, 413-421.
- [28] Su, D., Yuan, H., and Gadda, G. (2017) A Reversible, Charge-Induced Intramolecular C4a-S-Cysteinyl-Flavin in Choline Oxidase Variant S101C, *Biochemistry* 56, 6677-6690.
- [29] Ghanem, M., Fan, F., Francis, K., and Gadda, G. (2003) Spectroscopic and kinetic properties of recombinant choline oxidase from *Arthrobacter globiformis*, *Biochemistry* 42, 15179-15188.
- [30] Finnegan, S., Yuan, H., Wang, Y.-F., Orville, A. M., Weber, I. T., and Gadda, G. (2010) Structural and kinetic studies on the Ser101Ala variant of choline oxidase: Catalysis by compromise, *Archives of biochemistry and biophysics* 501, 207-213.
- [31] Ghanem, M., and Gadda, G. (2005) On the Catalytic Role of the Conserved Active Site Residue His466 of Choline Oxidase, *Biochemistry* 44, 893-904.
- [32] Salomaa, P., Schaleger, L. L., and Long, F. A. (1964) Solvent Deuterium Isotope Effects on Acid-Base Equilibria, *Journal of the American Chemical Society* 86, 1-7.
- [33] Lakowicz, J. R. (2006) *Principles of Fluorescence Spectroscopy*, Springer Science + Business Media, LLC, New York.
- [34] Kasha, M. (1950) Characterization of electronic transitions in complex molecules, *Discussions of the Faraday Society* 9, 14-19.
- [35] Berlman, I. (1971) *Handbook of fluorescence spectra of aromatic molecules*, Academic Press, New York.
- [36] IUPAC (1997) *Compendium of Chemical Terminology* 2nd ed., Blackwell Scientific Publications, Oxford.
- [37] Li, G., and Glusac, K. D. (2008) Light-triggered proton and electron transfer in flavin cofactors, *The journal of physical chemistry. A* 112, 4573-4583.
- [38] Saprygina, N. N., Morozova, O. B., Grampp, G., and Yurkovskaya, A. V. (2014) Effect of Amino Group Charge on the Photooxidation Kinetics of Aromatic Amino Acids, *The Journal of Physical Chemistry A* 118, 339-349.
- [39] Westheimer, F. H. (1961) The Magnitude of the Primary Kinetic Isotope Effect for Compounds of Hydrogen and Deuterium, *Chemical reviews* 61, 265-273.
- [40] Karen, A., Sawada, M. T., Tanaka, F., and Mataga, N. (1987) DYNAMICS OF EXCITED FLAVOPROTEINS—PICOSECOND LASER PHOTOLYSIS STUDIES, *Photochemistry and photobiology* 45, 49-53.
- [41] He, T.-F., Guo, L., Guo, X., Chang, C.-W., Wang, L., and Zhong, D. (2013) Femtosecond dynamics of short-range protein electron transfer in flavodoxin, *Biochemistry* 52, 9120-9128.
- [42] Mataga, N., Chosrowjan, H., Shibata, Y., Tanaka, F., Nishina, Y., and Shiga, K. (2000) Dynamics and Mechanisms of Ultrafast Fluorescence Quenching Reactions of Flavin Chromophores in Protein Nanospace, *The Journal of Physical Chemistry B* 104, 10667-10677.
- [43] Moser, C. C., Keske, J. M., Warncke, K., Farid, R. S., and Dutton, P. L. (1992) Nature of biological electron transfer, *Nature* 355, 796-802.
- [44] Zhong, D. (2007) Ultrafast catalytic processes in enzymes, *Current opinion in chemical biology* 11, 174-181.

7 CHAPTER 7: GENERAL DISCUSSION AND CONCLUSIONS

This dissertation focuses on the spectroscopic and mechanistic investigations of flavin-dependent nitronate monooxygenase and choline oxidase, with the aid of mutagenesis, rapid kinetics, steady-state kinetics, kinetic isotope and pH effects, and spectroscopic probes such as UV-visible absorption and fluorescence spectroscopy. These studies allowed the understanding the role of conserved residues in Class I nitronate monooxygenase (NMO) in substrate P3N binding and catalysis. The capability of thermodynamically stabilizing both the anionic and neutral forms of flavin semiquinone in NMO from *Pseudomonas aeruginosa* (*Pa*NMO) provided a single protein system to compare the photophysical properties of the flavin semiquinone in two ionization states without the effects exerted by different surrounding protein environments. The mechanism for both charge and photo-induced flavin C4a adducts were investigated in choline oxidase, underscoring the chemical versatility of flavin-dependent protein.

Class I NMO catalyzes the oxidation of nitronates with molecular oxygen. It has been previously characterized by biochemical, structural, and bioinformatic approaches.^{1, 2} The results demonstrated that the enzymatic oxidation of propionate 3-nitronate (P3N) in Class I NMO begins with a single electron transfer from P3N to the enzyme-bound FMN, forming a P3N radical species and a flavin semiquinone. The P3N radical is proposed to react directly with molecular oxygen to generate a 3-peroxy-3-nitropropanoate radical. A subsequent electron transfer from the flavin semiquinone to the 3-peroxy-3-nitropropanoate radical gives 3-peroxy-3-nitropropanoate, which would decay to the products. Alternatively, the flavin semiquinone would donate an electron to molecular oxygen yielding superoxide anion, which subsequently reacts with P3N radical to form 3-peroxy-3-nitropropanoate.² Previous crystallographic study of *Pa*NMO established that in Class

I NMO there are three fully conserved tyrosine residues, Y109, Y299, and Y303 (numbering for *Pa*NMO).¹ A fourth tyrosine is conserved in ~70% of the amino acid sequences, being replaced with a histidine in ~25% of the sequences and phenylalanine and tryptophan in the remaining cases. Another fully conserved residue in Class I NMO is K307, which is located at the entrance of the active site.

The crystallographic structure of the eukaryotic *Cs*NMO from *Cyberlindnera saturnus* (*Cs*NMO) was resolved to 1.65 Å. The three-dimensional structure of *Cs*NMO is highly conserved compared to the prokaryotic *Pa*NMO with the exception of three additional loops on the surface of *Cs*NMO. Conserved residues Y119, H276, Y321, K329 and Y325 line the active site and entrance of *Cs*NMO, corresponding to Y109, Y254, Y299, K307 and Y303 in bacterial *Pa*NMO. The role of the conserved active-site residues in Class I NMO were investigated in *Pa*NMO by site-directed mutagenesis, steady-state kinetics and pH effects on the UV-visible absorption spectroscopy. The results demonstrate that one of the active-site tyrosines in *Pa*NMO with the pK_a value of 9.5 is required to be protonated for binding of the negatively charged substrate P3N. However, the replacement of any of the four tyrosine with phenylalanine or lysine with methionine does not affect substrate binding or catalysis involving electron transfer reactions.

Flavin semiquinones are essential intermediates in the photocycle of light-responsive flavoproteins, e.g. cryptochrome blue-light photoreceptors,^{3, 4} blue-light BLUF domains,⁵ DNA photolyase,^{6, 7} and LOV domains.⁸ However, the understanding of the photophysics and photochemistry of flavin semiquinones has lagged because they are not stable in solution⁹ and are transient, short-lived species in many catalytic cycles. This dissertation established that *Pa*NMO could stabilize FMN in several redox and protonation states, including both neutral and anionic forms of flavin semiquinone. *Pa*NMO thus serves as a useful model system for studying the

spectroscopy and photophysics of each of these states in a constant protein environment. Neutral FMN semiquinone (FMNH[•]) in *Pa*NMO yields a strong fluorescence when excited to the first excited state (S₁), but no fluorescence at higher excited states. The resulting fluorescence excitation spectrum of FMNH[•] does not mimic the general shape of its UV-visible absorption spectrum, which violates the Kasha-Vavilov's rule. Time-dependent density functional theory (TD-DFT) calculations reveal that in FMNH[•] the lowest excited state is a bright emissive $\pi\pi^*$ state. A dark $n\sigma\pi^*$ state exists in FMNH[•] above the fluorescent D₁ $\pi\pi^*$ state that is likely responsible for its anti-Kasha behavior. The fluorescence of anionic FMN semiquinone (FMN^{•-}) in *Pa*NMO is not observed. The lack of fluorescence of FMN^{•-} is likely due to the existence of D₁ and D₂ $\pi\pi^*$ states with low oscillator strength based on the TD-DFT calculations.

Choline oxidase serves as a paradigm for alcohol oxidation catalyzed by flavin-dependent enzymes. It carries out two-step oxidation of choline to glycine betaine, with betaine aldehyde as an intermediate.¹⁰ In the crystallographic structure of choline oxidase, the FAD cofactor is covalently bound to protein via H99 through an 8 α -N³-histidyl linkage.¹¹ 8 α -N-histidyl adduct has been previously studied and reported to increase the redox of oxidized flavin.¹² The histidine residue at the 466 position is located on an extended flexible loop composed of thirty amino acids on the *si* face of the flavin cofactor, approximately 4.0 Å from the C4a atom. The serine residue at the 101 position is located on a loop comprising eight amino acids with the hydroxyl oxygen atom pointing toward the flavin C4a atom at a ~ 4.3 Å distance. The redox activity and structural resemblance to light-responsive LOV domain allow choline oxidase being a model system to engineer a variant that could potentially be inhibited by light through the formation of a C4a flavin adduct.¹³

First, a charge-induced, reversible C4a-S-cysteinyl-flavin was engineered in the choline oxidase by replacing S101 with a cysteine. Formation of the C4a-S-cysteinyl-flavin linkage between the side chain of C101 and the 8α -N³-histidyl flavin in the active site of the S101C enzyme is triggered by the binding of protonated Tris in the active site of the enzyme. The presence of protonated Tris bound at the active site of the enzyme is required to deprotonate the cysteine and to trigger the formation of the C4a-S-cysteinyl-flavin, and for the stabilization of the C4a-S-cysteinyl-flavin, as indicated by the decay of the C4a-S-cysteinyl-flavin when the bound Tris is replaced by glycine betaine. The pH titration data of the UV-visible absorption spectrum of the enzyme-bound flavin have established that the C4a-S-cysteinyl-flavin is stabilized between pH ~7.0 and ~9.5, in which the side chain of C101 is unprotonated and the N5 atom of the C4a-S-cysteinyl-flavin is protonated. This study establishes that the *de novo* engineering of a bicovalent C4a-S-cysteinyl- 8α -N³-histidyl flavin is feasible in a flavoprotein.

Then a transient photoinduced C4a-N-histidyl-FAD was observed with fluorescence excitation spectroscopy at basic pH values. Formation of the C4a-N-histidyl-FAD linkage between the side chain of H466 and the 8α -N³-histidyl flavin in the active site of choline oxidase is triggered by light absorption of oxidized FAD. It is followed by photoinduced electron transfer from the adjacent deprotonated H466, which quenches the excitation deactivation of the oxidized FAD through fluorescence. Subsequently, the yielded FAD semiquinone and histidine radical react to give C4a-N-histidyl-FAD through radical recombination. The C4a-N-histidyl-FAD instantaneously ($\leq 10^{-15}$ s) absorbs a photon to its excited singlet state,¹⁴ followed by the excited state deactivation through fluorescence which is observed in the fluorescence excitation spectrum. The mutagenesis and solvent equilibrium isotope effects suggest the involvement of H466 in the formation of C4a-N-histidyl-FAD. The efficient quenching of the oxidized FAD fluorescence in

choline oxidase at basic pH support a mechanism involving photoinduced electron transfer for the formation of the C4a-N-histidyl-FAD. This study establishes that a photoinduced flavin C4a adduct could be formed in choline oxidase and illustrates the strong application of fluorescence excitation spectroscopy in understanding transient excited-state reactions in light-sensitive flavoproteins.

Overall in this dissertation, the studies on nitronate monooxygenase and choline oxidase have provided insight into the chemistry versatility of flavoproteins. NMO catalyzes the oxidation of nitronates involving a single electron transfer chemistry and represents the first flavoprotein capable of stabilizing both neutral and anionic flavin semiquinones thermodynamically. The 8 α -N³-histidyl flavin in choline oxidase not only serve as an electrophile in its ground state to form a C4a-S-cysteinyl-flavin linkage with a proximal cysteine, but also mediate photoinduced electron transfer in its excited state leading to the formation of a transient C4a-N-histidyl-flavin. These studies will provide useful information on the mechanistic, photochemical and photophysical properties of flavin in different redox states.

7.1 References

- [1] Salvi, F., Agniswamy, J., Yuan, H., Vercammen, K., Pelicaen, R., Cornelis, P., Spain, J. C., Weber, I. T., and Gadda, G. (2014) The combined structural and kinetic characterization of a bacterial nitronate monooxygenase from *Pseudomonas aeruginosa* PAO1 establishes NMO class I and II, *J Biol Chem* 289, 23764-23775.
- [2] Smitherman, C., and Gadda, G. (2013) Evidence for a transient peroxy acid in the reaction catalyzed by nitronate monooxygenase with propionate 3-nitronate, *Biochemistry* 52, 2694-2704.
- [3] Lin, C., Robertson, D. E., Ahmad, M., Raibekas, A. A., Jorns, M. S., Dutton, P. L., and Cashmore, A. R. (1995) Association of flavin adenine dinucleotide with the Arabidopsis blue light receptor CRY1, *Science* 269, 968-970.
- [4] Bouly, J. P., Schleicher, E., Dionisio-Sese, M., Vandenbussche, F., Van Der Straeten, D., Bakrim, N., Meier, S., Batschauer, A., Galland, P., Bittl, R., and Ahmad, M. (2007) Cryptochrome blue light photoreceptors are activated through interconversion of flavin redox states, *J Biol Chem* 282, 9383-9391.

- [5] Gauden, M., van Stokkum, I. H. M., Key, J. M., Lührs, D. C., van Grondelle, R., Hegemann, P., and Kennis, J. T. M. (2006) Hydrogen-bond switching through a radical pair mechanism in a flavin-binding photoreceptor, *Proc Natl Acad Sci USA* 103, 10895-10900.
- [6] Kim, S. T., Sancar, A., Essenmacher, C., and Babcock, G. T. (1993) Time-resolved EPR studies with DNA photolyase: excited-state FADH⁰ abstracts an electron from Trp-306 to generate FADH⁻, the catalytically active form of the cofactor, *Proc Natl Acad Sci USA* 90, 8023-8027.
- [7] Kao, Y. T., Saxena, C., Wang, L., Sancar, A., and Zhong, D. (2005) Direct observation of thymine dimer repair in DNA by photolyase, *Proc Natl Acad Sci USA* 102, 16128-16132.
- [8] Schleicher, E., Kowalczyk, R. M., Kay, C. W., Hegemann, P., Bacher, A., Fischer, M., Bittl, R., Richter, G., and Weber, S. (2004) On the reaction mechanism of adduct formation in LOV domains of the plant blue-light receptor phototropin, *J Am Chem Soc* 126, 11067-11076.
- [9] Ehrenberg, A., Müller, F., and Hemmerich, P. (1967) Basicity, Visible Spectra, and Electron Spin Resonance of Flavosemiquinone Anions, *Eur J Biochem* 2, 286-293.
- [10] Fan, F., and Gadda, G. (2005) On the catalytic mechanism of choline oxidase, *J Am Chem Soc* 127, 2067-2074.
- [11] Salvi, F., Wang, Y. F., Weber, I. T., and Gadda, G. (2014) Structure of choline oxidase in complex with the reaction product glycine betaine, *Acta Crystallogr D Biol Crystallogr* 70, 405-413.
- [12] Singer, T. P., and Edmondson, D. E. (1974) 8 alpha-substituted flavins of biological importance, *FEBS Lett* 42, 1-14.
- [13] Crosson, S., and Moffat, K. (2001) Structure of a flavin-binding plant photoreceptor domain: Insights into light-mediated signal transduction, *Proc Natl Acad Sci USA* 98, 2995.
- [14] Lakowicz, J. R. (2006) *Principles of Fluorescence Spectroscopy*, Springer Science + Business Media, LLC, New York.